

Matrix models from black hole geometries

Andrea Boido, Alice Lüscher and James Sparks

*Mathematical Institute, University of Oxford,
Andrew Wiles Building, Radcliffe Observatory Quarter,
Woodstock Road, Oxford, OX2 6GG, U.K.*

Abstract

Supersymmetric, magnetically charged (and possibly accelerating) black holes in AdS_4 that uplift on Sasaki-Einstein manifolds Y_7 to M-theory have a dual matrix model description. The matrix model in turn arises by localization of the 3d $\mathcal{N} = 2$ SCFTs, dual to the AdS_4 vacuum, on the black hole horizon geometry, which is a Riemann surface Σ_g (or a spindle Σ). We identify the imaginary part t of the continuously distributed eigenvalues in the matrix model, and their density function $\rho(t)$, with natural geometric quantities associated with the M-theory circle action $U(1)_M$ on the near-horizon geometry $\text{AdS}_2 \times Y_9$, the internal space Y_9 being a Y_7 fibration over Σ_g (or Σ). Moreover, we argue that the points where $\rho'(t)$ is discontinuous match with the classical action of BPS probe M2-branes wrapping AdS_2 and the M-theory circle. We illustrate our findings with the ABJM and ADHM theories, whose duals have $Y_7 = S^7/\mathbb{Z}_k$, and some of their flavoured variants corresponding to other toric Y_7 .

Contents

1	Introduction and overview	3
1.1	Introduction and background	3
1.2	Overview of results	6
2	M2-brane Chern-Simons theories	10
2.1	Geometric engineering	10
2.1.1	Type IIA construction	10
2.1.2	Moduli space of vacua	13
2.1.3	M-theory circle	15
2.2	Topologically twisted matrix model	17
2.2.1	Chemical potentials versus R-charges	18
2.2.2	Localization on $\Sigma_g \times S^1$	19
2.2.3	The large N limit	20
3	Gravity duals	24
3.1	AdS ₄ backgrounds in M-theory	25
3.2	Near-horizon geometry of AdS ₄ black holes	27
3.2.1	GK geometry and geometric extremization	27
3.2.2	Fibered Y_9	29
3.2.3	Flavour twist	30
3.3	Example: $Y_7 = S^7$	32
4	Matrix model geometry	34
4.1	Holography of free energies and R-charges	34
4.2	M-theory circle moment map	36
4.3	Eigenvalue density from geometry	40
4.4	M2-branes and Wilson loops	46
4.4.1	BPS probe M2-branes	47
4.4.2	Wilson loop dual	49
5	Matrix models on the spindle	53
5.1	Accelerating black holes and block formulas	53
5.2	Shifted eigenvalue densities	56

5.3	Connecting to the refined twisted index	59
6	Further toric examples	61
6.1	Generalities on toric cones	62
6.1.1	GK geometry with toric fibres	62
6.1.2	Critical points and M2-branes	65
6.1.3	Eigenvalue density	67
6.2	Example: $C(Y_7) = \mathbb{C} \times C(T^{1,1})$	69
6.2.1	Flavoured $U(N)$	71
6.2.2	Flavoured ABJM	73
6.3	Example: $Y_7 = Q^{1,1,1}/\mathbb{Z}_n$	76
6.3.1	Flavoured ABJM	77
7	Discussion	79
A	Bethe potential at large N	80
A.1	Flavoured $U(N)$ theories	81
A.2	Flavoured ABJM theories	83
A.2.1	Flavoured ABJM dual to $\mathbb{C} \times C(T^{1,1})$	84
B	Example: $Y_7 = S^7/\mathbb{Z}_k$ – Summary of results	86
B.1	ADHM – Model I	87
B.2	ABJM – Model II	89
C	BPS condition for M2-branes	90
D	Wilson loop duals and flat C-fields	92

1 Introduction and overview

One of the successes of string theory and M-theory has been to give a microstate counting of black hole entropy. While the seminal work of [1] applied to supersymmetric black holes in asymptotically flat spacetime, more recently a different approach was initiated in [2, 3] using holography for asymptotically AdS black holes. This relies on the fact that the partition function of the dual field theory may be evaluated exactly using supersymmetric localization, reducing the computation of the entropy to a matrix model calculation. The aim of the present work is to extend this matching further, identifying large N matrix model quantities in this setting to counterparts in the gravity duals.

1.1 Introduction and background

We consider a general class of supersymmetric, magnetically charged AdS₄ black holes in M-theory, where the internal space Y_7 is a Sasaki-Einstein manifold. Before introducing the black hole the vacuum of the theory is the Freund-Rubin solution AdS₄ × Y_7 . Dirac quantization imposes

$$N = \frac{1}{(2\pi\ell_p)^6} \int_{Y_7} \star_{11} G \in \mathbb{N}, \quad (1.1)$$

where G is the M-theory four-form, \star_{11} is the Hodge dual, and ℓ_p denotes the Planck length. The integer N fixes the overall scale, and may also be interpreted as the number of M2-branes sourcing the AdS solution, as we describe further below.

Via the Kaluza-Klein mechanism, if the isometry group of Y_7 contains a maximal torus $U(1)^s$ of rank s , then there are associated massless $U(1)$ gauge fields A_i , $i = 1, \dots, s$, in the four-dimensional spacetime. One can then consider introducing a supersymmetric black hole into this vacuum, carrying conserved charges under the gauge fields. Taking the black hole horizon to be a Riemann surface¹ Σ_g of genus g , we consider black holes with magnetic (but no electric) fluxes

$$p_i = \frac{1}{2\pi} \int_{\Sigma_g} dA_i \in \mathbb{Z}. \quad (1.2)$$

In the full M-theory geometry the p_i are Chern classes which describe how the internal space Y_7 is fibred, as an associated principal $U(1)^s$ bundle, over the horizon Σ_g . The

¹Later in the paper we will also consider the extension to supersymmetric *accelerating* black holes [4], where the horizon is a orbifold surface known as a spindle [5].

total space Y_9 is then a fibre bundle

$$Y_7 \hookrightarrow Y_9 \rightarrow \Sigma_g. \quad (1.3)$$

Such black hole solutions are in general difficult to construct explicitly, not least since in general we lack four-dimensional consistent truncations that keep the massless gauge fields A_i . Exceptions to this are the $U(1)^4 \subset SO(8)$ STU gauged supergravity model that arises from reduction on $Y_7 = S^7$, with the corresponding black holes and holographic microstate counting discussed in [2]; and the consistent truncation of [6] to minimal gauged supergravity that includes only the R-symmetry gauge field (the graviphoton) for the $U(1)_R$ isometry of Y_7 , where the corresponding “universal twist” black holes and microstate counting were discussed in [7].

Even with a consistent truncation it is not guaranteed to be able to solve the Einstein equations in closed form, and we shall instead follow the approach introduced in [8], and further developed in [9–11]. Here rather than studying the full supersymmetric extremal black holes, we instead focus on their near-horizon geometry. Such near-horizon solutions take the form $\text{AdS}_2 \times Y_9$, where the internal space Y_9 has the fibred form (1.3). Supersymmetric M-theory solutions of this type, with no internal four-form flux G on Y_9 , were classified in [12], and require that Y_9 is a “GK geometry” [13]. We shall review this in more detail in section 3, but for the purposes of this introduction we now briefly summarize some relevant features.

Firstly, Y_9 necessarily admits an R-symmetry Killing vector field ξ , meaning that the preserved Killing spinor of the supergravity solution is charged under ξ . If we introduce a normalized basis of Killing vectors ∂_{φ_i} , $i = 1, \dots, s$, generating the $U(1)^s$ isometry of the fibre Y_7 in (1.3), then we may generically write

$$\xi = \sum_{i=1}^s b_i \partial_{\varphi_i}. \quad (1.4)$$

The variables $b_i \in \mathbb{R}$ then specify how $U(1)_R \subset U(1)^s$. Secondly, the geometry transverse to the vector field ξ in Y_9 is Kähler, and in the fibre Y_7 in particular one can introduce a transverse Kähler class $[\omega] \in H_B^2(\mathcal{F}_\xi)$, where the latter is the basic cohomology for the foliation \mathcal{F}_ξ defined by the vector field ξ . As in [10, 14, 15] we then study a restricted class of *flavour twist solutions*, where by definition we assume

$$[\omega] = \Lambda[\varrho] \in H_B^2(\mathcal{F}_\xi). \quad (1.5)$$

Here $\Lambda \in \mathbb{R}$ is a constant (which is ultimately fixed by flux quantization in M-theory, as in (1.1)) and ϱ denotes the transverse Ricci form for the Kähler metric. The condition (1.5) may be motivated in a number of ways. It is in some sense imposing an Einstein equation on the transverse Kähler metric, at a cohomology level, but in general one can certainly turn on more general Kähler class parameters. These parameters are expected, since in addition to the massless gauge fields A_i that result from isometries of Y_7 , the Kaluza-Klein mechanism will also lead to “baryonic” $U(1)$ gauge fields, associated with five-cycles in Y_7 , with the number of these being $\dim H_5(Y_7, \mathbb{R})$. When the latter is zero (such as for $Y_7 = S^7$ discussed above) the condition (1.5) is automatically true, and the same condition also holds for the universal twist black holes, also discussed above. On the other hand, when (1.5) does *not* hold it is currently not understood how to match the black hole entropy to a localization calculation, due to associated flat directions for the baryonic symmetries at large N [10]. In fact, in this paper we shall find a new puzzle with interpreting supergravity solutions which do not satisfy the condition (1.5).

With these ingredients to hand, we can now state how the black hole entropy is computed using this formalism [9, 10]. First, we introduce the gravitational free energy

$$F_{\text{grav}}[\xi] = \sqrt{\frac{2\pi^6}{27\text{Vol}_S(Y_7)[\xi]}} N^{3/2}. \quad (1.6)$$

Here $\text{Vol}_S(Y_7)[\xi]$ is the Sasakian volume of Y_7 [16, 17], and as the notation suggests this may be computed just from the topology of Y_7 and fixing a choice of R-symmetry vector ξ . F_{grav} is the free energy (the holographically renormalized action) of the $\text{AdS}_4 \times Y_7$ vacuum discussed at the start of this section. The black hole entropy is then given by the elegant formula

$$\mathcal{S}[\xi] = 4 \sum_{i=1}^s p_i \frac{\partial}{\partial b_i} F_{\text{grav}}[\xi] \Big|_{b_1=1}, \quad (1.7)$$

where p_i are the magnetic charges (1.2), and we have chosen a basis for ∂_{φ_i} generating $U(1)^s$ such that the Killing spinor is charged only under ∂_{φ_1} , with charge $\frac{1}{2}$. Supersymmetry is then preserved for such solutions via a topological twist, which fixes $p_1 = 2g - 2$, in terms of the genus g of the horizon Σ_g , and the condition $b_1 = 1$ in (1.7) simply normalizes the R-symmetry correctly. Crucially, following [8], in [9, 10] it is shown that solutions to the equation of motion *extremize* the entropy function in (1.7) over the choice of ξ , parametrized in terms of b_i via (1.4). The extremal value of \mathcal{S} is then the Bekenstein-Hawking entropy of the corresponding black hole solution.

The dual field theory calculations, which reproduce the entropy in (1.7) for certain classes of models, were carried out in [18, 19], with an interesting alternative approach recently given in [20]. As we review in section 2, the field theories are generically described by 3d $\mathcal{N} = 2$ Chern-Simons-matter theories. These arise as the low-energy worldvolume theories on N M2-branes at the Calabi-Yau four-fold singularity $X_4 = C(Y_7)$, and flow to superconformal field theories (SCFTs) in the IR, dual to the $\text{AdS}_4 \times Y_7$ vacuum. This is itself a well-established story.

Introducing a supersymmetric black hole changes the spacetime geometry, and correspondingly the Euclidean conformal boundary on which the field theory is defined is then $\Sigma_g \times S^1$. The partition function Z of the Chern-Simons-matter theory on the latter background is called the “topologically twisted index”, and this localizes to a matrix model as we review in section 2. In general the gauge group consists of \mathcal{G} copies of $U(N)$, labelled by $I = 1, \dots, \mathcal{G}$, and one can introduce the complexified Cartan-valued variables $u_I = \beta(A_3^I + i\sigma^I)$. Here β is the radius of the S^1 , A_3^I is the component of the I -th gauge field along this circle direction, while σ^I is the scalar field in the corresponding vector multiplet. The localized partition function involves an integral over the matrix variables u_I , which in the large N limit take a continuum form

$$u_I(t) = iN^{1/2}t + v_I(t), \quad (1.8)$$

where the imaginary part $N^{1/2}t$ will play a crucial role in what follows. The continuum limit has an associated eigenvalue density $\rho(t)$, and the black hole entropy is identified with $\text{Re} \log Z$.

1.2 Overview of results

In this paper we extend the above matching further, and show that many quantities in the large N matrix model can be identified directly in the gravitational duals, described by the GK geometry on Y_9 .

Firstly, a given field theory dual involves specifying a choice of the M-theory circle S_M^1 . This is because the Chern-Simons-matter theories are typically engineered from brane configurations in type IIA string theory, which involve reducing on S_M^1 . This can be specified by picking a $U(1)_M$ action on the fibre internal space Y_7 , generated by a corresponding Killing vector field ζ_M . Analogously to the construction in [21], we then introduce an *M-theory Hamiltonian function* h_M , also called *moment map* in the

following, which satisfies the defining equation

$$dh_M = -\zeta_M \lrcorner \omega. \quad (1.9)$$

Recall here that ω is the transverse Kähler form for the fibre Y_7 . In fact there is a natural choice for the integration constant in h_M , with an alternative definition of h_M given later in the paper. Being a continuous function on a compact space Y_7 , the image

$$h_M(Y_7) = [\tau_{\min}, \tau_{\max}] \subset \mathbb{R} \quad (1.10)$$

is a compact interval in \mathbb{R} , where we denote the image by the variable τ . Our first result is that there is a natural identification between this variable in gravity and the large N eigenvalue distribution on $\Sigma_g \times S^1$, namely

$$\tau = \ell_p^3 N^{1/2} t, \quad (1.11)$$

where ℓ_p is the Planck length, *cf.* equation (1.8). We motivate this identification by following a chain of relationships in the set-up we have described, starting from the vacuum moduli space of the Chern-Simons-matter theory. We shall see in examples that the eigenvalues in the matrix model are then indeed supported on the t -interval corresponding to (1.10), but there are further checks on this identification, as we now describe.

Secondly, in the gravity dual we can introduce a one-parameter family of five-dimensional spaces

$$Y_\tau = h_M^{-1}(\tau)/U(1)_M, \quad (1.12)$$

parametrized by τ . These are ‘‘Sasakian quotients’’ of Y_7 by the M-theory circle action, where the associated moment map level is τ . We then find that the eigenvalue density $\rho(t)$ in the matrix model is given by the simple formula

$$\rho(t) = C \cdot \left. \frac{d}{d\Lambda} \text{Vol}(Y_\tau) \right|_{\tau=\ell_p^3 N^{1/2} t}. \quad (1.13)$$

Here the constant C is fixed by requiring that $\rho(t)$ is a normalized density, and again we shall give a more explicit general formula later in the paper. Notice the derivative with respect to the parameter Λ , which was introduced as a Kähler class parameter via (1.5).

Finally, we also study certain probe M2-branes in the near-horizon $\text{AdS}_2 \times Y_9$ geometries, wrapping the (Euclidean) AdS_2 part of the spacetime and the M-theory circle

direction (so that they are tangent to ζ_M). These correspond to fundamental strings upon reducing to type IIA, and, when supersymmetric, should map to BPS Wilson loops in the fundamental representation of the gauge group wrapping the Euclidean time circle in the dual field theory [22]. We find that such M2-branes are supersymmetric precisely if they wrap the R-symmetry direction, and so are tangent to ξ . This can happen only on loci where ξ and ζ_M are aligned, which are precisely the *critical points* of h_M . Denoting with \mathbf{p}_n any point in the n -th such (connected) locus, the image $h_M(\mathbf{p}_n) = \tau_n$ defines a value t_n in the matrix model via (1.11). The values t_n are precisely the points at which the derivative of the eigenvalue density $\rho'(t)$ is discontinuous, and we find them to be related to the renormalized action I_{M2} of the above BPS M2-branes as

$$I_{M2}|_{\mathbf{p}_n} = N^{1/2}t_n . \quad (1.14)$$

If we order $t_1 = t_{\min} < t_2 < \dots < t_{\max}$, the BPS Wilson loop in the fundamental representation is then

$$\log \langle W_{\text{fund}} \rangle = -I_{M2}|_{\mathbf{p}_1} = -N^{1/2}t_{\min} , \quad (1.15)$$

which is the BPS M2-brane with least action.

This is a very satisfying picture of how the large N matrix model, that arises from localizing the Chern-Simons-matter field theories on $\Sigma_g \times S^1$, is related to the gravitational dual. We should emphasize that some of the ingredients we have introduced above have analogues also in the original $\text{AdS}_4 \times Y_7$ vacua – for example, the eigenvalue density on S^3 was interpreted in [23] in terms of counting operators in the chiral ring of the gauge theory in flat spacetime. The fact that we find similar formulas for the black hole solutions is non-trivial. Firstly, although the large N matrix models on S^3 and $\Sigma_g \times S^1$ are closely related (as pointed out in [18]), before taking the large N limit they are very different. This is emphasized by the alternative approach to the topologically twisted index and its refinement given in [20], which we will briefly discuss momentarily and in section 5. Similarly, the fact that certain structures in the Sasaki-Einstein geometry of Y_7 have analogues in GK geometry for Y_9 which are fibrations, as in (1.3), only follows from the quite extensive work on developing GK geometry that has been cited above. In particular there are some key differences with previous literature, for example with the discussion of BPS M2-branes. Another important aspect of the results described above is that they are formally independent of the choice of magnetic charges p_i , which have no analogue in the $\text{AdS}_4 \times Y_7$ vacuum. The matching we describe in fact holds “off-shell”, for any choice of R-symmetry vector ξ ; in particular we do not

have to pick the superconformal R-symmetry which extremizes the entropy (1.7) (and thus depends implicitly on the magnetic charges p_i) in order for the above statements to hold, and *a priori* it is not clear that this had to be the case.

Many of the structures we have introduced above also extend to *accelerating* black holes, using the results of [14, 15], as we discuss in section 5. Here the black hole horizon is replaced by a spindle $\Sigma = \mathbb{WCP}^1_{[m_+, m_-]}$. This is topologically a two-sphere, but with conical deficit angles $2\pi(1 - 1/m_{\pm})$ at the poles. Crucially there is not yet any large N matrix model result to compare to, although this is expected to arise from a limit of the spindle index introduced in [24]. However, setting $m_+ = m_- = 1$ gives the two-sphere, but where unlike in (1.4) the R-symmetry vector ξ on Y_9 is now allowed to mix with rotations of the horizon S^2 . We find that the analogous quantities computed in GK geometry in this setting, for example BPS M2-brane actions which sit at the poles of the S^2 , precisely match the *refined* twisted index of [20] where an additional chemical potential is introduced for rotations of the S^2 , in the background $S^2 \times S^1$ on which the field theory is defined! We present gravity predictions for the large N limit of the spindle index for $\Sigma \times S^1$.

Plan of the paper

The plan of the rest of the paper is as follows. In section 2 we briefly review how 3d $\mathcal{N} = 2$ Chern-Simons-matter theories arise on the worldvolumes of N M2-branes at a Calabi-Yau four-fold singularity X_4 . Key to this is a choice of M-theory circle and reduction to type IIA string theory, with our main examples being the ABJM and ADHM field theories, where in both cases $X_4 = \mathbb{C}^4/\mathbb{Z}_k$. We summarize how the partition function of such Chern-Simons-matter theories on $\Sigma_g \times S^1$ (the “topologically twisted index”) localizes to a matrix model, and take a large N continuum limit. In section 3, which is also largely review, we give an overview of the gravity dual solutions, with the near-horizon limit of the supersymmetric extremal black holes being described by $\text{AdS}_2 \times Y_9$ GK geometries in M-theory. Here $X_4 = C(Y_7)$ is a cone over Y_7 , and in turn the internal space Y_9 is a fibration of Y_7 over the horizon Σ_g (1.3).

Having introduced both sides of the duality, in section 4 we proceed to match quantities on both sides in more detail. Motivated by the moduli space discussion in section 2 we introduce the M-theory Hamiltonian function on Y_9 and relate this to the continuous eigenvalue density in the matrix model. We show in detail how this works for our two main ABJM and ADHM examples, and also relate this to the matching of

BPS M2-brane probes in the gravity background and dual Wilson loop VEVs. Section 5 switches gears and discusses the generalization to accelerating black holes, for which the Riemann surface horizon is replaced by a spindle $\Sigma = \mathbb{WCP}_{[m_+, m_-]}^1$. In this case there is not yet a large N matrix model result to compare to, but using [15] our gravity constructions extend straightforwardly. Remarkably, setting $m_+ = m_- = 1$ so that $\Sigma = S^2$ our results and BPS M2-brane actions in gravity perfectly match the recent “refined twisted index”, introduced in [20]. Section 6 illustrates the matching described in section 4 with further examples, where the calculations utilize appropriate toric geometry methods. We conclude in section 7 with a brief discussion and outlook.

Some further details have been relegated to various appendices: Appendix A gives more details of the large N matrix models with flavours, Appendix B collects the key results for the two main ABJM and ADHM examples, Appendix C derives the BPS condition for probe M2-branes, and finally Appendix D discusses a subtlety in computing the M2-brane VEV in gravity, along with its resolution.

2 M2-brane Chern-Simons theories

2.1 Geometric engineering

In this section we review how one can construct 3d $\mathcal{N} = 2$ worldvolume theories for M2-branes in backgrounds $\mathbb{R}^{1,2} \times X_4$, where X_4 is a Calabi-Yau four-fold singularity. This is well-understood in cases where X_4 may be appropriately viewed as a fibration over a Calabi-Yau three-fold X_3 , and there is a corresponding interpretation in terms of D2-branes in type IIA string theory. The fibration is related to adding D6-branes and/or turning on Ramond-Ramond two-form flux in the type IIA setting. We will focus on two simple examples which illustrate the general features, where both describe M2-branes in quotients of flat spacetime $\mathbb{R}^{1,2} \times \mathbb{C}^4/\mathbb{Z}_k$. We will then refer to these as primary examples for illustration throughout the remainder of the paper.

2.1.1 Type IIA construction

We start by considering N D2-branes in the background $\mathbb{R}^{1,2} \times X_3 \times \mathbb{R}_t$, where $t \in \mathbb{R}$ parametrizes² the real line and X_3 is a Calabi-Yau three-fold cone singularity. The latter has conical metric $g_{X_3} = dr^2 + r^2 g_{Y_3}$, where $r \geq 0$ is a radial coordinate for

²Here t is not to be confused with the time direction in $\mathbb{R}^{1,2}$, which will play no particular role in this paper.

the cone and (Y_5, g_{Y_5}) is a Sasaki-Einstein five-manifold. There are by now many classes of such X_3 , including infinite families with both explicit metrics and also general existence results [25]. While X_3 could be arbitrary, we will illustrate our results with two particularly simple examples, which we refer to as Model I and Model II:

$$\begin{aligned} \text{Model I : } X_3^{\text{I}} &= \mathbb{C}^3, \\ \text{Model II : } X_3^{\text{II}} &= \{z_1 z_2 = z_3 z_4\} \subset \mathbb{C}^4. \end{aligned} \tag{2.1}$$

Here X_3^{II} is the well-known conifold singularity, with $Y_5^{\text{II}} = T^{1,1} \cong S^2 \times S^3$, while the background for Model I is simply flat spacetime, with $Y_5^{\text{I}} = S^5$ with its round metric. The D2-branes are placed at the conical singularity $r = 0$ of X_3 (which is the origin of $\mathbb{C}^3, \mathbb{C}^4$, respectively, in the two models (2.1)), and the origin $t = 0$ of \mathbb{R}_t .

The low-energy effective theory on the D2-branes in the $\mathbb{R}^{1,2}$ directions is generically a three-dimensional $\mathcal{N} = 2$ theory. When the singularity X_3 admits a resolution to a smooth Calabi-Yau, this effective theory is expected to be described by a quiver gauge theory with superpotential W . For example, this will be the case if X_3 is a toric Calabi-Yau singularity, where the gauge group may be taken to be $\mathcal{G} = U(N)^{\mathcal{G}}$ where \mathcal{G} is the Euler number of the Calabi-Yau resolution. In this picture, each copy of $U(N)$ arises as the gauge group on a fractional D-brane, wrapping various collapsed cycles at the singularity, and the bifundamental matter fields in the quiver are massless strings between these D-branes. For our two examples we have:

Model I₀: $\mathcal{N} = 8$ $U(N)$ SYM. In $\mathcal{N} = 2$ language this is a $U(N)$ vector multiplet, together with three adjoint chiral fields Φ_i , $i = 1, 2, 3$, and superpotential $W = \text{Tr}(\Phi_3[\Phi_1, \Phi_2])$.

Model II₀: Klebanov-Witten theory [26]. This is a $U(N)^2$ quiver gauge theory, with bifundamental chiral fields A_i, B_i ($i = 1, 2$), transforming in the $(\mathbf{N}, \overline{\mathbf{N}})$, $(\overline{\mathbf{N}}, \mathbf{N})$ representations, respectively, and superpotential $W = \text{Tr}(A_1 B_1 A_2 B_2 - A_1 B_2 A_2 B_1)$.

In particular for Model II₀ the resolved Calabi-Yau is the resolved conifold, which replaces the isolated singular point $\{r = 0\} = \{z_1 = z_2 = z_3 = z_4 = 0\} \in X_3^{\text{II}}$ by a copy of $\mathbb{C}\mathbb{P}^1 = S^2$.

To obtain the final models that we are interested in, we add two further ingredients:

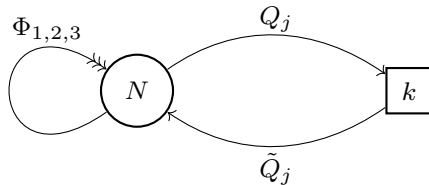


Figure 1: Quiver diagram for Model I: the ADHM theory.

D6-branes

We may add D6-branes to the above D2-brane set-up, without breaking any supersymmetry, provided these wrap divisors (complex codimension one submanifolds) in X_3 . From the low-energy D2-brane worldvolume perspective, this adds chiral matter fields in the fundamental/anti-fundamental representations, corresponding to massless strings stretching between the D2-branes and D6-branes [27, 28]. In particular, we define:

Model I: ADHM theory. We add k pairs of fundamental/anti-fundamental chiral fields (Q_j, \tilde{Q}_j) , $j = 1, \dots, k$ to Model I₀ [$\mathcal{N} = 8$ $U(N)$ SYM] above, with total superpotential

$$W = \text{Tr} \left(\Phi_3 [\Phi_1, \Phi_2] + \sum_{j=1}^k \tilde{Q}_j \Phi_3 Q_j \right). \quad (2.2)$$

Physically we have added k D6-branes to the original background, located at $\{z_3 = 0\} \subset \mathbb{C}^3$, and at the origin $t = 0$ of \mathbb{R}_t . The quiver for this theory is shown in Figure 1.

Chern-Simons terms

In $2 + 1$ dimensions we may instead add an $\mathcal{N} = 2$ Chern-Simons interaction for each $U(N)$ gauge group factor, proportional to the Chern-Simons levels $k_I \in \mathbb{Z}$, $I = 1, \dots, \mathcal{G}$. As explained in [29], such Chern-Simons interactions may be induced (via the Wess-Zumino couplings on D-branes) by turning on Ramond-Ramond (RR) fluxes in the original D2-brane background, where the flux threads the various (collapsed) cycles in X_3 . The sum $\sum_{I=1}^{\mathcal{G}} k_I = 2\pi\ell_s \mathcal{F}_0$, where ℓ_s is the string length and \mathcal{F}_0 is the Romans mass [30]. Thus provided $\mathcal{F}_0 = 0$ the resulting backgrounds uplift to M-theory. For Model II₀ above this leads to:

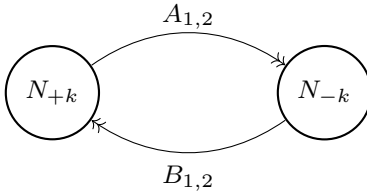


Figure 2: Quiver diagram for Model II: the ABJM theory.

Model II: ABJM theory [31]. This is the same Model II₀ D2-brane analogue of the Klebanov-Witten theory above, with superpotential

$$W = \text{Tr} (A_1 B_1 A_2 B_2 - A_1 B_2 A_2 B_1), \quad (2.3)$$

but with Chern-Simons levels $(k_1, k_2) = (k, -k)$, ensuring $\mathcal{F}_0 = 0$. This Chern-Simons coupling is induced by turning on k units of RR two-form flux through the (collapsed) $\mathbb{C}\mathbb{P}^1$ at the conifold singularity. The quiver for this theory is shown in Figure 2.

More generally, given any X_3 (with a Calabi-Yau resolution) one could add D6-branes, introducing fundamental matter in the field theory, and also turn on RR two-form flux, inducing Chern-Simons couplings in the field theory. Both types of deformation precisely fibre the M-theory circle S_M^1 over the original type IIA spacetime. The uplifted M-theory solution is then $\mathbb{R}^{1,2} \times X_4$, where $\mathcal{N} = 2$ supersymmetry fixes X_4 to be a Calabi-Yau four-fold, with the M-theory circle then necessarily complexified into $\mathbb{C}_M^* \equiv \mathbb{R}_t \times S_M^1$, and we may identify $X_3 = X_4/\mathbb{C}_M^*$. Both of our models uplift to $\mathbb{R}^{1,2} \times \mathbb{C}^4/\mathbb{Z}_k$, with different \mathbb{Z}_k quotients, as we describe in more detail in section 2.1.3.

2.1.2 Moduli space of vacua

The class of 3d $\mathcal{N} = 2$ field theories we have introduced have moduli spaces of vacua, and in this section we briefly comment on some aspects of this which will be relevant for the rest of the paper. A more complete discussion may be found in the original references [27–29, 32].

The Calabi-Yau geometry X_4 probed by the M2-branes appears directly in their vacuum moduli spaces. The reason for this is simple: for a single brane that probes a space X as a pointlike object, and is free to move anywhere on X , by definition X should appear as (a component of) the vacuum moduli space of the worldvolume field theory on that brane. Similarly, for N branes the vacuum moduli space should

contain a copy of $\text{Sym}^N X$, the symmetric product of N copies of X , corresponding to the moduli space of N indistinguishable pointlike objects probing X .

Let us describe this for a single D2-brane in $\mathbb{R}^{1,2} \times \mathbb{C}^3 \times \mathbb{R}_t$, setting $N = 1$ in Model I_0 described at the start of section 2.1.1. In $\mathcal{N} = 2$ language we have a $U(1)$ vector multiplet, which in addition to the gauge field contains a real scalar σ , together with three (uncharged) complex scalar fields Φ_i , $i = 1, 2, 3$. The superpotential W is zero for the Abelian theory, and thus the vacua are simply described by the vacuum expectation values (VEVs) of the Φ_i , which precisely parametrize $X_3^1 = \mathbb{C}^3$, together with the VEV of the real scalar σ , which parametrizes \mathbb{R}_t . As already mentioned above, in three dimensions we may also dualize the $U(1)$ gauge field into a periodic scalar field: in the M2-brane lift of the D2-brane, the VEV of this periodic scalar precisely parametrizes the M-theory circle S_M^1 . Moreover, after dualizing in this way the $\mathcal{N} = 2$ vector multiplet becomes a complex scalar field, living in \mathbb{C}_M^* . Extending to the non-Abelian $U(N)$ case, all of these fields become $N \times N$ matrices, transforming in the adjoint representation. Imposing the F-term relations $dW = 0$ from the superpotential $W = \text{Tr}(\Phi_3[\Phi_1, \Phi_2])$ implies that the Φ_i commute, and are thus simultaneously diagonalizable, parametrized by their N eigenvalues Φ_i^α , $\alpha = 1, \dots, N$. Similarly, σ is now a Hermitian $N \times N$ matrix, which is again parameterized by its N real eigenvalues σ^α . Altogether these parametrize $\text{Sym}^N(\mathbb{C}^3 \times \mathbb{R}_t) = (\mathbb{C}^3 \times \mathbb{R}_t)^N / S_N$, with the eigenvalues permuted by the Weyl group $\text{Weyl}(U(N)) = S_N$, which is the permutation group of N objects.

The M2-brane worldvolume theories of interest deform the original D2-brane theories by adding either D6-branes (fundamental/anti-fundamental matter) or turning on RR flux (Chern-Simons couplings). There is a similar, but more involved, discussion of their vacuum moduli spaces, which may be found in the original references [27–29, 32]. The main point we wish to emphasize here is that the branch of the vacuum moduli space which reproduces $\text{Sym}^N X_4$ has [32]

$$\sigma_1 = \sigma_2 = \dots = \sigma_{\mathcal{G}}, \quad (2.4)$$

where σ_I is the vector multiplet scalar for the I -th gauge group factor in $\mathcal{G} = U(N)^{\mathcal{G}}$. The N real eigenvalues σ_I^α of any one of the σ_I , where $\alpha = 1, \dots, N$, may again be thought of as parametrizing the positions of the D2/M2-branes along the \mathbb{R}_t direction. We shall return to this point again in the next subsection, and also when we consider the holographic duals.

In 3d gauge theories one can introduce pointlike *monopole operators*, which by def-

initiation create magnetic flux for a gauge field through an S_{pt}^2 surrounding that point. For M2-brane theories with gauge group $\mathcal{G} = U(N)^{\mathcal{G}}$ an important role is played by the diagonal monopole operators $T^{(n)}$, which by definition create flux

$$\int_{S_{\text{pt}}^2} \text{Tr } F_I = n \in \mathbb{Z}, \quad I = 1, \dots, \mathcal{G}. \quad (2.5)$$

Here F_I is the field strength for the I 'th gauge field, and it is convenient to further define $T \equiv T^{(1)}$, $\tilde{T} \equiv T^{(-1)}$. In a Chern-Simons theory such monopole operators also carry electric charges under the gauge group \mathcal{G} . An alternative way to introduce T, \tilde{T} is to first notice that in a quiver gauge theory nothing is charged under the diagonal $U(1)_{\text{diag}} \subset U(N)^{\mathcal{G}}$. This Abelian gauge field may then be dualized to a periodic scalar field τ , with period $2\pi/\mathcal{G}$ [32]. The diagonal monopole operators may then be promoted to complex chiral fields by identifying $T = |T| e^{i\mathcal{G}\tau}$, $\tilde{T} = |\tilde{T}| e^{-i\mathcal{G}\tau}$ [27].

For quiver gauge theories without D6-branes, and hence without fundamental/anti-fundamental matter, such as Model II, one can describe the vacuum moduli space without introducing T, \tilde{T} ; or rather one can introduce them, but they are essentially then immediately redundant, satisfying the trivial relation $T\tilde{T} = 1$. However, for theories that contain fundamental/anti-fundamental matter, the charges of T, \tilde{T} under both gauge and global symmetries in the quantum theory obtain anomalous contributions from fermion zero modes in that matter [27, 28]. The classical vacuum moduli space is correspondingly corrected in the quantum theory, and one necessarily needs to introduce T, \tilde{T} to describe this quantum-corrected moduli space. This leads to:

Model I: The monopole operators satisfy the quantum F-term relation

$$T\tilde{T} = \Phi_3^k. \quad (2.6)$$

This will be important, both for discussing the matrix model in section 2.2, and also for comparing to the gravity dual in section 4.

2.1.3 M-theory circle

As mentioned at the end of section 2.1.1, adding RR two-form flux and/or D6-branes to a type IIA spacetime fibres the M-theory circle S_M^1 , resulting in a total 11d spacetime of the form $\mathbb{R}^{1,2} \times X_4$. Equivalently, one can start with the latter spacetime and a specific choice of M-theory circle, and then reduce to type IIA. In practice we may fix a Calabi-Yau four-fold X_4 and pick a $U(1) \equiv U(1)_M$ action on X_4 . The flow of

the associated Killing vector ζ_M generates the M-theory circle action. Moreover, as explained in the last subsection the field theory moduli space for the Abelian theory precisely realizes X_4 .

For our models of interest recall that $X_4 = \mathbb{C}^4/\mathbb{Z}_k$, where we denote standard complex coordinates on \mathbb{C}^4 by $z_a = |z_a|e^{i\phi_a}$, and the a -th copy of \mathbb{C} is rotated by ∂_{ϕ_a} with weight one. The \mathbb{Z}_k quotient is precisely along $\mathbb{Z}_k \subset U(1)_M$, but where the M-theory circle action depends on the model. Let us see this explicitly:

Model I: Recall that this theory adds the fundamental/anti-fundamental fields $Q_j, \tilde{Q}_j, j = 1, \dots, k$, to the $\mathcal{N} = 8$ Maxwell theory. The branch of the *classical* vacuum moduli space where $Q_j = 0 = \tilde{Q}_j$ is identical to that for a D2-brane in flat spacetime, namely $\mathbb{C}_M^* \times \mathbb{C}^3$, which has the wrong topology.³ However, as shown in [27], the quantum-corrected moduli space for this theory may be parametrized by the three complex scalars Φ_1, Φ_2, Φ_3 , together with the diagonal monopole operators T, \tilde{T} , which recall satisfy the additional quantum constraint (2.6). The latter equation defines an $A_{k-1} = \mathbb{C}^2/\mathbb{Z}_k \subset \mathbb{C}^3$ singularity, where the \mathbb{C}^3 here has coordinates (T, \tilde{T}, Φ_3) . We immediately see that the quantum vacuum moduli space is $X_4^I = \mathbb{C}^2/\mathbb{Z}_k \times \mathbb{C}^2$, with (Φ_1, Φ_2) parametrizing the second factor of \mathbb{C}^2 . We may then identify

$$T = z_1^k, \quad \tilde{T} = z_2^k, \quad \Phi_1 = z_3, \quad \Phi_2 = z_4, \quad (2.7)$$

in terms of the standard coordinates z_a on \mathbb{C}^4 . The operators above have charges

$$U(1)_M^I : (1, -1, 0, 0), \quad (2.8)$$

under the M-theory circle action $U(1)_M$. The \mathbb{Z}_k quotient is precisely along $\mathbb{Z}_k^I \subset U(1)_M^I$, and we introduce the associated generating vector field $\zeta_M = \frac{1}{k}(\partial_{\phi_1} - \partial_{\phi_2})$, whose orbits are precisely the M-theory circles S_M^1 of the quotient. On the other hand, the fixed point set of the circle action $\{z_1 = z_2 = 0\}$ corresponds to the D6-brane locus in the type IIA spacetime. The

³There will be an additional ‘‘Higgs branch’’, where Q_j, \tilde{Q}_j may obtain vacuum expectation values, but from the F-term equations $dW = 0$ this can only happen where $\Phi_3 = 0$, which geometrically is then the D2-branes and D6-brane are coincident. This Higgs branch does not play any role in our discussion.

original type IIA spacetime $X_3^I = \mathbb{C}^3$ arises as the (Geometric Invariant Theory) quotient

$$\mathbb{C}^4/(\mathbb{C}_M^*)^I = X_3^I = \mathbb{C}^3, \quad (2.9)$$

where recall that $(\mathbb{C}_M^*)^I$ is the complexification of $U(1)_M^I$.

Model II: There are no quantum corrections in this theory, and we may hence describe the vacuum moduli space without introducing T, \tilde{T} . In the Abelian $N = 1$ theory the superpotential W is zero, and the vacuum moduli space is hence parametrized by the four scalar fields

$$A_1 = z_1, \quad B_1 = z_2, \quad A_2 = z_3, \quad B_2 = z_4. \quad (2.10)$$

Nothing is charged under the $U(1)_{\text{diag}} \subset U(1)^2$ diagonal gauge group, while we may identify the remaining $U(1)$ (to be concrete, the second $U(1)$ in $U(1)^2$) with the M-theory circle action. Thus the coordinates z_a on \mathbb{C}^4 have charges

$$U(1)_M^{\text{II}} : (1, -1, 1, -1). \quad (2.11)$$

The vacuum moduli space is then $X_4^{\text{II}} = \mathbb{C}^4/\mathbb{Z}_k^{\text{II}}$, with the $\mathbb{Z}_k^{\text{II}} \subset U(1)_M^{\text{II}}$ quotient arising due to a residual discrete gauge symmetry [31], and we correspondingly introduce the vector field $\zeta_M = \frac{1}{k}(\partial_{\phi_1} - \partial_{\phi_2} + \partial_{\phi_3} - \partial_{\phi_4})$. In this example the circle action is free, and hence there are no D6-branes. However Kaluza-Klein reduction along $U(1)_M^{\text{II}}$ gives rise to RR fluxes corresponding to Chern Simons coupling in the field theory. The original type IIA spacetime is the quotient

$$\mathbb{C}^4/(\mathbb{C}_M^*)^{\text{II}} = X_3^{\text{II}} = \{z_1 z_2 = z_3 z_4\} \subset \mathbb{C}^4. \quad (2.12)$$

2.2 Topologically twisted matrix model

The class of 3d $\mathcal{N} = 2$ Chern-Simons-matter theories we have introduced may be put on $\Sigma_g \times S^1$ with a topological twist along Σ_g , preserving supersymmetry, where Σ_g is a Riemann surface of genus g .⁴ The path integral of such a theory is called the topologically twisted index. In the following we review the localization of the latter, which leads to an effective matrix model description whose properties can be extracted in the large N limit. Our discussion follows the original references [2, 33, 34].

⁴From the type IIA perspective, this is achieved by wrapping the D2-branes on Σ_g .

2.2.1 Chemical potentials versus R-charges

The topologically twisted index is a function of background magnetic fluxes \mathbf{n}_A and fugacities y_A for the flavour symmetries of the theory. The fugacities $y_A = e^{i\pi\Delta_A}$ are equivalently expressed in terms of the chemical potentials Δ_A and these are the variables we use in the following.⁵ Another important fugacity is that for the topological symmetry, namely $\xi = e^{i\pi\Delta_m}$.

On the other hand, the partition function on S^3 instead depends on trial R-charges, which are also denoted Δ_A in the literature. We shall use $\Delta_A^{S^3}$ to distinguish them where necessary. The chemical potentials and the R-charges appear in an identical fashion in the computation of the large N partition functions on $\Sigma_g \times S^1$ and S^3 respectively, which leads to the formal identification $\Delta_A = \Delta_A^{S^3}$ in [18]. The latter reference also noticed that for the topological symmetry these parameters are related up to a sign $\Delta_m = -\Delta_m^{S^3}$. These identifications are crucial for this work, as holographically the parameters matched to geometry are the R-charges, and then by extension the chemical potentials. Additionally, it is also expected that the chemical potentials should be R-charges for the 1d supersymmetric theory that appears on flowing to the IR, after compactification on Σ_g . We will make some of these statements more precise in section 4.1. In line with this comment, we introduce the formal variables Δ_T and $\Delta_{\tilde{T}}$ which we identify with the R-charges of the diagonal monopole operators, such that

$$\Delta_m = -\Delta_m^{S^3} = -\frac{1}{2}(\Delta_T^{S^3} - \Delta_{\tilde{T}}^{S^3}) = -\frac{1}{2}(\Delta_T - \Delta_{\tilde{T}}). \quad (2.13)$$

The second equality is the definition of the “bare” monopole charge $\Delta_m^{S^3}$ [35]. Recall that the monopole operators T and \tilde{T} also obey an F-term relation, which translates into a constraint on their R-charges, and by extension to our variables. Together with (2.13) this gives two constraints on Δ_T and $\Delta_{\tilde{T}}$, and it is consistent to phrase any result in terms of these rather than Δ_m . As we shall see, many of the results we shall obtain take a more simple, universal form when expressed in terms of $\Delta_{T,\tilde{T}}$.

Finally, we note that the above variables are not all independent, but rather obey constraints coming from the superpotential. First, the invariance of the superpotential under global symmetries imposes $\prod_A y^A = 1$ in each term of the superpotential, such

⁵Note that we take a different convention from [2], namely $\Delta^{\text{there}} = \pi\Delta$.

that⁶

$$\sum_{A \in W} \Delta_A = 2, \quad (2.14)$$

where the sum runs over the fields appearing in each monomial of the superpotential. On the other hand the superpotential has charge 2 under the R-symmetry $\Delta_W = 2$, giving rise to the constraint $\sum_A \Delta_A^{S^3} = 2$. This guarantees that the identification $\Delta_A = \Delta_A^{S^3}$ is sensible. Second, there is also a constraint on the fluxes arising because we are imposing a topological twist to preserve supersymmetry on the Riemann surface Σ_g

$$\sum_{A \in W} \mathfrak{n}_A = 2g - 2. \quad (2.15)$$

Note that we take a different sign convention from [2] for the fluxes, in order to match the geometry conventions of [15] later on.

2.2.2 Localization on $\Sigma_g \times S^1$

The index can be evaluated *exactly* using supersymmetric localization [36]. That is, for BPS observables the path integral is exactly equal to a (finite-dimensional) integral over certain supersymmetric field configurations, dressed by a one-loop determinant that captures fluctuations. Recall that $\mathcal{N} = 2$ theories have vector multiplets with fields $(A_\mu, \lambda, \sigma, D)$, where A_μ is the gauge field with curvature $F_{\mu\nu}$, λ is an adjoint-valued Dirac fermion, while σ, D are adjoint-valued scalars. The BPS configurations for an $\mathcal{N} = 2$ vector multiplet on $\Sigma_g \times S^1$, denoting the Σ_g directions with orthonormal frame directions e^1, e^2 and the S^1 with e^3 , are such that $D = iF_{12}$, $F_{13} = F_{23} = 0$, while σ and A_3 take constant values along S^1 . The BPS moduli space is then characterized by the Cartan-valued variables

$$u = \beta(A_3 + i\sigma), \quad \mathfrak{m} = \frac{1}{2\pi} \int_{\Sigma_g} F, \quad (2.16)$$

where β is the radius of the S^1 and the gauge magnetic fluxes \mathfrak{m} take values in the co-root lattice of the gauge group.⁷ For each $U(N)$ gauge group, u takes the form of an $N \times N$ matrix, which can be diagonalized by a gauge transformation. Then, for the I 'th gauge group factor,

$$u_I = \text{diag}(u_I^1, \dots, u_I^N), \quad (2.17)$$

⁶Looking only at the constraint on the fugacities it appears that we could have $\sum_A \Delta_A = 2\ell$, $\ell \in \mathbb{Z}$ in general. However it has been argued in [18] that any $\ell \neq 1$ either does not give a consistent solution, or gives a solution related to the $\ell = 1$ solution by discrete symmetries.

⁷This BPS locus is to be contrasted with the one on S^3 where only $\sigma = -D$ is non-zero, and in particular there are no gauge magnetic fluxes.

such that the full BPS moduli space is parametrized by the \mathcal{G} sets of N eigenvalues u_I^α , $\alpha = 1, \dots, N$, $I = 1, \dots, \mathcal{G}$.

The localized partition function can then be recast into a contour integral over u_I and a sum over \mathbf{m} .

$$Z(\Delta, \mathbf{n}) = \sum_{\mathbf{m}} \oint_c Z_{\text{int}}(u, \mathbf{m}; \Delta, \mathbf{n}). \quad (2.18)$$

We are not interested in the explicit form of the integrand at this stage. What we want to highlight is that even though the moduli space depends on the gauge content of the model only, the path integral itself also includes the matter content. Therefore, as mentioned before, it is a function of the chemical potentials and the flavour magnetic fluxes of the theory. Deforming the contour and performing the sum in (2.18), the twisted index reduces to a contour integral with simple poles at $e^{iB_I^\alpha} - 1 = 0$ where $e^{iB_I^\alpha}$ depends on the field content; explicit rules to build this function can be found in [18]. The index is therefore given by a sum of residues evaluated at the solutions of the so-called Bethe ansatz equations (BAEs)

$$e^{iB_I^\alpha} = 1 \implies B_I^\alpha + 2\pi n_I^\alpha = 0, \quad (2.19)$$

where the variables n_I^α parameterize the phase ambiguities, and are chosen in order to cancel the long range forces [2]. Furthermore, the BAEs can be obtained as critical points of a function known as the Bethe potential \mathcal{U} ,

$$\text{BAEs : } \frac{\partial \mathcal{U}}{\partial u_I^\alpha} = 0. \quad (2.20)$$

In summary, this reformulates the problem of evaluating the index to the one of extremizing the Bethe potential.

2.2.3 The large N limit

In the large N limit, (2.20) can be solved numerically by taking the following ansatz for the eigenvalues, which is partly based on some analytical arguments and on the numerical simulations in [2],

$$u_I^\alpha = it^\alpha N^{1/2} + v_I^\alpha + o(N^0), \quad (2.21)$$

where t^α , v_I^α are real and taken to be $\mathcal{O}(N^0)$ in the large N limit. Notice that (2.21) may equivalently be written as

$$\text{Im } u_1 = \dots = \text{Im } u_{\mathcal{G}} = \text{diag}(t^1, \dots, t^N) N^{1/2}. \quad (2.22)$$

Note this condition implies that $\sigma_1 = \dots = \sigma_g$, which is *precisely* the same condition that arises on the vacuum moduli space – see equation (2.4). This is a non-trivial statement: (2.22) describes the large N eigenvalue distribution of the field theory localized on $\Sigma_g \times S^1$, while (2.4) is a statement about the moduli space of the same field theory on flat spacetime $\mathbb{R}^{1,2}$. Recall that in the latter case we interpreted $\sigma_1 = \dots = \sigma_g$ as the position of the corresponding D2-branes in \mathbb{R}_t . We will return to this comment in section 4, when we come to interpret the large N saddle point distribution directly in the gravity dual.

The numerical simulations also show that the imaginary parts of the eigenvalues t^α become dense at large N , and are distributed over a finite interval $[t_{\min}, t_{\max}]$. We may order the eigenvalues using Weyl transformations so that t^α are increasing, and introduce the corresponding (discrete) density function

$$\rho(t) = \frac{1}{N} \sum_{\alpha=1}^N \delta(t - t^\alpha), \quad \int_{t_{\min}}^{t_{\max}} dt \rho(t) = 1. \quad (2.23)$$

In the $N \rightarrow \infty$ limit the eigenvalues t^α become a continuous variable t , with continuous eigenvalue density $\rho(t)$. In particular (2.21) becomes a continuous function

$$u_I(t) = itN^{1/2} + v_I(t). \quad (2.24)$$

In fact, the Bethe potential can be formulated in terms of $\rho(t)$ and $v_I(t)$, and the solutions of the BAEs are found by extremizing the potential with respect to these functions. Again there are rules, which can be found in [18] and that we review in Appendix A, to build \mathcal{U} in terms of these variables directly from the field content of the theory. The normalization of ρ is imposed via the introduction of a Lagrange multiplier μ , and the quantity to extremize is actually

$$\frac{\mathcal{U}}{iN^{3/2}} - \pi\mu \left(\int dt \rho(t) - 1 \right). \quad (2.25)$$

We now present the results of this extremization, which may be found in [19] and [2] respectively:

Model I: The chemical potentials satisfy the constraints

$$\sum_{i=1}^3 \Delta_{\Phi_i} = 2, \quad \Delta_T + \Delta_{\bar{T}} = k\Delta_{\Phi_3}, \quad (2.26)$$

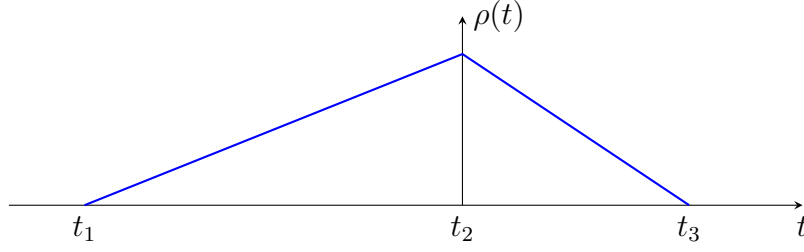


Figure 3: Schematic behaviour of the piecewise linear distribution of eigenvalues in the large N limit for the Model I ADHM theory.

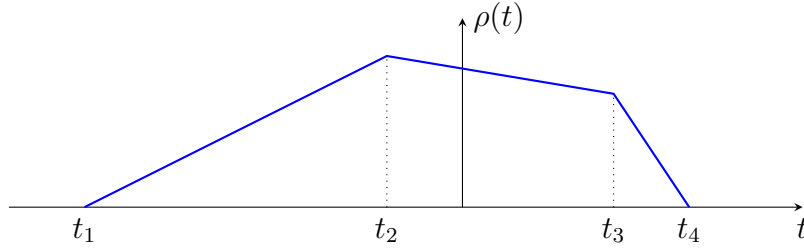


Figure 4: Schematic behaviour of the piecewise linear distribution of eigenvalues in the large N limit for the Model II ABJM theory.

leaving three independent. The first constraint is simply the superpotential one, where the W is given in (2.2), while the second constraint follows from (2.6). The saddle point eigenvalue density is

$$\rho(t) = \begin{cases} \frac{\mu + \Delta_{\tilde{T}} t}{\pi^2 \Delta_{\Phi_1} \Delta_{\Phi_2} \Delta_{\Phi_3}}, & t_{\min} < t < 0, \\ \frac{\mu - \Delta_T t}{\pi^2 \Delta_{\Phi_1} \Delta_{\Phi_2} \Delta_{\Phi_3}}, & 0 \leq t < t_{\max}, \end{cases} \quad (2.27)$$

where the endpoints are given by

$$t_{\min} = -\frac{\mu}{\Delta_{\tilde{T}}}, \quad t_{\max} = \frac{\mu}{\Delta_T}, \quad (2.28)$$

and the extremal value of the Lagrange multiplier is

$$\mu = \pi \sqrt{\frac{2}{k} \Delta_{\Phi_1} \Delta_{\Phi_2} \Delta_T \Delta_{\tilde{T}}}. \quad (2.29)$$

In particular for generic chemical potentials, $\rho(t)$ is linear in two regions (see Figure 3).

Model II: The chemical potentials Δ_{A_i} , Δ_{B_i} , $i = 1, 2$, satisfy the single superpotential constraint

$$\Delta_{A_1} + \Delta_{B_1} + \Delta_{A_2} + \Delta_{B_2} = 2, \quad (2.30)$$

where W is given by (2.3). Without loss of generality, we may assume that $\Delta_{A_1} \leq \Delta_{A_2}$, $\Delta_{B_1} \leq \Delta_{B_2}$. One finds the following eigenvalue density

$$\rho(t) = \begin{cases} \frac{\mu + k\Delta_{B_1}t}{\pi^2(\Delta_{A_1} + \Delta_{B_1})(\Delta_{A_2} + \Delta_{B_1})(\Delta_{B_2} - \Delta_{B_1})}, & t_1 < t < t_2, \\ \frac{2\mu + k(\Delta_{B_1}\Delta_{B_2} - \Delta_{A_1}\Delta_{A_2})t}{\pi^2(\Delta_{A_1} + \Delta_{B_1})(\Delta_{A_1} + \Delta_{B_2})(\Delta_{A_2} + \Delta_{B_1})(\Delta_{A_2} + \Delta_{B_2})}, & t_2 < t < t_3, \\ \frac{\mu - k\Delta_{A_1}t}{\pi^2(\Delta_{A_1} + \Delta_{B_1})(\Delta_{A_1} + \Delta_{B_2})(\Delta_{A_2} - \Delta_{A_1})}, & t_3 < t < t_4. \end{cases} \quad (2.31)$$

which is linear in the three regions separated by

$$t_1 = -\frac{\mu}{k\Delta_{B_1}}, \quad t_2 = -\frac{\mu}{k\Delta_{B_2}}, \quad t_3 = \frac{\mu}{k\Delta_{A_2}}, \quad t_4 = \frac{\mu}{k\Delta_{A_1}}, \quad (2.32)$$

where $t_{\min} = t_1 < t_2 < t_3 < t_4 = t_{\max}$, as depicted in Figure 4. The extremal value of the Lagrange multiplier is

$$\mu = \pi\sqrt{2k\Delta_{A_1}\Delta_{A_2}\Delta_{B_1}\Delta_{B_2}}. \quad (2.33)$$

The free energy $F = -\log Z$ can also be computed directly from the Bethe potential evaluated on the BAEs solutions [18]

$$\log Z_{\Sigma_g \times S^1}(\Delta, \mathbf{n}) = \frac{1}{\pi} \sum_A \left[\mathbf{n}_A \frac{\partial \bar{\mathcal{U}}(\Delta)}{\partial \Delta_A} \right], \quad (2.34)$$

$$\bar{\mathcal{U}}(\Delta) \equiv -i\mathcal{U}|_{\text{BAEs}} = \frac{2\pi\mu}{3} N^{3/2}, \quad (2.35)$$

where the sum runs over all the fields in the quiver, as well as the monopole operators. Note that some fields can be eliminated using the constraints (2.14) and (2.15). For our examples, this recovers some known results:

Model I

$$\log Z_{\Sigma_g \times S^1}^{\text{ADHM}} = \frac{\pi}{3} \sqrt{\frac{2}{k} \Delta_{\Phi_1} \Delta_{\Phi_2} \Delta_T \Delta_{\tilde{T}}} \left(\frac{\mathbf{n}_{\Phi_1}}{\Delta_{\Phi_1}} + \frac{\mathbf{n}_{\Phi_2}}{\Delta_{\Phi_2}} + \frac{\mathbf{n}_T}{\Delta_T} + \frac{\mathbf{n}_{\tilde{T}}}{\Delta_{\tilde{T}}} \right) N^{3/2}, \quad (2.36)$$

and

$$\frac{2}{\pi} \bar{\mathcal{U}}(\Delta) = \frac{4\pi}{3} \sqrt{\frac{2}{k} \Delta_{\Phi_1} \Delta_{\Phi_2} \Delta_T \Delta_{\tilde{T}}} N^{3/2} = F_{S^3}^{\text{ADHM}}. \quad (2.37)$$

Model II

$$\log Z_{\Sigma_g \times S^1}^{\text{ABJM}} = \frac{\pi}{3} \sqrt{2k\Delta_{A_1}\Delta_{A_2}\Delta_{B_1}\Delta_{B_2}} \left(\frac{\mathbf{n}_{A_1}}{\Delta_{A_1}} + \frac{\mathbf{n}_{A_2}}{\Delta_{A_2}} + \frac{\mathbf{n}_{B_1}}{\Delta_{B_1}} + \frac{\mathbf{n}_{B_2}}{\Delta_{B_2}} \right) N^{3/2}, \quad (2.38)$$

and

$$\frac{2}{\pi} \bar{\mathcal{U}}(\Delta) = \frac{4\pi}{3} \sqrt{2k\Delta_{A_1}\Delta_{A_2}\Delta_{B_1}\Delta_{B_2}} N^{3/2} = F_{S^3}^{\text{ABJM}}. \quad (2.39)$$

There are two things to notice here. First, the similarity of the expressions between the two models. This is easily understood from looking at the dual geometries which we will do in section 4.1. Second, that $\bar{\mathcal{U}}$ corresponds to the expression of the free energy on S^3 upon identifying the chemical potential with the R-charges, which has already been noted in [18]. There is no *a priori* reason for these quantities to be related from a purely field theoretic point of view. For some related discussion in the gravity dual, see [9].

Finally we shall also be interested in the expectation values of supersymmetric Wilson loop operators. Recall that a Wilson loop in a representation \mathcal{R} is defined as

$$W_{\mathcal{R}} = \text{Tr}_{\mathcal{R}} \mathcal{P} \exp \oint d\tau (iA_{\mu} \dot{x}^{\mu} + \sigma |\dot{x}|). \quad (2.40)$$

In order for the Wilson loop to be supersymmetric, it needs to wrap the S^1 direction [33]. It then reduces to $W_{\mathcal{R}} = \text{Tr}_{\mathcal{R}} \exp(iu)$ with u defined in (2.16). The expectation value is obtained by inserting this loop operator into the path integral, and normalizing by a factor of $1/Z$, so that $\langle 1 \rangle = 1$. In the large N limit, the factors of the partition function simply cancel. Therefore, in the fundamental representation,

$$\langle W_{\text{fund}} \rangle = \sum_{I=1}^{\mathcal{G}} \sum_{\alpha=1}^N e^{iu_{I}^{\alpha}} = N \sum_{I=1}^{\mathcal{G}} \int_{t_{\min}}^{t_{\max}} dt \rho(t) e^{-N^{1/2}t + iv_I(t)}, \quad (2.41)$$

such that at leading order in N

$$\log \langle W_{\text{fund}} \rangle = -N^{1/2} t_{\min}. \quad (2.42)$$

Compare this with the discussion in [21], on S^3 , which is similar.

3 Gravity duals

In this section we introduce and then further study the geometry of the M-theory backgrounds dual to the 3d field theories introduced in section 2. Firstly, we briefly introduce the vacuum $\text{AdS}_4 \times Y_7$ solutions, with Y_7 being a 7d Sasaki-Einstein manifold, which are dual to the field theories placed on S^3 (the conformal boundary of global Euclidean AdS_4). Next, we consider inserting a black hole with horizon Σ_g into such a background. This is the gravity setting relevant for reproducing the topologically twisted index at large N discussed in section 2.2, as the conformal boundary with the insertion of a black hole is $\Sigma_g \times S^1$ rather than S^3 .

The near-horizon geometry of such extremal black holes takes the form of $\text{AdS}_2 \times Y_9$ with Y_9 a GK manifold [12, 13]. More specifically Y_9 here is the total space of a fibration with base Σ_g and fibre Y_7 , as in (1.3). We present the main properties of such fibred Y_9 geometries and summarize the geometric extremization procedure to get the entropy and the R-charges in gravity. Finally, we illustrate concretely all the above constructions by looking at case where Y_7 is a 7-sphere (or a \mathbb{Z}_k quotient thereof), which corresponds to the gravity dual of the Models I and II previously introduced.

3.1 AdS_4 backgrounds in M-theory

To set the stage, we briefly illustrate the near-horizon limit of the 11d geometries corresponding to the 3d SCFTs on S^3 we introduced in section 2. This will also allow us to introduce various notation and geometric concepts that will be needed for the black hole generalization, where the internal manifold Y_7 will fiber over the horizon Σ_g in the later subsections.

The starting point consists of $\mathbb{R}^{1,2} \times X_4$ backgrounds in M-theory where X_4 is a Calabi-Yau four-fold cone. There are many classes of constructions of such Calabi-Yau's, including explicit metrics and existence results, and some of these will be considered later in section 6. However, for the sake of clarity, we mainly focus on the simplest possible example, namely $X_4 = \mathbb{C}^4$ (or a \mathbb{Z}_k quotient thereof), which leads to the Model I and II introduced previously in section 2. Following [16] we go “off-shell” and consider X_4 equipped with a Kähler, but not necessarily Ricci-flat, cone metric

$$ds_{X_4}^2 = dr^2 + r^2 ds_{Y_7}^2. \quad (3.1)$$

When the cone (3.1) is Kähler the induced metric $ds_{Y_7}^2$ on $Y_7 = \{r = 1\} \subset X_4$ is by definition Sasakian and therefore comes equipped with a unit length Killing vector field ξ called *Reeb vector field*. In particular the metric on Y_7 can be written as

$$ds_{Y_7}^2 = \eta_7^2 + ds_{6d}^2(\omega_S), \quad (3.2)$$

where η_7 is the one-form dual to ξ , i.e. $\xi \lrcorner \eta_7 = 1$ (and $\xi \lrcorner d\eta_7 = 0$). The metric (3.2) itself is transversely Kähler, with Kähler two-form ω_S and $d\eta_7 = 2\omega_S$.⁸ The transverse Kähler form on the base of the cone can be related with the Kähler form \mathcal{J} on the cone itself in the following way

$$\mathcal{J} \equiv \frac{1}{2} d(r^2 \eta_7) = r dr \wedge \eta_7 + r^2 \omega_S \quad \implies \quad \mathcal{J} \Big|_{r=1} = \omega_S. \quad (3.3)$$

⁸The superscript in ω_S is meant to highlight that this Kähler two-form is such that the metric (3.2) is Sasakian. Later on we will lift this assumption and consider a generic Kähler two-form ω .

The holomorphic $(4, 0)$ -form $\Psi_{(4,0)}$ on the cone $X_4 = C(Y_7)$ has charge 4 under ξ i.e.

$$\mathcal{L}_\xi \Psi_{(4,0)} = 4i\Psi_{(4,0)}. \quad (3.4)$$

We assume that Y_7 has a $U(1)^s$ isometry with $1 \leq s \leq 4$, and we call the corresponding generating vector fields ∂_{φ_i} , $i = 1, \dots, s$, with the coordinates φ_i having period 2π . The case $s = 4$ corresponds to a toric cone and will be considered in more detail in section 6.1.1. Having introduced the coordinates φ_i , we may parameterize the Reeb vector field ξ as

$$\xi = \sum_{i=1}^s b_i \partial_{\varphi_i}. \quad (3.5)$$

In particular, we choose the basis in (3.5) in such a way that $\Psi_{(4,0)}$ has charge 1 under ∂_{φ_1} and is uncharged under all other ∂_{φ_i} , so that (3.4) is achieved by setting $b_1 = 4$.

Placing N M2-branes at the singular point $\{r = 0\} \in X_4$, including their backreaction and then taking the near-horizon limit, results in the associated AdS₄ backgrounds

$$\begin{aligned} ds_{11}^2 &= L^2 \left(\frac{1}{4} ds_{\text{AdS}_4}^2 + ds_{Y_7}^2 \right), \\ G &= \frac{3}{8} L^3 \text{vol}_{\text{AdS}_4}. \end{aligned} \quad (3.6)$$

Here g_{AdS_4} is the metric on a unit radius AdS₄, with $\text{vol}_{\text{AdS}_4}$ the corresponding volume form, while G is the M-theory four-form. The constant length scale L is fixed by flux quantization via

$$L^6 = \frac{(2\pi\ell_p)^6 N}{6\text{Vol}_S(Y_7)}, \quad (3.7)$$

where ℓ_p is the eleven-dimensional Planck length, $\text{Vol}_S(Y_7)$ is the volume of the Sasakian metric on Y_7 , and the integer flux N given by (1.1) is the number of M2-branes.

The holographically renormalized gravitational free energy of such backgrounds is

$$F_{\text{grav}}[\xi] = \frac{\pi}{2G_4} = \sqrt{\frac{2\pi^6}{27\text{Vol}_S(Y_7)[\xi]}} N^{3/2}, \quad (3.8)$$

where G_4 is the four-dimensional effective Newton constant. Here $\text{Vol}_S(Y_7)[\xi]$ highlights the fact that the Sasakian volume of Y_7 is a function of the Reeb vector field ξ [16, 17]. The eleven-dimensional metric and four-form in (3.6) give an $\mathcal{N} = 2$ supersymmetric solution to eleven-dimensional supergravity precisely when the Sasakian metric $ds_{Y_7}^2$ is also Einstein, or equivalently when the Kähler cone metric (3.1) is also Ricci-flat, i.e. Calabi-Yau. In [16, 17] it was shown that such metrics precisely minimize the volume

$\text{Vol}(Y_7)[\xi]$, as a function of ξ subject to the charge constraint (3.4) which fixes its normalization. It immediately follows that the extremal value of ξ then maximizes the holographic free energy F_{grav} in (3.8).

3.2 Near-horizon geometry of AdS_4 black holes

From a geometric engineering perspective, taking an M2-brane worldvolume field theory and putting it on a Riemann surface Σ_g amounts to wrapping the M2-branes at the tip of the CY cone X_4 over Σ_g . When taking the near-horizon limit this set-up results in a particular class of $\text{AdS}_2 \times Y_9$ backgrounds where Y_9 is a GK manifold [12, 13] taking the particular form of a fibration over Σ_g with fibres Y_7 as in (3.2), although with Kähler form ω in general different from the Sasakian Kähler form ω_S . These are the near-horizon limits of supersymmetric, asymptotically AdS_4 , magnetically charged black holes, that we began our discussion with at the start of the paper.

3.2.1 GK geometry and geometric extremization

We start by describing the M-theory background arising from a general GK manifold Y_9 . We consider solutions of the form

$$ds_{11}^2 = e^{-2B/3} (ds_{\text{AdS}_2}^2 + ds_{Y_9}^2), \quad (3.9)$$

$$G = \text{vol}_{\text{AdS}_2} \wedge F, \quad (3.10)$$

where $ds_{\text{AdS}_2}^2$ is the metric on AdS_2 with unit radius, and B and F are respectively a function and a closed two-form on a compact manifold Y_9 . Via Dirac quantization the seven-form flux $\star G$ needs to be quantized over a set of codimension 2 submanifolds $\Sigma_\Upsilon \subset Y_9$, which constitute a basis for the free part of $H_7(Y_9, \mathbb{Z})$:

$$\frac{1}{(2\pi\ell_p)^6} \int_{\Sigma_\Upsilon} \star G = \mathcal{N}_\Upsilon \in \mathbb{Z}. \quad (3.11)$$

Imposing supersymmetry, *i.e.* the existence of Killing spinors, it can be shown [13] that the 9d Riemannian manifold Y_9 is equipped with a unit norm Killing vector field ξ , now called the R-symmetry vector,⁹ whose dual one-form we call η . The metric on Y_9 is adapted to the corresponding foliation \mathcal{F}_ξ , taking the form

$$ds_{Y_9}^2 = \eta^2 + e^B ds_{\text{8d}}^2(J). \quad (3.12)$$

⁹The reason we used the same symbol to denote the R-symmetry vector and the Reeb vector in section 3.1 will become clear momentarily.

Here $ds_{8d}^2(J)$ is the 8d transverse metric, which is Kähler with Kähler two-form J , Ricci two-form $\varrho = dP$, and a positive Ricci scalar $R > 0$. Note that in local coordinates we may write

$$\xi = \partial_z, \quad \eta = dz + P, \quad (3.13)$$

so that $d\eta = \varrho$. The transverse Kähler form J fully determines this class of geometries as

$$e^B = \frac{R}{2}, \quad F = -J + d(e^{-B}\eta). \quad (3.14)$$

The cone $C(Y_9)$, with metric $ds_{C(Y_9)}^2 = dr^2 + r^2 ds_{Y_9}^2$, has a canonically defined integrable complex structure and it admits a closed nowhere-vanishing holomorphic $(5,0)$ -form $\Psi_{(5,0)}$, hence it is a Calabi-Yau in this sense [13]. Furthermore, $\Psi_{(5,0)}$ has definite charge under the $U(1)$ action generated by ξ :

$$\mathcal{L}_\xi \Psi_{(5,0)} = i\Psi_{(5,0)}. \quad (3.15)$$

The geometries described are supersymmetric and satisfy the 11d equations of motion provided that the transverse Kähler metric satisfies the equation

$$\square R = \frac{1}{2} R^2 - R_{ab}R^{ab}, \quad (3.16)$$

where R_{ab} is the Ricci tensor and \square the Laplacian. However, we will again go “off-shell” following [8] and we will not impose the PDE (3.16) on the Kähler two-form. Instead we will follow an alternative approach, which is the analogue of the constrained extremization mentioned at the end of section 3.1. This consists of two steps: rather than imposing (3.16), one instead imposes its *integral* over Y_9 to hold, namely

$$\int_{Y_9} \eta \wedge \varrho^2 \wedge \frac{J^2}{2} = 0. \quad (3.17)$$

It then makes sense to impose the flux quantization conditions (3.11), which read

$$\int_{\Sigma_{\Upsilon}} \eta \wedge \varrho \wedge \frac{J^2}{2} = (2\pi\ell_p)^6 \mathcal{N}_{\Upsilon}. \quad (3.18)$$

It can be proved that these integrals depend only on the (basic) cohomology classes of J and ϱ . The second step then involves varying the *supersymmetric action*

$$S_{\text{SUSY}}(\xi, [J]) = \int_{Y_9} \eta \wedge \varrho \wedge \frac{J^3}{3!}, \quad (3.19)$$

subject to the constraints (3.18) and (3.17). Solving these for the cohomology class of J , the result is a function depending on the R-symmetry vector ξ only, which is the

analogue of (3.8) in the AdS₄ case. This function is proportional to the “trial entropy” of the black hole

$$\mathcal{S} = \frac{4\pi}{(2\pi)^8 \ell_p^9} S_{\text{SUSY}} . \quad (3.20)$$

Extremizing \mathcal{S} over the R-symmetry vector ξ and imposing its positivity yields the on-shell entropy.

3.2.2 Fibered Y_9

As anticipated we want to put a black hole in the AdS₄ background and study its near-horizon limit. This amounts to consider AdS₂ \times Y_9 backgrounds as in (3.9) where Y_9 takes the fibered form

$$Y_7 \hookrightarrow Y_9 \rightarrow \Sigma_g , \quad (3.21)$$

where Y_7 is a manifold as in (3.2) with an *a priori* generic Kähler two-form ω instead of the Sasakian one. The R-symmetry vector ξ is assumed to be tangent to Y_7 , hence it can be parametrized in the same way as the Reeb vector of the fibre (3.5). Physically the fibration (3.21) may be achieved by turning on s $U(1)$ gauge fields A_i supported on Σ_g with integer magnetic fluxes

$$\frac{1}{2\pi} \int_{\Sigma_g} dA_i = p_i \in \mathbb{Z} , \quad (3.22)$$

which are nothing but the magnetic charges of the black hole. Mathematically, this amounts to constructing a principal $U(1)^s$ bundle over Σ_g with Chern numbers p_i . The holomorphic (5,0)-form $\Psi_{(5,0)}$ is obtained as a wedge product of the canonical (1,0)-form on Σ_g and the (4,0)-form $\Psi_{(4,0)}$, and differently from the AdS₄ case it has charge 1 under the $U(1)$ action generated by ξ , hence $b_1 = 1$. In order for $\Psi_{(5,0)}$ to be globally well-defined form, in our basis we need to set $p_1 = 2g - 2$ [37]. In the following we will refer to the integers p_i as *flavour twisting parameters*.

Denoting ψ_7 as the one-form such that locally $\omega = d\psi_7$, concretely the fibration amounts to replace

$$\eta_7 \rightarrow \eta_7^t \equiv \eta_7 \Big|_{d\varphi_i \rightarrow d\varphi_i + A_i} , \quad (3.23)$$

$$\psi_7 \rightarrow \psi_7^t \equiv \psi_7 \Big|_{d\varphi_i \rightarrow d\varphi_i + A_i} \quad (3.24)$$

where the superscript t stands for “twisted”. Then one can show that for Y_9 as in

(3.21) we have

$$\eta = \eta_7^t + \text{basic} , \quad (3.25)$$

$$J = d\psi_7^t + A \text{vol}_{\Sigma_g} + \text{basic exact} , \quad (3.26)$$

where we take the normalization to be $\int_{\Sigma_g} \text{vol}_{\Sigma_g} = 1$, A is parametrizing the Kähler class of the Riemann surface, and “basic” here is with respect to the R-symmetry foliation \mathcal{F}_ξ . Note that the equation $d\eta = \varrho$ at the cohomology level becomes

$$[d\eta_7^t] = [\varrho] \in H_B^2(\mathcal{F}_\xi) . \quad (3.27)$$

To summarize: we started from a manifold Y_7 with $U(1)^s$ isometry, within which we picked an R-symmetry vector field ξ , parametrized in terms of b_i as in (3.5). Then we built the fibration (3.21) specified by some twisting parameters $p_i \in \mathbb{Z}$. The resulting manifold is a foliation defined by the above choice of ξ , which furthermore depends on the Kähler form of the transverse metric (3.26), which is unspecified up to this point.

3.2.3 Flavour twist

As discussed in the introduction, in the remainder of the paper we will be interested in the so called “flavour twist”, which amounts to imposing that the Kähler class of the fibre is proportional to its Ricci form class, *i.e.*

$$[\omega] = \Lambda [\varrho_7] . \quad (3.28)$$

The full Kähler class $[J]$ is then parameterized by two parameters only: A and Λ . This is the case which is under control from the holographic perspective, where a holographic matching of the free energy has been achieved [9, 10]. Note that for manifolds Y_7 with no baryonic symmetries, *i.e.* $H^2(Y_7, \mathbb{R}) = 0$ (such as S^7 and \mathbb{Z}_k quotients thereof, as in our main examples), the condition (3.28) is automatically true.

With this assumption, the geometric extremization procedure summarized in section 3.2.1 simplifies, but we will not go through the steps here.¹⁰ In the present work all we will need is an expression for the Kähler class parameter Λ which can be obtained by picking the 7-cycle given by the fibre Y_7 itself in (3.18). Indeed, the resulting flux is equivalent to (1.1) and gives the number of M2-branes N , and it is quadratic in Λ

$$\frac{\Lambda^2}{2} \int_{Y_7} \eta_7 \wedge \varrho_7^3 = (2\pi\ell_p)^6 N . \quad (3.29)$$

¹⁰See [10] (and note that what we call “flavour twist” is dubbed “mesonic twist” in [10]).

Now note that the integral at the left hand side is proportional to the Sasakian volume of Y_7

$$\text{Vol}_S(Y_7) = \frac{1}{(2b_1)^3} \int_{Y_7} \eta_7 \wedge \frac{\varrho_7^3}{3!}, \quad (3.30)$$

hence we can solve (3.29) to obtain¹¹

$$\Lambda = \frac{(2\pi\ell_p)^3}{\sqrt{24b_1^3 \text{Vol}_S(Y_7)}} N^{1/2}. \quad (3.31)$$

Then the remaining equations in (3.17) and (3.18) fix A , and put constraints on the remaining quantized fluxes \mathcal{N}_Υ in terms of the R-symmetry vector b_i and the flavour twisting parameters p_i , and eventually one obtains the trial black hole entropy with a flavour twist

$$\mathcal{S}[\xi] = 4 \sum_{i=1}^s p_i \frac{\partial}{\partial b_i} F_{\text{grav}}[\xi] \Big|_{b_1=1}, \quad (3.32)$$

where $F_{\text{grav}}[\xi]$ is the trial free energy (3.8) of the vacuum AdS₄ solution we started with.¹²

It is useful to introduce further observables: the geometric R-charges. These are integrals associated to 5d $U(1)^s$ -invariant supersymmetric submanifolds in the fibres $S_a \subset Y_7$ and they are dual to the R-charges of baryonic operators associated with M5-branes wrapping them. In particular, they are defined as

$$R_a \equiv \frac{1}{N} \frac{4\pi}{(2\pi\ell_p)^6} \int_{S_a} \eta_7 \wedge \frac{\omega^2}{2}. \quad (3.33)$$

Analogously to what we did above, we can introduce the Sasakian volume of these submanifolds as

$$\text{Vol}_S(S_a) = \frac{1}{(2b_1)^2} \int_{S_a} \eta_7 \wedge \frac{\varrho_7^2}{2}, \quad (3.34)$$

so that in the flavour twist case the geometric R-charges reduce to the ratio between Sasakian volumes

$$R_a = \frac{2\pi}{3b_1} \frac{\text{Vol}_S(S_a)}{\text{Vol}_S(Y_7)}, \quad (3.35)$$

with $R_a > 0$ [15].

Finally, other relevant quantities associated to these submanifolds are the quantized fluxes M_a that are obtained by considering the integral in (3.18) on fibrations $S_a \hookrightarrow \Sigma_a \rightarrow \Sigma_g$. Note that these are different from the \mathcal{N}_Υ in (3.18) and in general they are

¹¹A thorough discussion of the choice of sign in taking the square root is given in [15].

¹²Note that the free energy appearing in (3.32) is intended to be before setting $b_1 = 4$.

non-vanishing even if $H_5(Y_7, \mathbb{R}) = 0$ (see [15] for more details on this). For the flavour twist they are related to the geometric R-charges R_a by

$$M_a = \frac{N}{2} \sum_{i=1}^4 p_i \frac{\partial}{\partial b_i} (b_1 R_a). \quad (3.36)$$

3.3 Example: $Y_7 = S^7$

In this section we illustrate the simplest example of the above geometry, corresponding to the fibre being a 7-sphere.

The cone $X_4 = C(S^7)$ in this case is simply \mathbb{C}^4 , hence we can introduce four complex coordinates $z_a = |z_a| e^{i\phi_a}$, $a = 1, 2, 3, 4$, with ϕ_a having period 2π . The holomorphic form $\Psi_{(4,0)}$ is the standard one on \mathbb{C}^4

$$\Psi_{(4,0)} = dz_1 \wedge dz_2 \wedge dz_3 \wedge dz_4. \quad (3.37)$$

The standard Kähler form for the flat metric on \mathbb{C}^4 is

$$\mathcal{J} = \frac{i}{2} \sum_{a=1}^4 dz_a \wedge d\bar{z}_a = \sum_{a=1}^4 d\left(\frac{1}{2}|z_a|^2\right) \wedge d\phi_a = \sum_{a=1}^4 dy_a \wedge d\phi_a, \quad (3.38)$$

where in the last step we introduced the coordinates $y_a = \frac{1}{2}|z_a|^2 \geq 0$. Note that the last form in (3.38) is still valid when we lift the Einstein condition on \mathbb{C}^4 , though the coordinates y_a are defined differently.

The number of independent $U(1)$ isometries is clearly $s = 4$, hence there has to exist a linear change of variables relating the vector fields ∂_{ϕ_a} rotating the coordinates z_a with weight one with the general basis introduced in (3.5)

$$\partial_{\phi_a} = \sum_{i=1}^4 v_{ai} \partial_{\varphi_i}, \quad (3.39)$$

where v_{ai} are 16 constants. Recalling that we require $\Psi_{(4,0)}$ to have charge one under ∂_{φ_1} and to be uncharged under the remaining ∂_{φ_i} we can read off

$$v_1 = (1, 0, 0, 0), \quad v_2 = (1, 1, 0, 0), \quad v_3 = (1, 0, 1, 0), \quad v_4 = (1, 0, 0, 1). \quad (3.40)$$

The Sasakian volume as a function of the R-symmetry vector is given by

$$\text{Vol}_S(S^7) = \frac{\pi^4}{3b_2 b_3 b_4 (b_1 - b_2 - b_3 - b_4)}. \quad (3.41)$$

Setting $z_a = 0$ selects a copy of $\mathbb{C}^3 \subset \mathbb{C}^4$ which is the cone over the submanifold S_a . The corresponding Sasakian volumes are given by

$$\text{Vol}_S(S_1) = \frac{\pi^3}{b_2 b_3 b_4}, \quad \text{Vol}_S(S_a) = \frac{\pi^3 b_a}{b_2 b_3 b_4 (b_1 - b_2 - b_3 - b_4)}, \quad a = 2, 3, 4. \quad (3.42)$$

From the quantities above we can directly read off the final results for the gravitational free energy of the AdS₄ solution (3.8), and the black hole entropy (3.32), the geometric R-charges (3.35), and the fluxes (3.36) through the submanifolds $\Sigma_a \subset Y_9$ of the AdS₂ solution:

$$\begin{aligned} F_{\text{grav}} &= \frac{\pi}{3} \sqrt{2b_2 b_3 b_4 (b_1 - b_2 - b_3 - b_4)} N^{3/2}, \\ \mathcal{S} &= \frac{4\pi}{3} N^{3/2} \sum_{i=1}^4 p_i \frac{\partial}{\partial b_i} \sqrt{2b_2 b_3 b_4 (b_1 - b_2 - b_3 - b_4)}, \\ R_1 &= \frac{2}{b_1} (b_1 - b_2 - b_3 - b_4), \quad R_a = \frac{2b_a}{b_1}, \quad a = 2, 3, 4, \\ M_1 &= N(p_1 - p_2 - p_3 - p_4), \quad M_a = N p_a, \quad a = 2, 3, 4. \end{aligned} \quad (3.43)$$

One should then set $b_1 = 1$ and extremize \mathcal{S} in order to obtain the on-shell quantities. Note that we have

$$\sum_{a=1}^4 R_a = 2, \quad \sum_{a=1}^4 M_a = (2g - 2)N. \quad (3.44)$$

It is also convenient to give an expression for the R-symmetry vector in terms of the original basis ∂_{ϕ_a} . One may check that

$$\xi = \frac{b_1}{2} \sum_{a=1}^4 R_a \partial_{\phi_a}. \quad (3.45)$$

Using this expression to compute $\xi \lrcorner \mathcal{J}$ with both (3.38) and (3.3) we find that the radius in the coordinates $\{y_a\}$ is

$$r^2 = \sum_{a=1}^4 R_a y_a. \quad (3.46)$$

Later we will be interested in \mathbb{Z}_k quotients of the 7-sphere. This will be reviewed for the two main models of interest in section 4.1. However, at the level of the various quantities obtained via integration introduced above, the quotient simply amounts to

adding a factor of $k \in \mathbb{Z}$ in the denominator of the volumes (3.41) and (3.42). Moreover, for later purposes it is useful to invert the relations (3.43) and express F_{grav} and \mathcal{S} in terms of the geometric R-charges, so that eventually we have

$$F_{\text{grav}} = \frac{4\pi}{3} \sqrt{2kR_1R_2R_3R_4} N^{3/2}, \quad (3.47)$$

$$\mathcal{S} = \frac{\pi}{3} \sqrt{2kR_1R_2R_3R_4} \sum_{a=1}^4 \frac{(M_a/N)}{R_a} N^{3/2}, \quad (3.48)$$

where we have already set $b_1 = 4$ in the former and $b_1 = 1$ in the latter. Finally, let us also give an expression for the Kähler class parameter (3.31) in the flavour twist as we will need it many times later

$$\Lambda = \frac{\pi \ell_p^3 N^{1/2}}{2} \sqrt{2kR_1R_2R_3R_4}. \quad (3.49)$$

4 Matrix model geometry

The topologically twisted matrix models described in section 2 are dual to the black hole near-horizon geometries presented in section 3. In this section we make a precise identification of various quantities on both sides of this duality. We start in section 4.1 by reviewing the matching between chemical potentials and R-charges, and the free energy with the entropy. In section 4.2 then we introduce the M-theory Hamiltonian function, which allows us to give a further geometrical interpretation of the matrix model, or more particularly its eigenvalue density discussed in section 4.3. The relation to probe M2-branes wrapping the M-theory circle, and their Wilson loop duals, is described in section 4.4. Along the way we describe the general matching for any Calabi-Yau four-fold cone X_4 , but illustrate with our two main examples where $X_4 = \mathbb{C}^4/\mathbb{Z}_k$; further examples are discussed in section 6.

4.1 Holography of free energies and R-charges

As already discussed in section 2.1.3, given any M-theory solution we may in principle make different choices of M-theory circle $U(1) \equiv U(1)_M$ acting on the spacetime, and reduce in different ways to type IIA. Starting with a given $\text{AdS}_2 \times Y_9$ background, with Y_9 a fibration of Y_7 over Σ_g as introduced in the previous section, different choices of M-theory circle acting on Y_7 lead to different Chern-Simons-matter theories on $\Sigma_g \times S^1$. Our principal examples of this are Models I and II, which are dual to M-theory

geometries with $Y_7 = S^7/\mathbb{Z}_k$ and $U(1)_M$ actions given in (2.8) and (2.11) respectively, where the \mathbb{Z}_k quotient is taken along the corresponding M-theory circle.

Having fixed a particular GK geometry and choice of M-theory circle, and hence a choice of UV field theory on $\Sigma_g \times S^1$, we would like to identify variables on each side of the duality. From a geometric engineering point of view, baryonic operators arise from M5-branes wrapping five-dimensional submanifolds $S_A \subset Y_7$. The R-charge of the corresponding field is then given in term of the Sasakian volume of S_A in the same way we defined the geometrical R-charges in (3.35);¹³ this was first studied in the D3-brane holographic context in [38]. Moreover, recalling the identification between chemical potentials and R-charges, we get the following chain of identifications

$$\Delta_A = \Delta_A^{S^3} = R_A. \quad (4.1)$$

Here A labels any field of the theory, including monopole operators whose chemical potentials are only formally defined. Similarly, the field theory fluxes \mathbf{n}_A through Σ_g are related in the same way to the geometrical fluxes:

$$\mathbf{n}_A = \frac{M(S_A)}{N}, \quad (4.2)$$

where $M(S_A)$ is the quantized flux through $S_A \hookrightarrow \Sigma_A \rightarrow \Sigma_g$, which is computed via (3.36).

Let us illustrate this for our two models:

Model I: The identifications (2.7) give the relation between the fields in this model and the divisors on $\mathbb{C}^4/\mathbb{Z}_k$. In this case, the submanifolds S_A directly correspond to (multiples of) S_a (recall the latter are defined by $\{z_a = 0\}$). Substituting this into (4.1) gives the identifications

$$\Delta_T = kR_1, \quad \Delta_{\bar{T}} = kR_2, \quad \Delta_{\Phi_1} = R_3, \quad \Delta_{\Phi_2} = R_4, \quad (4.3)$$

$$\mathbf{n}_T = k \frac{M_1}{N}, \quad \mathbf{n}_{\bar{T}} = k \frac{M_2}{N}, \quad \mathbf{n}_{\Phi_1} = \frac{M_3}{N}, \quad \mathbf{n}_{\Phi_2} = \frac{M_4}{N}. \quad (4.4)$$

Model II: We may again use (4.1) together with the identifications (2.10) to deduce the mapping

$$\Delta_{A_1} = R_1, \quad \Delta_{B_1} = R_2, \quad \Delta_{A_2} = R_3, \quad \Delta_{B_2} = R_4, \quad (4.5)$$

¹³The distinction between S_A and S_a is purely motivated by the fact that in some examples the choice we make in gravity for the latter submanifolds does not directly correspond to the S_A associated to physical operators but rather to linear combinations thereof. Correspondingly, the same will be true for any associated quantity *e.g.* R_A vs R_a .

$$\mathbf{n}_{A_1} = \frac{M_1}{N}, \quad \mathbf{n}_{B_1} = \frac{M_2}{N}, \quad \mathbf{n}_{A_2} = \frac{M_3}{N}, \quad \mathbf{n}_{B_2} = \frac{M_4}{N}. \quad (4.6)$$

Having made these identifications allows one to then match other physical quantities on both sides of the correspondence. In particular minus the free energy of the field theory on $\Sigma_g \times S^1$ reproduces the entropy \mathcal{S} :

$$\log Z_{\Sigma_g \times S^1}[\Delta, \mathbf{n}] = \mathcal{S}[R, M]. \quad (4.7)$$

The matching (4.7) has been verified in multiple examples [2, 9, 10], and is particularly straightforward to see in our main examples. For Model I, using the dictionary (4.3)–(4.4), $\log Z$ in (2.36) matches the entropy (3.48) on S^7 . Likewise for Model II, the dictionary (4.5)–(4.6) relates (2.38) with (3.48). In a similar fashion, a well-known matching is that of the free energy on S^3 with F_{grav} , which can be observed explicitly for both models as (2.39) and (2.37) match with (3.47). Interestingly F_{S^3} and F_{grav} are proportional to μ and Λ respectively, such that a direct consequence of their matching is

$$\Lambda = \frac{\ell^3 N^{1/2}}{2} \mu, \quad (4.8)$$

which is indeed what we observe by comparing (3.49) with (2.29) and (2.33).

4.2 M-theory circle moment map

Our aim in this section is to provide a geometric interpretation of the matrix model described in section 2.2.3, or more precisely the large N saddle point distribution. To this end, we would first like to identify the variable t from a geometric perspective in M-theory.

Recall that, in the large N limit, the variable t corresponds to the continuum limit of the imaginary parts of the eigenvalues in (2.21). On the other hand, before taking the large N limit the eigenvalues t^α , $\alpha = 1, \dots, N$, are simply defined as the values of the scalars σ^α (up to an overall proportionality constant). Physically the VEVs of the scalars σ^α also parametrize the position of the N D2-branes in the \mathbb{R}_t direction, as described in section 2.1.2. Via this chain of identifications, it is natural to conclude that the matrix model variable t , for the large N eigenvalue distribution, should be related to the coordinate parametrizing \mathbb{R}_t in the type IIA construction. The aim of the rest of this section will be to make this statement precise.

Let us start by considering the uplifted geometry in M-theory without the branes' backreaction. Recall from section 2.1.3 that the Killing vector ζ_M by definition gener-

ates the $U(1)_M$ isometry of the M-theory circle action. This $U(1)_M$ action is Hamiltonian on X_4 , namely there exists a function $\mu_M: X_4 \rightarrow \mathbb{R}$, called the moment map, such that

$$d\mu_M = -\zeta_M \lrcorner \mathcal{J}, \quad (4.9)$$

where \mathcal{J} is the original Kähler form on X_4 . The crucial point is that the image of μ_M is precisely identified with the \mathbb{R}_t direction. In fact, from a physical perspective, the D-term equations that fix the VEVs of σ^α (*i.e.* the position of the M2-branes along \mathbb{R}_t), correspond geometrically to fixing level sets of the moment map [32]!

Let us illustrate this in the two examples with $X_4 = \mathbb{C}^4/\mathbb{Z}_k$. We will focus on the Abelian case ($N = 1$), where note that the Kähler form is given in (3.38).

Model I: From (2.8) we recall that the M-theory circle is given by $\zeta_M^I = \frac{1}{k}(\partial_{\phi_1} - \partial_{\phi_2})$. Hence, using the definition (4.9), the moment map in this case is simply

$$\mu_M^I(z_a) = \frac{1}{2k} (|z_1|^2 - |z_2|^2). \quad (4.10)$$

On the other hand the D-term equation for $k = 1$ reads [27]

$$|T|^2 - |\tilde{T}|^2 = \frac{\sigma}{2\pi}, \quad (4.11)$$

and hence from the identifications in (2.7) we can see that the D-term equation for $k = 1$ can be expressed as¹⁴

$$\mu_M^I(z_a) = \frac{\sigma}{\pi}. \quad (4.12)$$

Model II: Here, the M-theory circle is in (2.11) and reads $\zeta_M^{II} = \frac{1}{k}(\partial_{\phi_1} - \partial_{\phi_2} + \partial_{\phi_3} - \partial_{\phi_4})$. From (4.9) we then read the moment map

$$\mu_M^{II}(z_a) = \frac{1}{2k} (|z_1|^2 - |z_2|^2 + |z_3|^2 - |z_4|^2). \quad (4.13)$$

The D-term equation for this theory is [31]

$$\frac{1}{k} (|A_1|^2 - |B_1|^2 + |A_2|^2 - |B_2|^2) = \frac{\sigma}{2\pi}. \quad (4.14)$$

From the identifications (2.10) it follows that the D-term equation is again

$$\mu_M^{II}(z_a) = \frac{\sigma}{\pi}. \quad (4.15)$$

¹⁴Recall that $\mathbb{C}^2/\mathbb{Z}_k \subset \mathbb{C}^4/\mathbb{Z}_k = X_4$ is realized via the embedded equation $T\tilde{T} = \Phi_3^k$ in \mathbb{C}^3 (2.6). This means that for $k > 1$ we cannot identify T, \tilde{T} with the coordinates z_1, z_2 on the covering space \mathbb{C}^2 of $\mathbb{C}^2/\mathbb{Z}_k$, and correspondingly the classical metric on the field theory moduli space is different from the spacetime metric. However, these comments are only meant to motivate the precise identifications later.

Our claim is that this picture is “preserved”, in a sense that we will specify momentarily, when taking the large N limit in field theory and the near-horizon limit in gravity.

As explained in section 2.2.3, in field theory the eigenvalues u_I^α in the large N limit become infinite in number, and continuously distributed, with their imaginary part parametrized by the real variable t which takes values in a finite interval $[t_{\min}, t_{\max}]$. Moreover, this interval is divided into a certain number of subintervals, on each of which the eigenvalue density $\rho(t)$ is linear; in particular $\rho'(t)$ is discontinuous at the endpoints of each subinterval. The gravity duals are described by the $\text{AdS}_2 \times Y_9$ backgrounds in M-theory described in section 3.2. In this context, the $U(1)_M$ action on the fibre Y_7 is still Hamiltonian, and hence we can define the moment map h_M (now regarded as a function on Y_7) via

$$dh_M = -\zeta_M \lrcorner \omega . \quad (4.16)$$

Recall here that ω is the transverse Kähler form on Y_7 , and in the flavour twist case this is given by (3.28). From (3.3) and the fact that $d\eta_7 = \varrho_7$ it follows that, for the flavour twist case

$$h_M = 2\Lambda \mu_M \Big|_{r=1} = \Lambda \zeta_M \lrcorner \eta_7 , \quad (4.17)$$

where μ_M is the moment map on the cone X_4 introduced above in (4.9). Since h_M is a continuous real function defined on a compact space, its image is an interval

$$h_M(Y_7) = [\tau_{\min}, \tau_{\max}] \subset \mathbb{R} . \quad (4.18)$$

The function h_M is defined on Y_7 , rather than directly on a Kähler manifold (which is instead here a transverse Kähler structure), but nevertheless it is straightforward to import some standard results from the symplectic geometry literature (see *e.g.* [39]). Similar reasoning was used in [21]. First, the interval in (4.18) is divided into subintervals whose boundaries are given by the images of the critical points of the moment map, so $\{dh_M = 0\}$. In turn these are precisely the loci where ζ_M is aligned with the Reeb vector field ξ , so that along such a locus $\zeta_M \lrcorner \eta_7$ is a constant. This includes the special case where ζ_M is zero, which are fixed point sets signalling the presence of D6-branes. We shall return to what distinguishes these subintervals geometrically in the next subsection, while the relation of these points with physical observables will be discussed in section 4.4.

We conclude that there must be a holographic map between the field theory variable t and the geometry variable τ parametrizing the image of the moment map. In particular,

from the examples we are going to consider shortly and later in section 6, we find the precise identification is

$$\tau = \ell_p^3 N^{1/2} t. \quad (4.19)$$

Let us once again illustrate how this works concretely for the examples with $X_4 = \mathbb{C}^4/\mathbb{Z}_k$ i.e. $Y_7 = S^7/\mathbb{Z}_k$. Recall the radial coordinate on the cone is given by (3.46)

$$r^2 = \sum_{a=1}^4 R_a y_a, \quad (4.20)$$

with $y_a \geq 0$. Note that when $R_a = \frac{1}{2}$ for all $a = 1, 2, 3, 4$ we recover the usual radius for a round 7-sphere. Setting $r^2 = 1$ constrains the possible values of y_a , in particular

$$0 \leq y_a \leq \frac{1}{R_a}. \quad (4.21)$$

Model I: The moment map on S^7/\mathbb{Z}_k is given by

$$h_M^I = \frac{2\Lambda}{k} (y_1 - y_2) \Big|_{r^2=1}, \quad (4.22)$$

whose image is clearly

$$h_M^I(S^7/\mathbb{Z}_k) = \left[-\frac{2\Lambda}{kR_2}, \frac{2\Lambda}{kR_1} \right]. \quad (4.23)$$

Using (3.49) for the Kähler class parameter, this precisely maps to the interval $[t_{\min}, t_{\max}]$ with extrema (2.28) via (4.19) and the identification among the R-charges (4.3). Moreover, the only other fixed point locus of the $U(1)_M$ action on S^7/\mathbb{Z}_k is $\{z_1 = z_2 = 0\}$ which reproduces the point $t = 0$, arising from the D6-brane insertion.

Model II: Here we solve the constraint $r^2 = 1$ for one of the coordinates and substitute it back into the moment map. In order to obtain τ_{\min} it is convenient to solve for y_4 , so that

$$h_M^{\text{II}}(y_a) = \frac{2\Lambda}{k} \left[\left(1 + \frac{R_1}{R_4}\right) y_1 - \left(1 - \frac{R_2}{R_4}\right) y_2 + \left(1 + \frac{R_3}{R_4}\right) y_3 - \frac{1}{R_4} \right]. \quad (4.24)$$

In field theory we assumed a particular ordering for the chemical potentials which must be mirrored here: $R_1 \leq R_3$ and $R_2 \leq R_4$. As a consequence the coefficient of y_2 in the expression above is negative, and it is then clear that the minimum of $h_M^{\text{II}}(y_a)$ is achieved when

$$y_1 = y_3 = 0, \quad y_2 = \frac{1}{R_2} \quad \Longrightarrow \quad \tau_1 \equiv \tau_{\min} = -\frac{2\Lambda}{kR_2}. \quad (4.25)$$

Similarly, solving for y_3 it is easy to obtain the maximum

$$\tau_4 \equiv \tau_{\max} = \frac{2\Lambda}{kR_1}. \quad (4.26)$$

Notice that, as explained in general above, τ_{\min} and τ_{\max} are images of loci where ζ_M is aligned with the R-symmetry vector ξ , specifically here where $\{z_1 = z_3 = z_4 = 0\}$ and $\{z_2 = z_3 = z_4 = 0\}$. Indeed, there are other two such loci/image points:

$$\{z_1 = z_2 = z_3 = 0\} \implies \tau_2 = -\frac{2\Lambda}{kR_4}, \quad (4.27)$$

$$\{z_1 = z_2 = z_4 = 0\} \implies \tau_3 = \frac{2\Lambda}{kR_3}. \quad (4.28)$$

By virtue of (4.8), (4.5), and (4.19), $\tau_1, \tau_2, \tau_3, \tau_4$ are precisely matched with (2.32).

To conclude this section, let us notice that here neither the 3d space where the field theory lives, nor the fact that Y_7 is fibered over Σ_g , played a crucial role. Therefore, everything we have said holds, with minor adjustments, for both 3d theories localized on S^3 and on $\Sigma_g \times S^1$.

4.3 Eigenvalue density from geometry

In the previous section we identified the variable t in field theory as the value of the moment map associated to the M-theory circle action. We can actually do better and provide a prescription to compute the full eigenvalue density function of the matrix model $\rho(t)$ from the geometry of the near-horizon dual. Despite focusing on the $\text{AdS}_2 \times Y_9$ geometries, applying our approach to $\text{AdS}_4 \times Y_7$ is rather straightforward. Note that for a certain set of the latter geometries with toric Y_7 some results concerning this very same matter were already found in the past – see appendix C of [23] and section 3.6 of [21]. However, here we will give a much more complete picture which works off-shell and in principle also for non-toric Y_7 , and more specifically also for the near-horizon black hole GK geometries.

We start by using the moment map h_M defined in (4.17) to build a 5d space out of the fibre Y_7 , by restricting to the level set $h_M^{-1}(\tau) \subset Y_7$ and then quotienting by the M-theory circle action

$$Y_\tau \equiv h_M^{-1}(\tau)/U(1)_M. \quad (4.29)$$

In the special case when Y_7 is quasi-regular, namely that $b_i \in \mathbb{Q}$ for all $i = 1, \dots, s$, so that the orbits of the R-symmetry vector close, Y_τ has a particular structure which derives from the following mathematical construction. We first introduce the 6d Kähler base space K_6 obtained by quotienting

$$K_6 \equiv Y_7/U(1)_\xi . \quad (4.30)$$

Note that this quotient would be very badly behaved if we did not assume $b_i \in \mathbb{Q}$, because the generic orbits of ξ would then be open. In passing, let us highlight that the critical points of h_M which delimit the subintervals in the image $h_M(Y_7)$ correspond precisely to the fixed points of the $U(1)_M$ action on K_6 ; indeed these are either fixed points on Y_7 itself, which are related to D6-brane insertions, or points where ζ_M is aligned with ξ in the ambient space Y_7 , as in such a situation the former projects to zero in the quotient above.

Given that the moment map h_M is independent of ξ , it can be thought as a function on K_6 . We can then consider introducing a 4d subspace $K_\tau \subset K_6$ as a symplectic quotient with Fayet-Iliopoulos parameter τ

$$K_\tau \equiv K_6//U(1)_M , \quad (4.31)$$

and by construction K_τ is itself a Kähler space with a Kähler form ω_τ that is inherited from the original ω on K_6 . Finally, we restore the $U(1)_\xi$ direction by building the fibration

$$S^1_\xi \hookrightarrow Y_\tau \rightarrow K_\tau . \quad (4.32)$$

The induced Kähler class $[\omega_\tau]$ depends linearly on τ , with a different slope in each of the subintervals in the image of h_M delimited by the $U(1)_M$ fixed points [39]; therefore it is quite natural to relate it with $\rho(t)$. Our precise claim is that

$$\rho(t) \propto \frac{d}{d\Lambda} \int_{Y_\tau} \eta \wedge \frac{\omega_\tau^2}{2} \Big|_{\tau=\ell_p^3 N^{1/2} t} = \frac{d}{d\Lambda} \text{Vol}(Y_\tau) \Big|_{\tau=\ell_p^3 N^{1/2} t} . \quad (4.33)$$

The normalization constant is then fixed by requiring $\rho(t)$ to integrate to 1. Finally, in order for the construction above to make sense even when Y_7 is irregular ($b_i \notin \mathbb{Q}$), we note that $\text{Vol}(Y_\tau)$ depends continuously on the R-symmetry vector b_i , hence its expression can be extended to the general case by continuity.

Next, we will illustrate the above in the two examples with $Y_7 = S^7/\mathbb{Z}_k$, but first let us comment on how to go about computing the volume $\text{Vol}(Y_\tau)$. For toric Y_7 it is quite

straightforward and we will provide a general recipe later in section 6. In general, without further assumptions on the geometry of Y_τ , it may be difficult to produce closed form expressions. We envisage that an approach based on a fixed point formula, such as that in [40], could however be effective.

For $Y_\tau = S^7/\mathbb{Z}_k$ we use the coordinates $\{y_a, \phi_a\}$ introduced in section 3.3. Modulo angles, the space Y_τ is described by imposing both $r^2 = 1$ and $h_M(y_a) = \tau$ which result in the two linear equations describing hyperplanes in \mathbb{R}^4 . Recalling that r^2 is given by (4.20) and that $y_a \geq 0$, the former equation actually defines a tetrahedron with vertices

$$p_a = \frac{1}{R_a} e_a, \quad (4.34)$$

where e_a is the standard orthonormal basis on \mathbb{R}^4 . Imposing the moment map level set equation then amounts to slicing this tetrahedron with a hyperplane. The intersection of the two will be a 2d polygon Q_τ , particularly either a triangle or a quadrilateral. For the flavour twist, by definition the following cohomological relation holds

$$[\omega] = \Lambda[d\eta_\tau] = 2\Lambda[\omega_S]. \quad (4.35)$$

From (3.38) one can see that the measure induced via ω_S is simply the standard Euclidean measure on \mathbb{R}^4 (times a factor k^{-1} which comes from the \mathbb{Z}_k quotient), and correspondingly ω induces $(2\Lambda)^4$ times the Euclidean volume form. It follows that

$$\text{Vol}(Y_\tau) = \frac{(2\pi)^3}{k} (2\Lambda)^2 \text{Vol}_E(Q_\tau), \quad (4.36)$$

where Vol_E denotes the Euclidean volume, and the factor $(2\pi)^3$ comes from integrating over the angles.

Let us also introduce a notation for the vectors orthogonal to the two hyperplanes, which are nothing but ξ and ζ_M in coordinates. The former is

$$\xi = \frac{1}{2} (R_1, R_2, R_3, R_4), \quad (4.37)$$

while the latter will depend upon the model we are considering and we will denote it by ζ . It will also be useful to introduce a name for the component of ζ orthogonal to ξ , namely

$$\zeta_\perp \equiv \zeta - \frac{\zeta \cdot \xi}{|\xi|^2} \xi. \quad (4.38)$$

In both Model I and Model II, it turns out the properly normalized $\rho(t)$ is given in gravity by

$$\rho(t) = \frac{1}{32\pi^5 \ell_p^3 N^{1/2} |\xi| |\zeta_\perp|} \frac{d}{d\Lambda} \text{Vol}(Y_\tau) \Big|_{\tau = \ell_p^3 N^{1/2} t}. \quad (4.39)$$

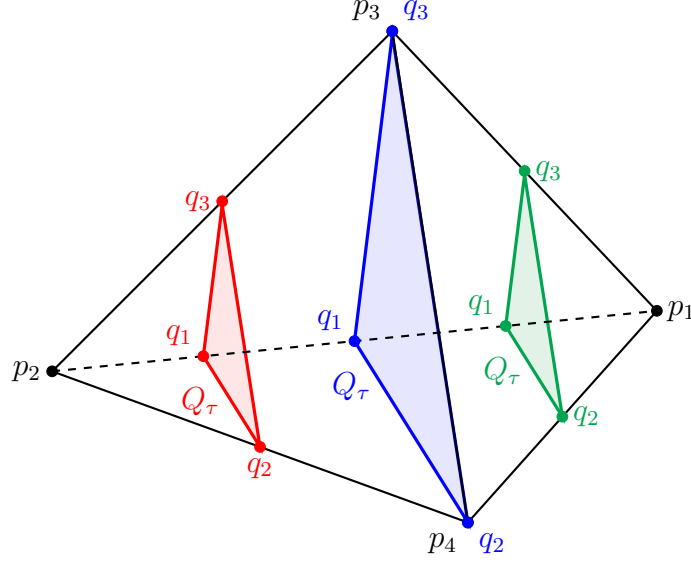


Figure 5: Tetrahedron describing S^7 and its slicing corresponding to Model I – ADHM theory. The red slice is for $\tau_{\min} < \tau < 0$, blue slice for $\tau = 0$, and green slice for $0 < \tau < \tau_{\max}$. The perimeter of Q_τ varies with τ qualitatively as ρ in Figure 3.

Model I: The hyperplane described by the level set equation of the M-theory circle moment map in (4.22) satisfies the equation

$$y_1 - y_2 = \frac{k}{2\Lambda} \tau, \quad (4.40)$$

with $-\frac{2\Lambda}{kR_2} \leq \tau \leq \frac{2\Lambda}{kR_1}$, and the vector ζ is

$$\zeta = \frac{1}{k} (1, -1, 0, 0). \quad (4.41)$$

Note that for $\tau = 0$, both vertices p_3 and p_4 of the tetrahedron belong to $Q_{\tau=0}$, therefore the hyperplane (4.40) is parallel to one of the edges of the tetrahedron. So Q_τ is always a triangle but we have to compute $\text{Vol}_E(Q_\tau)$ separately for $\tau < 0$ and $\tau > 0$, which corresponds to the two subintervals of the image of h_M^I that we identified in the previous section (see Figure 5). Let us start with $\tau < 0$. By standard linear algebra, one can find that the

vertices of Q_τ are

$$\begin{aligned} q_1 &= \left(\frac{2\Lambda + kR_2\tau}{2\Lambda(R_1 + R_2)}, \frac{2\Lambda - kR_1\tau}{2\Lambda(R_1 + R_2)}, 0, 0 \right), \\ q_2 &= \left(0, -\frac{k\tau}{2\Lambda}, \frac{2\Lambda + kR_2\tau}{2\Lambda R_3}, 0 \right), \\ q_3 &= \left(0, -\frac{k\tau}{2\Lambda}, 0, \frac{2\Lambda + kR_2\tau}{2\Lambda R_4} \right). \end{aligned} \quad (4.42)$$

Given that $\boldsymbol{\xi}$ and $\boldsymbol{\zeta}_\perp$ are both orthogonal to the plane where Q_τ lies, the volume of Q_τ can be related to the volume of the 4d parallelepiped whose edges are the aforementioned vectors plus two of the edges of Q_τ . Concretely

$$\begin{aligned} \text{Vol}_E(Q_{\tau < 0}) &= \frac{1}{2} \left| \det \left(\frac{\boldsymbol{\xi}}{|\boldsymbol{\xi}|}, \frac{\boldsymbol{\zeta}_\perp}{|\boldsymbol{\zeta}_\perp|}, q_2 - q_1, q_3 - q_1 \right) \right| \\ &= \frac{(2\Lambda + kR_2\tau)^2}{8\Lambda^2 R_3 R_4 (R_1 + R_2)} \sqrt{(R_1 + R_2)^2 + 2(R_3^2 + R_4^2)}. \end{aligned} \quad (4.43)$$

Similarly, for $\tau > 0$ we get the vertices

$$\begin{aligned} q_1 &= \left(\frac{2\Lambda + kR_2\tau}{2\Lambda(R_1 + R_2)}, \frac{2\Lambda - kR_1\tau}{2\Lambda(R_1 + R_2)}, 0, 0 \right), \\ q_2 &= \left(\frac{k\tau}{2\Lambda}, 0, \frac{2\Lambda - kR_1\tau}{2\Lambda R_3}, 0 \right), \\ q_3 &= \left(\frac{k\tau}{2\Lambda}, 0, 0, \frac{2\Lambda - kR_1\tau}{2\Lambda R_4} \right), \end{aligned} \quad (4.44)$$

and therefore the volume

$$\text{Vol}_E(Q_{\tau > 0}) = \frac{(2\Lambda - kR_1\tau)^2}{8\Lambda^2 R_3 R_4 (R_1 + R_2)} \sqrt{(R_1 + R_2)^2 + 2(R_3^2 + R_4^2)}. \quad (4.45)$$

From (4.43) and (4.45) we can directly compute $\rho(t)$ as explained above. Fixing the normalization as in (4.39), we find

$$\rho(t) = \frac{1}{\ell_p^3 N^{1/2}} \begin{cases} \frac{2\Lambda + kR_2\tau}{\pi^2 R_3 R_4 (R_1 + R_2)}, & -\frac{2\Lambda}{kR_2} < \tau < 0 \\ \frac{2\Lambda - kR_1\tau}{\pi^2 R_3 R_4 (R_1 + R_2)}, & 0 < \tau < \frac{2\Lambda}{kR_1} \end{cases} \Bigg|_{\tau = \ell_p^3 N^{1/2} t}, \quad (4.46)$$

which perfectly matches with the eigenvalue distribution (2.27) of the ADHM theory.

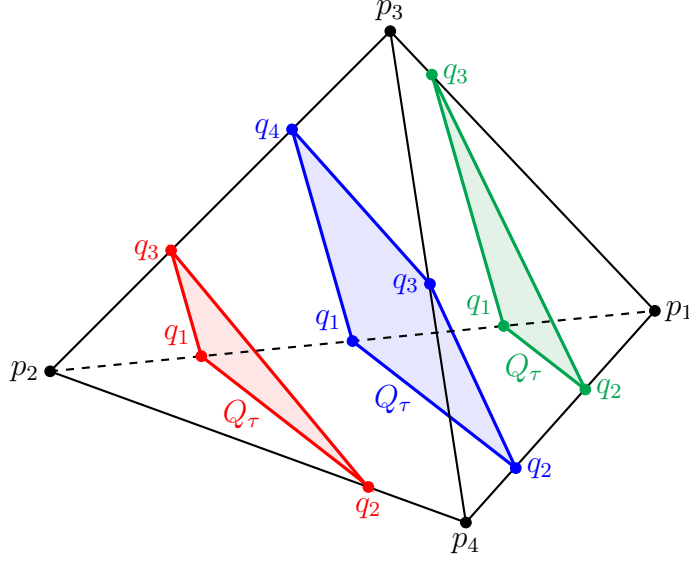


Figure 6: Tetrahedron describing S^7 and its slicing corresponding to Model II – ABJM theory. The red slice is for $\tau_1 < \tau < \tau_2$, blue slice for $\tau_2 < \tau < \tau_3$, and green slice for $\tau_3 < \tau < \tau_4$. The perimeter of Q_τ varies with τ qualitatively as ρ in Figure 4.

Model II: Here the hyperplane corresponding to the moment map level set is described by

$$y_1 - y_2 + y_3 - y_4 = \frac{k}{2\Lambda} \tau, \quad (4.47)$$

with $-\frac{2\Lambda}{kR_2} \leq \tau \leq \frac{2\Lambda}{kR_1}$ (recall we assumed $R_1 \leq R_3$ and $R_2 \leq R_4$), and the vector ζ is

$$\zeta = \frac{1}{k} (1, -1, 1, -1). \quad (4.48)$$

In this case there is no value of τ for which both p_3 and p_4 belong to the hyperplane (4.47), hence the latter hyperplane is not parallel to any edge and the situation is as depicted in Figure 6. In the intervals $\tau_{\min} = \tau_1 < \tau < \tau_2$ and $\tau_3 < \tau < \tau_4 = \tau_{\max}$ the polyhedron Q_τ is a triangle and the computation goes through similarly to Model I. Instead in the interval

$\tau_2 < \tau < \tau_3$, Q_τ is a quadrilateral whose vertices are

$$\begin{aligned} q_1 &= \left(\frac{2\Lambda + kR_2\tau}{2\Lambda(R_1 + R_2)}, \frac{2\Lambda - kR_1\tau}{2\Lambda(R_1 + R_2)}, 0, 0 \right), \\ q_2 &= \left(\frac{2\Lambda + kR_4\tau}{2\Lambda(R_1 + R_4)}, 0, 0, \frac{2\Lambda - kR_1\tau}{2\Lambda(R_1 + R_4)} \right), \\ q_3 &= \left(0, 0, \frac{2\Lambda + kR_4\tau}{2\Lambda(R_3 + R_4)}, \frac{2\Lambda - kR_3\tau}{2\Lambda(R_3 + R_4)} \right), \\ q_4 &= \left(0, \frac{2\Lambda - kR_3\tau}{2\Lambda(R_2 + R_3)}, \frac{2\Lambda + kR_2\tau}{2\Lambda(R_2 + R_3)}, 0 \right). \end{aligned} \quad (4.49)$$

The Euclidean volume of Q_τ can be computed as the sum of the volumes of two triangles, say those with vertices $\{q_1, q_2, q_3\}$ and $\{q_1, q_3, q_4\}$

$$\begin{aligned} \text{Vol}_E(Q_{\tau_2 < \tau < \tau_3}) &= \frac{1}{2} \left| \det \left(\frac{\boldsymbol{\xi}}{|\boldsymbol{\xi}|}, \frac{\boldsymbol{\zeta}_\perp}{|\boldsymbol{\zeta}_\perp|}, q_2 - q_1, q_3 - q_1 \right) \right| \\ &\quad + \frac{1}{2} \left| \det \left(\frac{\boldsymbol{\xi}}{|\boldsymbol{\xi}|}, \frac{\boldsymbol{\zeta}_\perp}{|\boldsymbol{\zeta}_\perp|}, q_3 - q_1, q_4 - q_1 \right) \right|. \end{aligned} \quad (4.50)$$

We do not write the explicit expression as it is long and not particularly insightful. Eventually, fixing the normalization as in (4.39), we find

$$\rho(t) = \frac{1}{\ell_p^3 N^{1/2}} \begin{cases} \frac{2\Lambda + kR_2\tau}{\pi^2(R_1 + R_2)(R_2 + R_3)(R_4 - R_2)}, & \tau_1 < \tau < \tau_2 \\ \frac{4\Lambda + k(R_2R_4 - R_1R_3)\tau}{\pi^2(R_1 + R_2)(R_2 + R_3)(R_1 + R_4)(R_3 + R_4)}, & \tau_2 < \tau < \tau_3 \\ \frac{2\Lambda - kR_1\tau}{\pi^2(R_1 + R_2)(R_1 + R_4)(R_3 - R_1)}, & \tau_3 < \tau < \tau_4 \end{cases} \Bigg|_{\tau = \ell_p^3 N^{1/2} t}, \quad (4.51)$$

with

$$\tau_1 = -\frac{2\Lambda}{kR_2}, \quad \tau_2 = -\frac{2\Lambda}{kR_4}, \quad \tau_3 = \frac{2\Lambda}{kR_3}, \quad \tau_4 = \frac{2\Lambda}{kR_1}, \quad (4.52)$$

which perfectly matches with the eigenvalue distribution (2.31) of the ABJM theory.

4.4 M2-branes and Wilson loops

In this section we place probe M2-branes in the black hole backgrounds from section 3. In particular, we are interested in M2-branes wrapping AdS_2 and an additional circle $S^1_{\text{M2}} \subset Y_9$ in the internal manifold. When these branes are BPS and wrap a particular S^1 copy, their classical action is related to BPS Wilson loop expectation values in the dual matrix model.

4.4.1 BPS probe M2-branes

Since we wish to ultimately match to the Euclidean localized field theory, we need to Wick rotate our background¹⁵

$$t^{(L)} = -it^{(E)}, \quad \text{vol}^{(L)} = -i \text{vol}^{(E)}, \quad iI^{(L)} = -I^{(E)}, \quad (4.53)$$

where the superscripts (L) and (E) denote respectively quantities in Lorentzian and Euclidean signature and I here stands for any action. Consequently, the backgrounds of interest become EAdS₂ × Y₉. In the rest of the section we will drop the superscripts and work in Euclidean signature unless otherwise stated.

The classical action of a probe M2-brane with worldvolume Σ_{M2} in Euclidean signature is [41]¹⁶

$$I_{M2} = \frac{1}{(2\pi)^2 \ell_p^3} \left[-\text{Vol}(\Sigma_{M2}) - i \int_{\Sigma_{M2}} C \right]. \quad (4.54)$$

Notice that this formula is gauge-invariant under shifts of the three-form gauge field $C \rightarrow C + d\Omega$, with Ω a two-form, provided that $\Omega|_{\partial\Sigma_{M2}} = 0$. However, the formula (4.54) requires careful interpretation, as we will discuss next. By virtue of (3.10) and (3.14), we can express C as

$$C = -i \text{vol}_{\text{EAdS}_2} \wedge \mathcal{A} + d\Omega, \quad (4.55)$$

where Ω parametrizes the gauge freedom and we have defined

$$\mathcal{A} = -\psi + e^{-B}\eta, \quad (4.56)$$

with $d\psi = J$. Notice here that J is closed, so we may always *locally* write $J = d\psi$, with ψ a transverse one-form (*i.e.* $\xi \lrcorner \psi = 0$), but in general this will not be globally well-defined. Indeed, $[J] \in H_B^2(\mathcal{F}_\xi)$ always defines a non-zero basic cohomology class – if it were a basic exact form then using Stokes' theorem the volume of Y₉ would necessarily be zero.¹⁷ Explicitly, recalling (3.26) we can write

$$\mathcal{A} = -(\psi_7^t + A \sigma_{\Sigma_g}) + e^{-B}\eta + \text{basic exact}, \quad (4.57)$$

where both ψ_7 and σ_{Σ_g} , such that $d\sigma_{\Sigma_g} = \text{vol}_{\Sigma_g}$, are *local* one-forms only. There is no possible choice of gauge fixing that turns the total C -field (4.55) into a globally defined

¹⁵In this instance $t^{(L)}$ is the time coordinate rather than the direction \mathbb{R}_t introduced at the beginning of section 2.1.1.

¹⁶We use the conventions of [42], Wick-rotated as in (4.53).

¹⁷This is a modification of a standard argument in Kähler geometry, showing that the Kähler class of a compact manifold is always non-zero.

form. However, in the following we will be interested in a particular case where S_{M2}^1 is tangent to the fibres Y_7 . Therefore, if we can turn C into a global form when restricted to the fibres, that would yield a well-defined M2-brane action when substituted into (4.54). Assuming the flavour twist condition (3.28), we can do this by choosing

$$\Omega = -i \text{vol}_{\text{EAdS}_2} \wedge (-\Lambda z) , \quad (4.58)$$

so that (4.55) reads (*cf.* (3.25))

$$C = -i \text{vol}_{\text{EAdS}_2} \wedge (-\Lambda \eta - A \sigma_{\Sigma_g} + e^{-B} \eta + \text{basic exact}) . \quad (4.59)$$

Restricting the above expression to a point on the Riemann surface, the term proportional to σ_{Σ_g} drops out and everything left is proportional to η , which itself is a global one-form since the only class in $H_B^2(\mathcal{F}_\xi)$ that is zero when pulled back to a class in $H^2(Y_9)$ is that generated by $[\varrho]$. In fact as discussed in [8] for the class of GK geometries we are considering in fact $H^2(Y_9) \cong H_B^2(\mathcal{F}_\xi)/[\varrho]$, where $\varrho = d\eta$ immediately implies that $[\varrho] = 0 \in H^2(Y_9)$.

Substituting (4.59) into (4.54) and recalling we are interested in the case where $\Sigma_{M2} = \text{EAdS}_2 \times S_{M2}^1$, we get

$$I_{M2} = \frac{1}{(2\pi)^2 \ell_p^3} \left[(-2\pi) \int_{S_{M2}^1} \left(-e^{-2B/3} \text{vol}_{S_{M2}^1} + \Lambda \eta - e^{-B} \eta \right) \right] , \quad (4.60)$$

where the factor (-2π) appearing in front of the first integral comes from the regularized volume¹⁸ of EAdS_2 [43]

$$\text{Vol}(\text{EAdS}_2) = -2\pi . \quad (4.61)$$

We are interested in computing the action (4.60) for BPS M2-branes. In general, a probe M2-brane will break the supersymmetry of the background, in the sense that acting with a supercharge on the configuration fields of the M2-brane yields a non-vanishing variation. However, the M2-brane action possesses another fermionic symmetry, called κ -symmetry [41],¹⁹ which we can use to compensate for the supersymmetry variation. In Appendix C we discuss in some detail the condition to retain some supersymmetry with the M2-brane insertion, and we find that the circle S_{M2}^1 needs to be aligned with the R-symmetry circle, *i.e.*

$$\text{vol}_{S_{M2}^1} = -e^{-B/3} \eta . \quad (4.62)$$

¹⁸Specifically, one can use holographic normalization to define this rigorously.

¹⁹This is a symmetry of the Green-Schwarz brane action which includes also fermionic degrees of freedom. However, when evaluating the Green-Schwarz action on a classical bosonic background such a contribution vanishes and one is left with the action (4.54).

Then, in the action (4.60) the first and third terms inside the first integral cancel to give the final result

$$I_{\text{M2}}^{\text{BPS}} = -\frac{\Lambda}{2\pi\ell_p^3} \int_{S_{\text{M2}}^1} \eta, \quad (4.63)$$

where Λ is given explicitly in (3.31), and depends on $\text{Vol}_S(Y_7)^{-1/2}$ and $N^{1/2}$. Note that this integral is a quantity that will differ from model to model and from point to point and will have to be computed in each example. For ease of notation, we will drop the BPS superscript in the following, and by I_{M2} we will always mean the action of a BPS M2-brane.

Finally, let us make a further comment on the C -field (4.59). This is valid for solutions in the flavour twist class, but outside this class it is not clear how to generalize the gauge-fixing we have carried out. More specifically, it is not clear how to assign well-defined M2-brane actions outside the flavour twist class. Notice that while the action of an M2-brane is invariant under gauge transformations of the C -field, the issue in this case is that we are working with a complex solution, with purely imaginary C -field, and the saddle point solution then in general manifestly depends on the (complex) gauge choice. On the other hand, the holographic matching of quantities in gravity and localized field theory/matrix models only seems to hold for the same flavour twist class, and it is possible that these observations are related.

4.4.2 Wilson loop dual

In order for the probe M2-branes to be holographically dual to Wilson loops in the fundamental representation, they should wrap $\text{EAdS}_2 \times S_M^1$ – see Figure 7.^{20,21} Indeed Wilson loops are dual to fundamental strings from the type IIA perspective [22], so we should take $S_{\text{M2}}^1 = S_M^1$.²² In the previous subsection we derived that the M2-branes were BPS for S_{M2}^1 aligned with the R-symmetry circle. Then further imposing that they wrap the M-theory circle, the branes are BPS at the points where ζ_M is aligned with the R-symmetry vector ξ . There are a finite number of such connected loci, which can be determined explicitly for each choice of Y_7 together with a $U(1)_M$ action. Let us denote by \mathbf{p}_n a point in the n -th such locus. Holographically the dual Wilson loop

²⁰Similar M2-branes were considered in [21], although without any black hole in AdS_4 present.

²¹Note that we can use a probe approximation because we are interested in Wilson loops in the fundamental representation which are “light”, meaning that the corresponding brane has negligible backreaction. The equivalent statement in field theory is that the insertion of the Wilson loop in the path integral does not affect the eigenvalue density itself, to leading order.

²²Note that, as anticipated, this circle is always tangent to the fibres Y_7 , hence the expression (4.60) is well-defined.

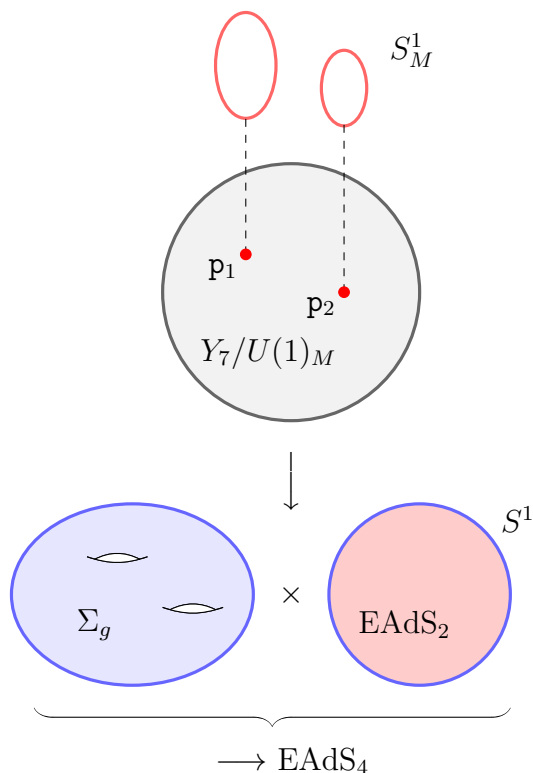


Figure 7: We consider an extremal black hole with Euclidean near horizon geometry $EAdS_2 \times \Sigma_g$ in $EAdS_4$. The full geometry is $EAdS_2 \times Y_9$ with Y_9 a fibration of Y_7 over Σ_g . The probe M2-branes wrap the $EAdS_2$ and a copy of the M-theory circle S_M^1 at the points \mathbf{p}_n (red) where ζ_M is aligned with the R-symmetry vector ξ at \mathbf{p}_n . The dual field theory lives on $\Sigma_g \times S^1$ (blue), with S^1 being the boundary of $EAdS_2$. This S^1 is also the direction wrapped by the Wilson loop, in order for it to be BPS.

expectation value is determined by the M2-brane action evaluated at \mathbf{p}_n , where we should sum (or integrate) over all the possible configurations

$$\langle W_{\text{fund}} \rangle = \sum_n \int d\mathbf{p}_n e^{-I_{M2}|\mathbf{p}_n} . \quad (4.64)$$

Interestingly the value of the action only depends on the locus and not on the specific point within. One should also presumably integrate over the locus, with some measure, although the choice of measure is a subleading effect in N , and we have correspondingly been schematic in writing (4.64). Another interesting point is that the Wilson loop for the class of supersymmetric black holes we are considering is not zero due to integration over gauge-equivalent configurations, discussed in [44]. This is a subtle point, but clearly important for the identification that follows, and the way that the argument in [44] is evaded in this setting is discussed further in Appendix D.

The ordering of the loci is arbitrary from the geometry point of view, and we order them such that $I_{\text{M2}}|_{\mathbf{p}_n}$ is increasing with n . At large N we only consider the dominant contribution in the sum in (4.64), which comes from the most negative M2-brane action

$$\log \langle W_{\text{fund}} \rangle = -I_{\text{M2}}|_{\mathbf{p}_1}. \quad (4.65)$$

Comparing with the expression for the Wilson loop at large N in field theory (2.42), we have a matching $I_{\text{M2}}|_{\mathbf{p}_1} = N^{1/2}t_{\text{min}}$. Our claim is that more is true and actually the M2-brane action reproduces all the points t_n at which the derivative of the eigenvalue density is discontinuous:

$$I_{\text{M2}}|_{\mathbf{p}_n} = N^{1/2}t_n, \quad (4.66)$$

where recall that \mathbf{p}_n is a point in the n -th region where ζ_M and ξ are aligned. Let us denote β_n the factor of proportionality at such a point,

$$\zeta_M = \beta_n \xi \quad \Longrightarrow \quad \int_{S_M^1|_{\mathbf{p}_n}} \eta = -2\pi\beta_n, \quad (4.67)$$

as $\xi \lrcorner \eta = 1$ and the sign is due to the orientation determined in (4.62). Therefore the action of a BPS M2-brane dual to a Wilson loop reads

$$I_{\text{M2}}|_{\mathbf{p}_n} = \frac{\Lambda}{\ell_p^3} \beta_n. \quad (4.68)$$

The statement (4.66) is actually equivalent to the argument in section 4.2 that the discontinuity points of ρ' are reproduced by the fixed points of the moment map. Indeed recall that $h_M = \Lambda \zeta_M \lrcorner \eta$, and we already mentioned that the critical points of h_M were those where ζ_M and ξ are aligned. At a point \mathbf{p}_n where $\zeta_M = \beta_n \xi$ we have $\tau_n \equiv h_M|_{\mathbf{p}_n} = \Lambda\beta_n$, such that

$$t_n = \frac{\tau_n}{\ell_p^3 N^{1/2}} = \frac{\Lambda\beta_n}{\ell_p^3 N^{1/2}} = \frac{I_{\text{M2}}|_{\mathbf{p}_n}}{N^{1/2}}. \quad (4.69)$$

Let us next examine this in our favourite examples. Recall that on S^7/\mathbb{Z}_k

$$\xi = \sum_{a=1}^4 \frac{R_a}{2} \partial_{\phi_a}. \quad (4.70)$$

Model I: For ADHM

$$\zeta_M^{\text{I}} = \frac{1}{k} (\partial_{\phi_1} - \partial_{\phi_2}), \quad (4.71)$$

such that $\zeta_M^I = \beta_n \xi$ in the regions $\mathbf{p}_1 \in (0, z_2, 0, 0)$, $\mathbf{p}_2 \in (0, 0, z_3, z_4)$, $\mathbf{p}_3 \in (z_1, 0, 0, 0)$, with

$$\beta_1 = -\frac{2}{kR_2}, \quad \beta_2 = 0, \quad \beta_3 = \frac{2}{kR_1}. \quad (4.72)$$

This reproduces the points in (2.28), recalling the relation (4.8) between Λ and μ .

Model II: For ABJM

$$\zeta_M^{\text{II}} = \frac{1}{k}(\partial_{\phi_1} - \partial_{\phi_2} + \partial_{\phi_3} - \partial_{\phi_4}), \quad (4.73)$$

such that ζ_M^{II} and ξ are aligned on the regions where only one of the coordinate is non-zero. Ordering them by increasing β_n we denote $\mathbf{p}_1 \in (0, z_2, 0, 0)$, $\mathbf{p}_2 \in (0, 0, 0, z_4)$, $\mathbf{p}_3 \in (0, 0, z_3, 0)$, $\mathbf{p}_4 \in (z_1, 0, 0, 0)$, giving

$$\beta_1 = -\frac{2}{kR_2}, \quad \beta_2 = -\frac{2}{kR_4}, \quad \beta_3 = \frac{2}{kR_3}, \quad \beta_4 = \frac{2}{kR_1}, \quad (4.74)$$

which exactly reproduces the subinterval points in (2.32).

In the case where some of the R-charges are equal the regions may change topology. In particular when $R_a = 1/2$ for all a , there are two loci on which ζ_M^{II} and ξ are aligned, namely $\mathbf{p}_1 \in \{z_1 = z_3 = 0\}$, $\mathbf{p}_2 \in \{z_2 = z_4 = 0\}$, where

$$\beta_1 = -\frac{4}{k}, \quad \beta_2 = \frac{4}{k}, \quad (4.75)$$

and $\rho(t) = 2\mu/\pi$ is just a constant function between these two points. In our polytope picture this corresponds to the moment map plane being parallel to both the edge between p_1 and p_3 and that between p_2 and p_4 , so that Q_τ is always a quadrilateral. In this case, we also have

$$\Lambda = \frac{\pi \ell_p^3 N^{1/2}}{8} \sqrt{2k} = \frac{\pi \ell_p^3 N^{1/2}}{2} \mu. \quad (4.76)$$

This particular case describes the so-called ‘‘universal twist’’, which is an explicitly known black hole solution of minimal 4d gauged supergravity that uplifts on general classes of internal space Y_7 [7], including S^7/\mathbb{Z}_k discussed here.

5 Matrix models on the spindle

In this section we generalize the results obtained so far to the case where the black hole has a further parameter corresponding to the acceleration. The near-horizon geometry remains of the form described in section 3.2.1, with an internal GK manifold Y_9 , but the Riemann surface in the fibration (3.21) is replaced by the 2d orbifold $\Sigma \equiv \mathbb{WCP}^1_{[m_+, m_-]}$, where $m_{\pm} \in \mathbb{N}$ are coprime and determine the acceleration [14, 15]. The space Σ , known as a spindle, is topologically a two-sphere with conical singularities at the two poles parametrized by the positive integers m_{\pm} . Notice that we recover S^2 by setting $m_+ = m_- = 1$.

We first review the relevant geometric properties of said fibrations, based on the discussion in [15], and then proceed to outline how we expect the large N matrix model arising from localizing the dual 3d $\mathcal{N} = 2$ SCFT on $\Sigma \times S^1$ to behave. There are currently no results concerning such large N matrix models from a purely field theoretic approach, though some related work on the “refined twisted index”, with which we make contact here, has been carried out in [20], and may be matched to our gravitational formulas.

5.1 Accelerating black holes and block formulas

In [14] it was conjectured that any supersymmetric, magnetically charged, and accelerating black hole in AdS_4 , which uplifts to M-theory on a Sasaki-Einstein manifold like (3.2), has a near-horizon geometry of the form (3.9) where Y_9 takes the fibred form

$$Y_7 \hookrightarrow Y_9 \rightarrow \Sigma. \quad (5.1)$$

Here Σ is a spindle parametrized by $m_{\pm} \in \mathbb{N}$. These fibrations were constructed explicitly in [15], and their main difference with respect to (3.21) is that the R-symmetry vector ξ is not necessarily orthogonal to Σ ; in general it may have a component tangent to the spindle, which is the black hole horizon. Denoting ∂_{φ_0} the generator of the $U(1)$ isometry which rotates Σ about its axis, and keeping the notation ∂_{φ_i} for a basis of generators for the $U(1)^4$ action on the fibre Y_7 , we parametrize ξ as

$$\xi = \sum_{\mu=0}^s b_{\mu} \partial_{\varphi_{\mu}}, \quad (5.2)$$

with $b_0 \neq 0$ in general and $b_1 = 1$ as before. Other than this, the twisting is obtained by turning on s gauge magnetic fluxes analogous to those in (3.22)

$$\frac{1}{2\pi} \int_{\Sigma} dA_i = \frac{p_i}{m_+ m_-}, \quad p_i \in \mathbb{Z}. \quad (5.3)$$

The $i = 1$ direction is special and we need to set

$$p_1 = -\sigma m_+ - m_-, \quad (5.4)$$

where $\sigma = \pm 1$ determines whether the mechanism for preserving supersymmetry is the “twist” or the “anti-twist”, which are both distinct from the topological twist for preserving supersymmetry on a Riemann surface [45]. Note that in the twist case $\sigma = +1$ when setting $m_{\pm} = 1$ we have $p_1 = -2$, which agrees with what we had in section 3.2.2 for $g = 0$.

Differently from the Riemann surface case, here the topology of the fibres in (5.1) do depend on the specific point of the base. We will be particularly interested in the fibres over the two poles of the spindle

$$Y_{\pm} \equiv Y_7 / \mathbb{Z}_{m_{\pm}}. \quad (5.5)$$

The vector fields $V_+ = \sum_{\mu=0}^s v_{+\mu} \partial_{\varphi_{\mu}}$ and $V_- = \sigma \sum_{\mu=0}^s v_{-\mu} \partial_{\varphi_{\mu}}$ which rotate the normal directions to Y_{\pm} are given by

$$v_+ = (m_+, 1, -a_+ p_2, \dots, -a_+ p_s), \quad v_- = (-\sigma m_-, 1, -\sigma a_- p_2, \dots, -\sigma a_- p_s), \quad (5.6)$$

where a_{\pm} are coprime integers satisfying $a_- m_+ + a_+ m_- = 1$.²³ Thanks to (5.6), we can introduce two new vectors fields ξ_{\pm} as the orthogonal projections of the R-symmetry vector ξ onto Y_{\pm}

$$\xi_{\pm} \equiv \xi \mp \frac{b_0}{m_{\pm}} V_{\pm} = \sum_{i=1}^s b_i^{(\pm)} \partial_{\varphi_i}, \quad (5.7)$$

where we define the shifted vectors

$$b_i^{(+)} \equiv b_i - \frac{b_0}{m_+} v_{+i}, \quad b_i^{(-)} \equiv b_i + \frac{b_0}{\sigma m_-} v_{-i}. \quad (5.8)$$

By applying a simple lemma in differential geometry, in [15] it was shown that in this set-up many geometric quantities that are integrals over Y_9 receive contributions

²³The integers a_{\pm} exist by Bezout’s lemma but are not unique. However, this is not an issue as they drop out from any on-shell physical quantity.

only from the two poles of the spindle and hence reduce to integrals over the fibres Y_{\pm} , resulting in the so-called *block formulas*.²⁴ In particular, this is the case for all the quantities of physical interests such as the supersymmetric action (3.19), the constraint (3.17), and the quantized fluxes (3.18). Moreover, the geometric R-charges defined in (3.33) get doubled as we can define both R_a^+ and R_a^- by integrating over S_a^{\pm} *i.e.* the copies of the codimension two submanifold $S_a \subset Y_7$ over the two poles of the spindle. For a more detailed discussion and the explicit expressions we refer the reader to [15], while here we will directly focus on the flavour twist case.

In order to implement the flavour twist condition here we cannot simply impose (3.28), as the transverse Kähler form of the fibres ω is not guaranteed to be the same at every point of the spindle – and it is not in general. However, the analogous conditions in this case are instead

$$[J|_{Y_{\pm}}] = \Lambda_{\pm}[\varrho|_{Y_{\pm}}], \quad \Lambda_{\pm} \in \mathbb{R}. \quad (5.9)$$

The two Kähler class parameters are specified by imposing flux quantization through the fibres at the poles and read

$$\Lambda_+ = \frac{(2\pi\ell_p)^3}{\sqrt{24b_1^3 \text{Vol}_S(Y_7)|_{b_i^{(+)}}} } N^{1/2}, \quad \Lambda_- = \sigma \frac{(2\pi\ell_p)^3}{\sqrt{24b_1^3 \text{Vol}_S(Y_7)|_{b_i^{(-)}}} } N^{1/2}. \quad (5.10)$$

Note that these are the same functional expressions as (3.31), though evaluated with the shifted vectors $b_i^{(\pm)}$. This is a characteristic feature of physical quantities in these fibred geometries: most get contributions from the two poles, taking the same form we had in the Riemann surface case but evaluated with the orthogonal projections of the R-symmetry vector onto the fibres (5.7). Indeed, the off-shell entropy is given by

$$\mathcal{S} = \frac{4}{b_0} (F_{\text{grav}}[\xi_+] - \sigma F_{\text{grav}}[\xi_-]) \Big|_{b_1=1}. \quad (5.11)$$

Moreover, as anticipated we have now two sets of geometric R-charges associated to supersymmetric submanifolds of the fibres $S_a \subset Y_7$

$$R_a^{\pm} = \frac{2\pi}{3b_1} \frac{\text{Vol}_S(S_a)}{\text{Vol}_S(Y_7)|_{b_i^{(\pm)}}}, \quad (5.12)$$

with $R_a^+ > 0$ and $\sigma R_a^- > 0$. The corresponding integer fluxes M_a through the codimension two fibrations $S_a \hookrightarrow \Sigma_a \rightarrow \Sigma$ inside Y_9 are given in terms of these R-charges

²⁴These block formulas in GK geometry have recently been derived using a fixed point formula for an equivariant version of the master volume in [46].

by

$$M_a = \frac{b_1}{2b_0} (R_a^+ - R_a^-) N . \quad (5.13)$$

Note that all of the above expressions reduce to those in section 3.2.3 upon setting $\sigma = 1$, $m_+ = m_- = 1$, and sending $b_0 \rightarrow 0$, hence recovering the result for $\Sigma_g = S^2$.

5.2 Shifted eigenvalue densities

Besides an investigation of the localized index on $\Sigma \times S^1$ at finite N [24], there are currently no systematic studies of the field theory dual to the accelerating black holes whose near-horizon geometry we presented above. This renders the task of providing a geometric characterization of the corresponding matrix models harder, especially given that part of the picture we presented in section 4 was motivated heuristically, albeit with concrete computational checks. Nevertheless, we can exploit the lessons learned so far to describe some of the features of said matrix models, leaving a more thorough analysis to future work.

First of all, let us notice that at the fixed points of V_\pm , that is at the respective poles of Σ , the geometry of the internal space becomes equivalent to that described in section 3.2.2 (with Σ_g replacing the spindle), upon using the shifted R-symmetry vectors $b_i \rightarrow b_i^{(\pm)}$. Moreover, the vector field ζ_M generating the $U(1)_M$ action is a characteristic feature of the original geometric engineering set-up, and as such it only rotates directions inside the fibres Y_7 , and does not act on the spindle itself – that is, it does not have any component along ∂_{φ_0} . Hence it is clear that at the two poles of the spindle the geometric set-up is much the same as what we had before, and thus we can envisage having a doubling of all the quantities associated to the matrix model, with a copy at the “+” pole and another at the “−” pole.

We begin by noting that the $U(1)_M$ action is Hamiltonian on Y_\pm , and therefore we can define two associated moment maps h_M^\pm at the poles of the spindle to be such that

$$dh_M^\pm = -\zeta_M \lrcorner J|_{Y_\pm} . \quad (5.14)$$

From here, everything goes through as in section 4, although with the shifted R-symmetry vector $b_i^{(\pm)}$ and consequently the shifted Kähler class parameters Λ_\pm and the shifted R-charges R_a^\pm . Parametrizing with τ the images of h_M^\pm , we can define two quotients of the fibres Y_\pm

$$Y_\tau^\pm \equiv (h_M^\pm)^{-1}(\tau)/U(1)_M . \quad (5.15)$$

The volumes of Y_τ^\pm can be obtained from $\text{Vol}(Y_\tau)$, as computed in the Riemann surface case, by shifting the R-symmetry vectors and dividing by a factor m_\pm which accounts for the \mathbb{Z}_{m_\pm} quotient in (5.5)

$$\text{Vol}(Y_\tau^\pm) = \frac{1}{m_\pm} \text{Vol}(Y_\tau) \Big|_{b_i^{(\pm)}} . \quad (5.16)$$

Note that τ is just a label at this stage, and there is no reason why it should be the same at the two poles, hence we will rename it to τ^\pm . We can correspondingly define two “shifted densities” $\rho_\pm(t^\pm)$ as in (4.33). In particular, denoting with $\rho_{\Sigma_g}(t)$ the eigenvalue density of a certain field theory on Σ_g , the same field theory on the spindle will have

$$\rho_\pm(t^\pm) = \rho_{\Sigma_g}(t^\pm) \Big|_{b_i^{(\pm)}} . \quad (5.17)$$

Moreover, the derivatives $\rho'_\pm(t)$ are discontinuous at the critical points of h_M^\pm , namely where ζ_M is aligned with ξ_\pm and are simply given by

$$t_n^\pm = t_n \Big|_{b_i^{(\pm)}} , \quad (5.18)$$

where t_n are the points of discontinuity of $\rho'_{\Sigma_g}(t)$.

This last point can be corroborated by looking at probe M2-branes in this background. The discussion about supersymmetry we carried out in section 4.4.1 goes through without any change as it relies only on the fact that Y_9 is a GK manifold. There we showed that the M2-branes are BPS when ζ_M is aligned with ξ , and from (5.7) we can see that in the loci where V_\pm are zero, namely the respective poles of the spindle, this is equivalent to requiring ζ_M to be aligned with ξ_\pm , as stated above. With suitable tweaks, also the gauge fixing in section 4.4 goes through, albeit it has to be done separately at the two poles, and we find that BPS M2-branes wrapping $E\text{AdS}_2 \times S_M^1$ can sit at either poles of Σ , and their action matches (5.18)

$$I_{\text{M2}} \Big|_{\mathbf{p}_n^\pm} = N^{1/2} t_n^\pm . \quad (5.19)$$

Here \mathbf{p}_n^\pm are points in the n -th locus where $\zeta_M \propto \xi_\pm$. Correspondingly, in field theory a Wilson loop in the fundamental representation wrapping the Euclidean time circle is supersymmetric when it sits at either of the two poles, and its expectation value at leading order in N will be

$$\log \langle W_{\text{fund}}^\pm \rangle = -I_{\text{M2}} \Big|_{\mathbf{p}_1^\pm} . \quad (5.20)$$

All the quantities introduced up to now should then match with the corresponding quantities derived from a purely field theoretic computation. In particular, for 3d

$\mathcal{N} = 2$ SCFTs on $\Sigma \times S^1$ it is convenient to introduce the shifted chemical potentials

$$\Delta_A^+ = \Delta_A + \frac{\epsilon}{2} \left(\mathbf{n}_A - \frac{r_A}{2} \frac{m_- - \sigma m_+}{m_+ m_-} \right), \quad (5.21)$$

$$\Delta_A^- = \Delta_A - \frac{\epsilon}{2} \left(\mathbf{n}_A + \frac{r_A}{2} \frac{m_- - \sigma m_+}{m_+ m_-} \right), \quad (5.22)$$

where ϵ is an extra parameter which will enter the extremization procedure and the r_A are subject to the constraint $\sum_{A \in W} r_A = 2$ but are otherwise free. We expect all physical quantities to have natural expressions in terms of these, and the holographic matching to be achieved by suitably identifying Δ_A^\pm with linear combinations of R_a^\pm and ϵ with $2b_0$.

To summarize, the matrix model arising from considering the large N limit of the localized partition function on $\Sigma \times S^1$ is expected to factorize into two different matrix models, which can be studied independently and result in the densities $\rho_\pm(t^\pm)$ introduced above. We expect that the information contained in said ‘‘shifted’’ densities can be used to recover the total $\rho_\Sigma(t)$, as a function of a single variable t obtained from t^\pm . This picture is also motivated by several results in the literature where in various different contexts a factorization of physical observables have been observed, ultimately related to a fixed point formula. Of these, the refined twisted index discussed in [20] is directly relevant, and will be discussed in more detail in the next subsection.

Since we have left most of the formulas in this section rather implicit, we conclude by presenting the explicit BPS M2-brane actions for the ABJM model on a spindle. There are 4 such BPS M2-branes, wrapping an aligned M-theory circle and R-symmetry vector over each \pm pole of the spindle, giving 8 formulas in total. From (5.19) and the results in Appendix B we can simply write down

$$I_{\text{M2}}|_{\mathfrak{p}_a^\pm} = N^{1/2} t_a^\pm, \quad a = 1, 2, 3, 4, \quad (5.23)$$

where

$$t_1^\pm = -\frac{\mu^\pm}{kR_2^\pm}, \quad t_2^\pm = -\frac{\mu^\pm}{kR_4^\pm}, \quad t_3^\pm = \frac{\mu^\pm}{kR_3^\pm}, \quad t_4^\pm = \frac{\mu^\pm}{kR_1^\pm}, \quad (5.24)$$

and

$$\mu^\pm = \pi \sqrt{2kR_1^\pm R_2^\pm R_3^\pm R_4^\pm}. \quad (5.25)$$

Here the R-charges R_a^\pm satisfy the constraints [15]

$$R_a^+ - R_a^- = 2b_0 \frac{M_a}{N} = 2b_0 \mathbf{n}_a, \quad \sum_{a=1}^4 R_a^+ = 2 - \frac{2b_0}{m_+}, \quad \sum_{a=1}^4 R_a^- = 2 + \frac{2b_0}{\sigma m_-}, \quad (5.26)$$

which should be matched to the chemical potential variables Δ_a^\pm in (5.21), (5.22), where the fluxes \mathbf{n}_a for the twist and anti-twist cases are constrained to obey

$$\sum_{a=1}^4 \mathbf{n}_a = -\frac{\sigma m_+ + m_-}{m_+ m_-}. \quad (5.27)$$

Here we identify $\epsilon = 2b_0$, as in the next subsection. This gives a very precise prediction for the large N matrix model behaviour of the ABJM theory on a spindle, with (5.24) giving the points at which the expected eigenvalue density blocks have discontinuities in their derivatives. More physically, as we have explained the least such M2-brane action computes a BPS Wilson loop VEV in the field theory on the spindle.

5.3 Connecting to the refined twisted index

To conclude the discussion on the spindle index, we will make contact with the recent field theory results of [20]. There the authors studied the matrix models arising from the large N limit of the *refined* twisted index $Z_{S^2 \times S^1}$, which is defined for the genus $g = 0$ case as a further refinement of the topologically twisted index with respect to the axial $U(1)$ isometry of the two-sphere (see section 4 of [33]). This index depends on an extra parameter ϵ , which “rotates” the S^1 relative to the S^2 . Holographically, its logarithm has been matched with the entropy of supersymmetric, magnetically charged, and also rotating black holes in AdS₄ [47], with ϵ identified with the chemical potential conjugate to the angular momentum of the black hole [48].

We shall see in this section that the field theory results of [20] may *also* be matched to GK geometries for which $Y_7 = S^7$ is fibred over S^2 , and where the R-symmetry vector also rotates the S^2 . Specifically, we shall see that the field theory parameter $\epsilon = 2b_0$, in terms of the component b_0 of ξ that rotates the S^2 . A similar matching was pointed out in [14], and also relies on some observations in [49]. In order to explain this, one first observes for the twisted $S^2_\epsilon \times S^1$, the R-symmetry Killing vector field bilinear for this rigid supersymmetric background is [33, 49]²⁵

$$K = \bar{\zeta} \gamma^\mu \zeta \partial_\mu = \partial_\theta + \frac{1}{2} \epsilon \partial_{\varphi_0}. \quad (5.28)$$

Here ζ is the Killing spinor of the background, θ has period 2π and parametrizes the S^1 , while φ_0 parametrizes the axial direction on the S^2 and is also normalized to have canonical period 2π . The expression (5.28) is a more invariant geometric way to

²⁵The fugacity was denoted $e^{i\epsilon} = e^{i\epsilon/2}$ in [33], which explains the factor of $\frac{1}{2}$ in (5.28).

characterize the parameter ϵ , in terms of specifying the R-symmetry vector field of the background on which one is localizing. On the other hand, the bulk black hole solution inherits the same Killing vector field, and when lifted to 11d M-theory this explains why $\epsilon = 2b_0$, since by definition b_0 parameterizes the component of the R-symmetry vector of the full solution along the horizon direction Σ , precisely as in equation (5.2). This is all detailed quite explicitly for the class of dyonically charged, accelerating and rotating black holes studied in [4, 49] (which lie in the universal truncation of [6]), but the same arguments should go through also for the more general class of purely magnetically charged black holes in this paper, with general choice of Y_7 and magnetic fluxes, but with a trial R-symmetry vector field that also rotates the horizon S^2 . We then expect the entropy function in (5.11) to match $\log Z_{S^2 \times S^1}$ in the twist case $\sigma = 1$ and in the limit $m_{\pm} = 1$, which we find is indeed the case. This is then consistent with the conjecture in [14]: that b_0 may be regarded as a chemical potential for angular momentum J , with the entropy of *rotating* versions of the black holes in this paper obtained via a Legendre transform. Moreover, given the results earlier in the paper, we may go further and also match matrix model quantities in the refined field theory calculation, and GK geometry with $b_0 \neq 0$.

When considering the refined index, the summation over the gauge magnetic fluxes \mathbf{m} in (2.18) cannot be performed directly and instead one should keep them as variables when taking the large N limit. In particular, in [20] the authors supplement the ansatz (2.21) with²⁶

$$\mathbf{m}_I^\alpha = iN^{1/2} \mathbf{s}^\alpha + \mathbf{p}_I^\alpha \quad \longrightarrow \quad \mathbf{m}_I(t) = iN^{1/2} \mathbf{s}(t) + \mathbf{p}_I(t). \quad (5.29)$$

Moreover, the partition function takes the form of a product of holomorphic blocks [50], which at large N can be expressed in terms of shifted Bethe potentials

$$\log Z_{S^2 \times S^1} = -\frac{i}{\pi\epsilon} \left[\mathcal{U}(\rho_+(t^+), v_I^+(t^+), \Delta_A^+) - \mathcal{U}(\rho_-(t^-), v_I^-(t^-), \Delta_A^-) \right], \quad (5.30)$$

where \mathcal{U} is the same Bethe potential we introduced in section 2.2.2 and the various quantities appearing are defined as

$$t^\pm = t \pm \frac{\pi\epsilon}{2} \mathbf{s}(t), \quad \rho_\pm(t^\pm) = \frac{\rho(t)}{1 \pm \frac{\pi\epsilon}{2} \mathbf{s}'(t)}, \quad v_I^\pm(t^\pm) = v_I(t) \pm \frac{\pi\epsilon}{2} \mathbf{p}_I(t), \quad (5.31)$$

$$\Delta_A^\pm = \Delta_A \pm \frac{\epsilon}{2} \mathbf{n}_A,$$

²⁶Our notation differs from that of [20] in the following way: $\mathbf{s}^{\text{there}} = -\mathbf{n}$, $\mathbf{n}^{\text{there}} = \mathbf{s}$, $\epsilon^{\text{there}} = \pi\epsilon$, $\Delta^{\text{there}} = \pi\Delta$, $T_{\text{there}}^{(\pm)} = t^\pm$, $\widetilde{\mathcal{W}}^{\text{there}} = -\mathcal{U}$.

and the shifted chemical potentials satisfy the constraints

$$\sum_{A \in W} \Delta_A^\pm = 2 \mp \epsilon. \quad (5.32)$$

Note that the Δ_A^\pm introduced for the spindle in (5.21) and (5.22) precisely reduce to those in (5.31) when $\sigma = 1$ and $m_+ = m_- = 1$.

At this point, one should extremize (5.30) with respect to $\rho(t)$, $v_I(t)$, $\mathfrak{s}(t)$, and $\mathfrak{p}_I(t)$, but in [20] the authors observed that this is actually equivalent to extremizing independently the two Bethe potentials with respect to $\rho_\pm(t^\pm)$ and $v_I^\pm(t^\pm)$. With a suitable map between the variables this is equivalent to the unrefined case and therefore the results are the same

$$\rho_\pm(t^\pm) = \rho_{\Sigma_g}(t^\pm)|_{\Delta_A^\pm}, \quad v_I^\pm(t^\pm) = v_I^{\Sigma_g}(t^\pm)|_{\Delta_A^\pm}. \quad (5.33)$$

The physical $\rho(t)$ and the other functions of t of the matrix model are then obtained by going backwards through the definitions of the shifted quantities in (5.31) and imposing some consistency conditions which will not be detailed here. Substituting (5.33) into (5.30) one obtains

$$\log Z_{S_\epsilon^2 \times S^1} = \frac{1}{\pi\epsilon} \left[\bar{\mathcal{U}}(\Delta_A^+) - \bar{\mathcal{U}}(\Delta_A^-) \right] = \frac{1}{2\epsilon} \left[F_{S^3}(\Delta_A^+) - F_{S^3}(\Delta_A^-) \right]. \quad (5.34)$$

As anticipated, this matches perfectly with the entropy function (5.11) when $\sigma = 1$ and $m_+ = m_- = 1$ if we identify $\epsilon = 2b_0$ and Δ_A^\pm with suitable linear combinations of $R_a^\pm(\xi_\pm)$.²⁷ Furthermore, notice that the densities (5.33) are exactly the same as those we defined from GK geometry, for the spindle matrix model, in (5.17)!

6 Further toric examples

In this final section we illustrate our results with some further examples. We will consider other toric choices of Calabi-Yau cones X_4 , which are dual to various flavoured variants of the two quivers we already discussed. These are somewhat more involved computationally, but there are no extra ingredients entering the picture besides some toric geometry machinery, which we will use as a tool for computing the relevant quantities.

²⁷Recall that $F_{S^3} = F_{\text{grav}}|_{b_1=4} = 16F_{\text{grav}}|_{b_1=1}$ upon identifying Δ_A with the same linear combinations of $R_a(\xi)$.

We first revisit briefly the toric version of the GK geometry described in section 3.2 and explain how the extra structure provides an algorithmic way to compute both the eigenvalue density and the discontinuity points of its derivative. We then apply the above to the examples where $X_4 = \mathbb{C} \times C(T^{1,1})$ and $X_4 = C(Q^{1,1,1}/\mathbb{Z}_n)$.

6.1 Generalities on toric cones

6.1.1 GK geometry with toric fibres

In the examples we will consider, the cone $X_4 = C(Y_7)$ is a complex toric cone. The advantage of dealing with toric spaces is that geometric quantities can be expressed in terms of sums over combinatorial data, the *toric data*, including integrals over the internal space or its cycles. For ease of exposition in this section we generally take Y_7 to be the simply-connected covering space, re-establishing quotients by \mathbb{Z}_k or \mathbb{Z}_n in final formulas as appropriate, much as we did in section 3.3.

The complex cone (3.1) is toric if $s = 4$ *i.e.* Y_7 has $U(1)^4$ isometry, generated by the Killing vector fields ∂_{φ_i} as before. At each fixed radius $r > 0$ sits a homothetic copy of Y_7 , with the original Y_7 embedded naturally at $r = 1$. A toric cone is fully described by a set of $d \geq 4$ primitive integer vectors $v_a \in \mathbb{Z}^4$, $a = 1, \dots, d$. In particular, we introduce the polyhedral cone \mathcal{C} as the cone whose d facets have v_a as inward-pointing normal vectors

$$\mathcal{C} \equiv \left\{ y \in \mathbb{R}^4 \mid \sum_{i=1}^4 y^i v_{ai} \geq 0, a = 1, \dots, d \right\}. \quad (6.1)$$

This polyhedral cone is also the image of the moment map $\mu: C(Y_7) \rightarrow \mathbb{R}^4$ associated to the $U(1)^4$ action, given explicitly by²⁸

$$\mu_i = y^i = \frac{1}{2} r^2 \partial_{\varphi_i} \lrcorner \eta. \quad (6.2)$$

The set $\{y^i, \varphi_i\}$, $i = 1, 2, 3, 4$ constitutes a system of coordinates for $C(Y_7)$ and the latter can be built as a $U(1)^4$ fibration over the polyhedral cone \mathcal{C} itself in the following way: in the interior of the cone \mathcal{C}_{int} the fibration is trivial, while on each facets at the boundary $\partial\mathcal{C}$ a single $U(1) \subset U(1)^4$ copy shrinks to a point. In particular, at the a^{th} facet the $U(1)$ copy that shrinks is identified by the vector field

$$\nu_a = \sum_{i=1}^4 v_{ai} \partial_{\varphi_i}. \quad (6.3)$$

²⁸This should not be confused with the moment map associated to the $U(1)_M$ action we introduced in (4.9). The one given in (6.2) is defined to satisfy $d\mu_i = -\partial_{\varphi_i} \lrcorner \mathcal{J}$.

Complex codimension one submanifolds of $C(Y_7)$ which are invariant under the $U(1)^4$ action are called toric divisors and their images under the moment map μ are precisely the d facets of the cone \mathcal{C} . Note that the freedom of changing basis for the $U(1)^4$ action results in the freedom of making an $SL(4, \mathbb{Z})$ transformation of the toric data v_{ai} and the toric map coordinates μ_i . The basis we use is such that the condition (3.15) holds and $v_a = (1, \vec{w}_a)$, with $\vec{w}_a \in \mathbb{Z}^3$.

Notice that any consistent choice of toric data for $d = 4$ is related to that in (3.40) by an $SL(4, \mathbb{Z})$ transformation, and indeed $\mathbb{C}^4 = C(S^7)$ is the simplest example of toric cone. In that case the toric divisors coincide with the cones over the submanifolds obtained setting the complex coordinates $z_a = 0$ whose volumes are (3.42), and the vectors ν_a are nothing but those rotating said coordinates, *i.e.* $\nu_a = \partial_{\phi_a}$. When $d > 4$ instead, the v_a cannot be all linearly independent, and indeed there exists a $d \times (d - 4)$ constant matrix q_A^a (the *kernel matrix*), such that

$$\sum_{a=1}^d q_A^a v_a = 0, \quad \forall A = 1, \dots, d - 4. \quad (6.4)$$

This relation can also be seen as the fact that the toric divisors are not independent cycles because $\dim H_5(Y_7, \mathbb{R}) = d - 4$.²⁹ It is then clear that the vectors ν_a do not constitute a basis for the $U(1)^4$ action as they are not linearly independent, hence we will stick with the ∂_{φ_i} basis, unlike what we did for $Y_7 = S^7$ where ∂_{ϕ_a} is a more natural (or certainly democratic) choice.

The image of Y_7 under the moment map is a subset of \mathcal{C} which we call the *Sasakian polytope*. Introducing the vector $b = (b_1, b_2, b_3, b_4)$ as the coordinate vector for the Reeb vector field (3.5), the Sasakian polytope is given by

$$P(b) = \mathcal{C} \cap H(b), \quad (6.5)$$

where $H(b)$ is the Reeb hyperplane, defined as

$$H(b) \equiv \left\{ y \in \mathbb{R}^4 \mid \sum_{i=1}^4 y^i b_i = \frac{1}{2} \right\}. \quad (6.6)$$

One can show that the Sasakian volume (3.30) can be obtained from the Euclidean volume of the polytope $P(b)$ as

$$\text{Vol}_S(Y_7) = \frac{(2\pi)^4}{|b|} \text{Vol}_E(P), \quad (6.7)$$

²⁹An alternative way to construct the toric cone X_4 is to start with the space \mathbb{C}^d with coordinates z_a , and then take a (GIT) quotient by a $(\mathbb{C}^*)^{d-4}$ action with weights q_A^a .

where $|b|$ denotes the Euclidean norm of the vector b and the factor $(2\pi)^4$ comes from integrating over the angles φ_i . This is useful because computing $\text{Vol}_E(P)$ is just a matter of basic linear algebra involving the toric data v_a and the Reeb vector b . Note that the cones over the submanifolds S_a we introduced above (3.33) are precisely the toric divisors and are mapped to the facets of \mathcal{C} via the moment map μ . Hence, the Sasakian volume $\text{Vol}_S(S_a)$ is similarly obtained from the Euclidean volume of the facets P_a of the polytope P

$$\text{Vol}_S(S_a) = \frac{(2\pi)^3}{|b|} \text{Vol}_E(P_a). \quad (6.8)$$

All the discussion so far was true for Sasakian Y_7 . However, in order to implement the GK extremization procedure, we want to depart from this assumption and consider a general Kähler form ω (transverse to the foliation \mathcal{F}_ξ generated by ξ). In particular, the transverse cohomology class of ω can be parametrized by d real parameters $\lambda_a \in \mathbb{R}$ as

$$[\omega] = -2\pi \sum_{a=1}^d \lambda_a c_a, \quad (6.9)$$

where $c_a \in H_B^2(\mathcal{F}_\xi)$ are the Poincaré duals of the toric divisors. The Sasakian case with ω_S is recovered when $\lambda_a = -\frac{1}{2b_1}$ for all $a = 1, \dots, d$. Likewise, the flavour twist is achieved by setting $\lambda_a = -\Lambda$ as in (3.31) for all $a = 1, \dots, d$.³⁰ For now it will be convenient to stick with the general case and we will impose the flavour twist at a later stage. Allowing for a general Kähler class amounts to shifting the facets of the polytope (6.5)

$$P(b) \rightarrow \mathcal{P}(b, \lambda_a) \equiv \left\{ y \in H(b) \mid \sum_{i=1}^4 (y^i - y_*^i) v_{ai} \geq \lambda_a, \quad a = 1, \dots, d \right\}, \quad (6.10)$$

where y_*^i is an arbitrary point in the Reeb hyperplane. For the following, it will be convenient to take

$$y_* = \left(\frac{1}{2b_1}, 0, 0, 0 \right). \quad (6.11)$$

Note that saturating the a^{th} inequality in (6.10) defines the a^{th} facet \mathcal{P}_a . The corresponding generalization of the Sasakian volume (6.7) is the so-called *master volume*

$$\mathcal{V}_7 = \text{Vol}(Y_7) \equiv \int_{Y_7} \eta_7 \wedge \frac{\omega^3}{3!} = \frac{(2\pi)^4}{|b|} \text{Vol}_E(\mathcal{P}), \quad (6.12)$$

³⁰There is a subtlety here that we are slightly glossing over. Since $\dim H_B^2(\mathcal{F}_\xi) = d - 3$, the d parameters λ_a are not uniquely specified in (6.9). There is then a related “gauge invariance”, acting as the shifts $\lambda_a \rightarrow \lambda_a + \sum_{i=1}^4 \gamma^i (v_{ai} b_1 - b_i)$, γ^i being the arbitrary gauge parameters. More precisely then, we recover the flavour twist when there exist a gauge in which $\lambda_a = -\Lambda$.

which itself is a function of the Reeb vector b and the Kähler class parameters λ_a . Concretely, \mathcal{V}_7 can be computed again using basic linear algebra notions (see [9]). The supersymmetric action (3.19), the constraint equation (3.17), and the quantized fluxes (3.18) can all be expressed in terms of \mathcal{V}_7 and its derivatives. We refer to [9, 37] for more details as we will not need these expressions.

Next, note that whenever the cone X_4 is toric, the geometric R-charges (3.35) satisfy the constraints

$$\sum_{a=1}^d R_a \nu_{ai} = \frac{2}{b_1} b_i. \quad (6.13)$$

The $i = 1$ component tells us that the R_a sum to 2, which in turn imposes a constraint on the fluxes

$$\sum_{a=1}^d M_a = p_1 N = (2g - 2)N, \quad (6.14)$$

which is a manifestation of the fact that supersymmetry for these geometries is being implemented via a topological twist over the Riemann surface Σ_g . Moreover, from (6.13) it is possible to express the R-symmetry vector (3.5) in terms of the vectors ν_a in (6.3)

$$\xi = \frac{b_1}{2} \sum_{a=1}^d R_a \nu_a, \quad (6.15)$$

which agrees with (3.45), as it should.

Finally, to connect back to the flavour twist case of interest, we note that the Sasakian volumes can be recovered from \mathcal{V}_7 in the following way

$$\text{Vol}_S(Y_7) = \mathcal{V}_7 \Big|_{\lambda_a = -\frac{1}{2b_1}}, \quad \text{Vol}_S(S_a) = -\frac{1}{2\pi} \frac{\partial \mathcal{V}_7}{\partial \lambda_a} \Big|_{\lambda_a = -\frac{1}{2b_1}}. \quad (6.16)$$

Substituting these expressions into the relevant quantities of section 3.2.3 yields the physical observables in the toric flavour twist case.³¹

6.1.2 Critical points and M2-branes

Recall that the moment map h_M associated to the $U(1)_M$ action defined in (4.17) maps Y_7 to the interval $[\tau_{\min}, \tau_{\max}]$ which gives the support of the eigenvalue density. Let us

³¹In practice we imposed the flavour twist condition before the toric condition. Alternatively, we could have started from the toric expressions for the supersymmetric action, constraint, and flux quantization conditions and imposed the flavour twist by setting λ_a all equal. The two procedures are completely equivalent.

compute h_M explicitly. Firstly, note that for general toric Y_7 we have [37, 51]

$$\partial_{\varphi_i} \lrcorner \omega = -dx^i, \quad (6.17)$$

where $x^i = (y^i - y_*^i)$. Defining ζ_i to be the coefficient of the M-theory killing vector ζ_M in the toric basis, *i.e.* $\zeta_M = \sum_{i=1}^4 \zeta_i \partial_{\varphi_i}$, it follows that

$$h_M(y^i) = \sum_{i=1}^4 \zeta_i (y^i - y_*^i). \quad (6.18)$$

The coefficients ζ_i depend on the particular physical model we consider, and will be specified in each example.

Recall also that the image of h_M is divided in subintervals whose extrema correspond to its value at the critical points, *i.e.* where $dh_M = 0$. In turn such points are those where ζ_M is proportional to ξ , and we can find them explicitly by employing the following strategy. We firstly find all the linear combinations of the form

$$\zeta_M = \beta \xi + \sum_{a \in F} \alpha_a \nu_a, \quad (6.19)$$

where F is any set of toric indices $\{a\}$ such that all the corresponding facets $\{\mathcal{P}_a\}$ have at least one point in common. By definition, in the intersection $\bigcap_{a \in F} \mathcal{P}_a$ all the vectors ν_a with $a \in F$ collapse, and therefore $\zeta_M = \beta \xi$ which is precisely the condition for criticality of h_M . Note that here β could also be vanishing, which signals the presence of D6-branes. In all the examples we look at, the intersection above is either a single point in the toric polytope or one of its edges. Ultimately, the extrema of the subintervals in the image of h_M are obtained by evaluating

$$h_M(y_F), \quad y_F \in \bigcap_{a \in F} \mathcal{P}_a, \quad (6.20)$$

for each set F defined as above, where note that different sets F do not always lead to different points in the image.

Furthermore, we can directly make contact with the M2-brane discussion of section 4.4. In particular, from (4.67) we see that β determines precisely the value of the action of the probe M2-brane, which becomes BPS when it sits at y_F

$$I_{\text{M2}} = \frac{\Lambda}{\ell_p^3} \beta. \quad (6.21)$$

6.1.3 Eigenvalue density

We now want to compute the eigenvalue density as the volume of the quotient space (4.29) for any choice of toric X_4 . In fact, recall that in section 4.3 we stated that

$$\rho(t) \propto \frac{d}{d\Lambda} \text{Vol}(Y_\tau) \Big|_{\tau=\ell_p^3 N^{1/2} t}, \quad (6.22)$$

where Y_τ is defined as a quotient of the τ level set of h_M . In the toric setting we can always follow the strategy we exploited for the two examples considered earlier in section 4.3, and decouple the coordinates $y^i \in \mathbb{R}^4$ with Euclidean metric³² from the angles $\varphi_i \in U(1)^4$, which simply give a contribution of 2π each. Firstly, we note that the polytope (6.10) is the generalization of the tetrahedron defined by $r^2 = 1$ in section 4.3. The shape of such a polytope will depend on the toric data v_a . Saturating the a^{th} inequality, *i.e.*

$$(y^i - y_*^i) v_{ai} = \lambda_a, \quad (6.23)$$

defines the plane where the a^{th} facet \mathcal{P}_a lies, and changing the corresponding Kähler class parameter λ_a amounts to shifting the facet parallel to itself. Upon setting the flavour twist condition $\lambda_a = -\Lambda$, all the facets move together when changing Λ . We then restrict to the level set of the moment map (6.18) imposing

$$(y^i - y_*^i) \zeta_i = \tau. \quad (6.24)$$

This equation describes a hyperplane in \mathbb{R}^4 which slices the polytope \mathcal{P} . The intersection of the two will be a polygon \mathcal{Q}_τ whose shape depends on the value of τ and whose Euclidean area determines directly the volume we are interested in

$$\text{Vol}(Y_\tau) = (2\pi)^3 \text{Vol}_E(\mathcal{Q}_\tau). \quad (6.25)$$

Every time the plane (6.24) crosses a vertex or an edge of the polytope, the expression for $\text{Vol}_E(\mathcal{Q}_\tau)$ changes, hence it is clear that these correspond to the discontinuity points in the derivative of the density, *i.e.* the critical points of the previous subsection. Note that here we have a clear geometric interpretation of what it means taking the derivative with respect to Λ in (6.22): given what we said below (6.23), it is clear that $\frac{d}{d\Lambda} \text{Vol}_E(\mathcal{Q}_\tau)$ is (proportional to) the length of the perimeter of the polygon \mathcal{Q}_τ .

³²Differently from section 4.3, here the Kähler class parameter is absorbed into the coordinates y^i . This has some repercussions on the normalization of quantities. In particular, this is why we distinguish \mathcal{Q}_τ from Q_τ (see (6.25) versus (4.36)) which are otherwise conceptually the same quantity.

In general, for a fixed τ a vertex $q_{ab} \in \mathbb{R}^4$ of \mathcal{Q}_τ is computed by imposing simultaneously two equations like (6.23) for adjacent facets \mathcal{P}_a and \mathcal{P}_b , the Reeb hyperplane condition $y \in H(b)$, and the moment map level set in (6.24)

$$\begin{aligned} (q_{ab}^i - y_*^i) v_{ai} &= -\Lambda, \\ (q_{ab}^i - y_*^i) v_{bi} &= -\Lambda, \\ (q_{ab}^i - y_*^i) b_i &= 0, \\ (q_{ab}^i - y_*^i) \zeta_i &= \tau. \end{aligned} \tag{6.26}$$

These are four linear equations for four variables q_{ab}^i , $i = 1, \dots, 4$, hence the vertices of \mathcal{Q}_τ are uniquely determined in terms of Λ , τ and b (for fixed examples v_a and ζ are fixed)³³, and we pick $y_* = (1/2b_1, 0, 0, 0)$ for convenience. This system should be solved for any pair of adjacent facets. Note that it may not admit any solution, for certain pairs, indicating that the moment map hyperplane cuts the polytope parallel to the edge between these two facets. Further imposing that the solution indeed lies inside the polytope

$$(q_{ab}^i - y_*^i) v_{ci} \geq -\Lambda, \quad \forall c = 1, \dots, d \tag{6.27}$$

gives the range of τ for which q_{ab} is a vertex of \mathcal{Q}_τ . Therefore the set of vertices of \mathcal{Q}_τ , and consequently the expression for its perimeter (which recall is the quantity identified with the eigenvalue density ρ), changes on each such interval of τ . Once the sets of vertices are found, the surface area of \mathcal{Q}_τ on each interval can be computed by splitting it into triangles and computing the area of each triangle as a determinant as we did in the examples in section 4.3. More concretely, let us call ζ the vector in \mathbb{R}^4 with components ζ_i and introduce

$$\zeta_\perp \equiv \zeta - \frac{\zeta \cdot b}{|b|^2} b. \tag{6.28}$$

This is the equivalent of (4.38) but all the vectors here are expressed in toric coordinates. Then, the area of a triangle with vertices $q_{a_1 a_2}, q_{a_3 a_4}, q_{a_5 a_6} \in \mathbb{R}^4$ can be computed as

$$\frac{1}{2} \left| \det \left(\frac{b}{|b|}, \frac{\zeta_\perp}{|\zeta_\perp|}, q_{a_3 a_4} - q_{a_1 a_2}, q_{a_5 a_6} - q_{a_1 a_2} \right) \right|, \tag{6.29}$$

and $\text{Vol}_E(\mathcal{Q}_\tau)$ will be a finite sum of such determinants. Note that it is crucial to have ζ_\perp rather than ζ in (6.29) because only ζ_\perp is orthogonal to both the triangle and to

³³Note that in the examples we will express b in terms of geometrical R-charges R , as in (6.15), for better comparison with the dual field theory results.

b , so that the volume of the parallelotope computed by the determinant is simply the area of the triangle times the length of the two “heights”, which are both 1. We refer the reader to the examples in the next subsections to see how this procedure works more concretely.

Finally, let us highlight that we are now able to justify the normalization in (4.39). Let us compute the integral of the RHS of (6.22)

$$\mathcal{I} \equiv \int_{t_{\min}}^{t_{\max}} dt \frac{d}{d\Lambda} \text{Vol}(Y_\tau) = \frac{(2\pi)^3}{\ell_p^3 N^{1/2}} \frac{d}{d\Lambda} \int_{\tau_{\min}}^{\tau_{\max}} d\tau \text{Vol}_E(\mathcal{Q}_\tau), \quad (6.30)$$

where in the last step we exchanged the integral and the derivative and changed the variable of integration from t to τ . Now the integral above with a suitable measure is nothing but the volume of the entire polytope \mathcal{P} , which can be expressed in terms of the master volume \mathcal{V}_7

$$\int_{\tau_{\min}}^{\tau_{\max}} \frac{d\tau}{|\zeta_\perp|} \text{Vol}_E(\mathcal{Q}_\tau) = \text{Vol}_E(\mathcal{P}) = \frac{|b|}{(2\pi)^4} \mathcal{V}_7. \quad (6.31)$$

Substituting this back into (6.30) we obtain

$$\mathcal{I} = \frac{|b||\zeta_\perp|}{2\pi\ell_p^3 N^{1/2}} \frac{d\mathcal{V}_7}{d\Lambda} = \frac{|b||\zeta_\perp|}{2\pi\ell_p^3 N^{1/2}} (2\pi\ell_p)^6 N, \quad (6.32)$$

where the second equality is the toric equivalent of the flux quantization (3.29) [9]. Hence, the correct normalization for (6.22) is

$$\rho(t) = \frac{1}{\mathcal{I}} \frac{d}{d\Lambda} \text{Vol}(Y_\tau) \Big|_{\tau=\ell_p^3 N^{1/2} t} = \frac{1}{32\pi^5 \ell_p^3 N^{1/2} |b||\zeta_\perp|} \frac{d}{d\Lambda} \text{Vol}(Y_\tau) \Big|_{\tau=\ell_p^3 N^{1/2} t}, \quad (6.33)$$

which is exactly what we had in (4.39). If Y_7 is a quotient space by a \mathbb{Z}_n action, similarly to section 4, there is an additional factor of n relating the volumes of Y_τ and \mathcal{Q}_τ (the unquotiented case is $n = 1$), and the final expression for ρ reads

$$\rho(t) = \frac{1}{4\pi^2 \ell_p^3 N^{1/2} |b||\zeta_\perp| n} \frac{d}{d\Lambda} \text{Vol}(\mathcal{Q}_\tau) \Big|_{\tau=\ell_p^3 N^{1/2} t}. \quad (6.34)$$

6.2 Example: $C(Y_7) = \mathbb{C} \times C(T^{1,1})$

We now illustrate the procedure outlined in the previous subsection on the toric cone $X_4 = \mathbb{C} \times C(T^{1,1})$, which admits two field theory duals depending on the choice of the

M-theory circle action. First let us describe some properties of this geometry. The toric vectors are

$$\begin{aligned} v_1 &= (1, 0, 0, 0), & v_2 &= (1, 0, 0, 1), & v_3 &= (1, 0, 1, 1), \\ v_4 &= (1, 0, 1, 0), & v_5 &= (1, 1, 0, 0), \end{aligned} \tag{6.35}$$

and the corresponding toric diagram is shown in Figure 8. A subtle point to address is that the space Y_7 has a singularity and therefore computing the master volume naively leads to the wrong result. As discussed in [9] this is fixed by imposing a restriction on the Kähler class parameters

$$\lambda_1 - \lambda_2 + \lambda_3 - \lambda_4 = 0. \tag{6.36}$$

Incidentally, this constraint also enforces the flavour twist condition (3.28), which is precisely what we need to compare with field theory results. The Sasakian volume of the link Y_7 of $\mathbb{C} \times C(T^{1,1})$ is

$$\text{Vol}_S(Y_7) = \frac{\pi^4(b_1 - b_2)}{3b_2b_3b_4(b_1 - b_2 - b_3)(b_1 - b_2 - b_4)}. \tag{6.37}$$

The geometric R-charges are

$$\begin{aligned} R_1 &= \frac{2(b_1 - b_2 - b_3)(b_1 - b_2 - b_4)}{b_1(b_1 - b_2)}, & R_2 &= \frac{2b_4(b_1 - b_2 - b_3)}{b_1(b_1 - b_2)}, \\ R_3 &= \frac{2b_3b_4}{b_1(b_1 - b_2)}, & R_4 &= \frac{2b_3(b_1 - b_2 - b_4)}{b_1(b_1 - b_2)}, & R_5 &= \frac{2b_2}{b_1}, \end{aligned} \tag{6.38}$$

so they satisfy

$$\sum_{a=1}^5 R_a = 2, \quad R_1R_3 - R_2R_4 = 0. \tag{6.39}$$

Note that the second constraint implements the partial extremization over the baryonic directions in field theory. Finally, the Kähler class parameter defined in (3.31) can be expressed in terms of the R-charges as

$$\Lambda = \frac{\ell_p^3 N^{1/2} \pi}{2} \sqrt{\frac{2(R_1 + R_2)(R_3 + R_4)(R_1 + R_4)(R_2 + R_3)R_5}{R_1 + R_2 + R_3 + R_4}}. \tag{6.40}$$

Notice that the denominator may also be expressed as $2 - R_5$.

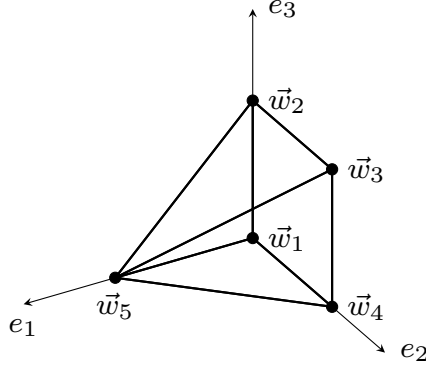


Figure 8: Toric diagram for $\mathbb{C} \times C(T^{1,1})$.

6.2.1 Flavoured $U(N)$

Geometry The first choice of $U(1)_M$ action we consider has weights $(1, -1, 0, 0, 0)$ on the complex coordinates z_a in the ambient space of the GIT quotient defining X_4 (see footnote 29), which are rotated by $\partial_{\phi_a} \equiv \nu_a = \sum_i v_{ai} \partial_{\varphi_i}$ [27]. Using the toric data (6.35), the M-theory circle action on X_4 therefore reads

$$\zeta_M = -\partial_{\varphi_4}. \quad (6.41)$$

For this choice of ζ_M and toric data (6.35), (6.19) admits two non-trivial solutions for β ,³⁴ which we multiply by Λ to obtain τ

$$\tau_{\min} = -\frac{2\Lambda}{R_2 + R_3}, \quad \tau_{\max} = \frac{2\Lambda}{R_1 + R_4}. \quad (6.42)$$

The non-zero α_a coefficients for these solutions are $\{\alpha_1, \alpha_4, \alpha_5\}$ and $\{\alpha_2, \alpha_3, \alpha_5\}$ respectively, which is reflected by the vertices in Figure 9. Note that $\beta = \tau/\Lambda = 0$ is also a solution for either $\{\alpha_1, \alpha_2\}$ or $\{\alpha_3, \alpha_4\}$ non-vanishing. Recall that these results also correspond to the action of BPS M2-branes via (4.69).

Next we want to obtain the full distribution ρ by solving the system (6.26). We find solutions for $\{q_{14}, q_{15}, q_{45}, q_{23}, q_{25}, q_{35}\}$. We do not report the explicit expressions of the vertices as they are not particularly insightful. They have a similar structure to the ones presented in the examples of section 4.3. Further imposing the inequalities (6.27), we find that the first three solutions are the vertices of \mathcal{Q}_τ for $\tau \in [\tau_{\min}, 0]$, while the last three define \mathcal{Q}_τ for $\tau \in [0, \tau_{\max}]$, where we reproduce the expression of τ_{\min}, τ_{\max} in (6.42). \mathcal{Q}_τ is therefore a triangle in both regions, and its area can be

³⁴In practice we solve the system in terms of b_i and then convert the results in the R_a variables using (6.38).

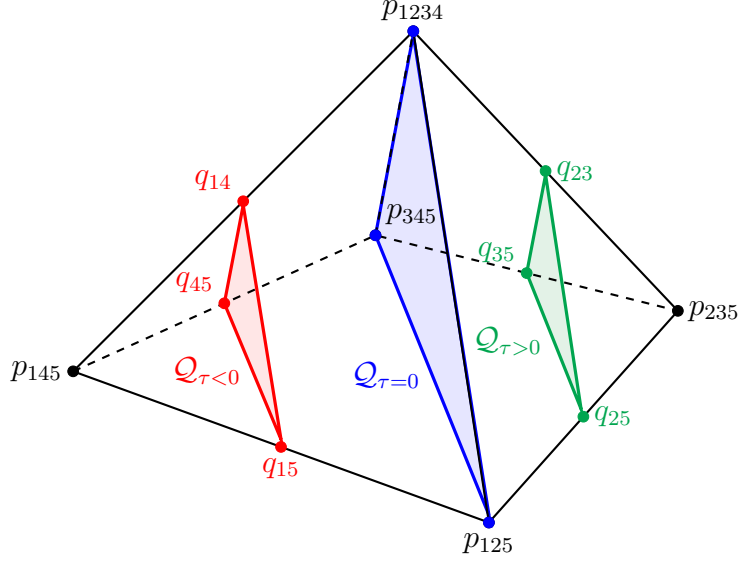


Figure 9: Pyramid describing $\mathbb{C} \times C(T^{1,1})$ and its slicing corresponding to flavoured $U(N)$. The red slice is \mathcal{Q}_τ for $\tau_{\min} < \tau < 0$, the blue slice for $\tau = 0$, and the green slice for $0 < \tau < \tau_{\max}$. Each vertex p_{abc} denotes the intersection of the facets \mathcal{P}_a , \mathcal{P}_b , \mathcal{P}_c , and the Reeb hyperplane. The perimeter of \mathcal{Q}_τ varies with τ qualitatively as ρ in Figure 3.

computed via the determinant (6.29) first for $\{q_{14}, q_{15}, q_{45}\}$ and then for $\{q_{23}, q_{25}, q_{35}\}$, see Figure 9. Finally taking the Λ derivative to obtain the perimeter and normalizing by the appropriate factor (6.34) gives the geometrical density

$$\rho(t) = \frac{1}{\ell_p^3 N^{1/2}} \left\{ \begin{array}{l} \frac{2\Lambda + (R_2 + R_3)\tau}{\pi^2(R_1 + R_2)(R_3 + R_4)R_5}, \quad \tau_{\min} < \tau < 0 \\ \frac{2\Lambda - (R_1 + R_4)\tau}{\pi^2(R_1 + R_2)(R_3 + R_4)R_5}, \quad 0 < \tau < \tau_{\max} \end{array} \right\} \Bigg|_{\tau = \ell_p^3 N^{1/2} t}. \quad (6.43)$$

Field theory The dual field theory to this geometry is a flavoured $U(N)$ theory which contains two pairs of fundamental chiral fields $\{Q^{(1)}, \tilde{Q}^{(1)}\}$, $\{Q^{(2)}, \tilde{Q}^{(2)}\}$ and three adjoint chiral fields Φ_i , $i = 1, 2, 3$, see Figure 10, and has superpotential

$$W = \text{Tr} \left[\Phi_1[\Phi_2, \Phi_3] + \tilde{Q}^{(1)}\Phi_1 Q^{(1)} + \tilde{Q}^{(2)}\Phi_2 Q^{(2)} \right], \quad (6.44)$$

such that

$$T\tilde{T} = \Phi_1\Phi_2 \implies \Delta_T + \Delta_{\tilde{T}} = \Delta_{\Phi_1} + \Delta_{\Phi_2}. \quad (6.45)$$

The results can be derived from the Bethe potential given in Appendix A, and read [19]

$$t_{\min} = -\frac{\mu}{\Delta_{\tilde{T}}}, \quad t_{\max} = \frac{\mu}{\Delta_T}, \quad (6.46)$$

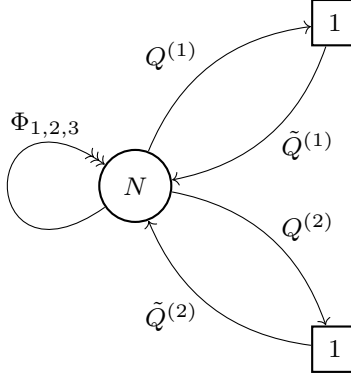


Figure 10: Quiver diagram of the flavoured $U(N)$ theory.

$$\rho(t) = \begin{cases} \frac{\mu + \Delta_{\tilde{T}} t}{\pi^2 \Delta_{\Phi_1} \Delta_{\Phi_2} \Delta_{\Phi_3}}, & t_{\min} < t < 0, \\ \frac{\mu - \Delta_T t}{\pi^2 \Delta_{\Phi_1} \Delta_{\Phi_2} \Delta_{\Phi_3}}, & 0 < t < t_{\max}, \end{cases}, \quad (6.47)$$

with

$$\mu = \pi \sqrt{\frac{2\Delta_{\Phi_1} \Delta_{\Phi_2} \Delta_{\Phi_3} \Delta_T \Delta_{\tilde{T}}}{\Delta_{\Phi_T} + \Delta_{\Phi_{\tilde{T}}}}}. \quad (6.48)$$

Matching The field theory and geometrical parameters are related as [9]

$$\begin{aligned} \Delta_{\Phi_1} &= R_1 + R_2, & \Delta_{\Phi_2} &= R_3 + R_4, & \Delta_{\Phi_3} &= R_5, \\ \Delta_T &= R_1 + R_4, & \Delta_{\tilde{T}} &= R_2 + R_3. \end{aligned} \quad (6.49)$$

As expected, under this identification, $\mu = 2\Lambda/(\ell_p^3 N^{1/2})$. It is then easy to see that the discontinuity points of $\rho'(t)$ match, and also that we reproduce $\rho(t)$.

6.2.2 Flavoured ABJM

Geometry A second possible choice of $U(1)_M$ is to have weights $(1, 0, 0, 0, -1)$ on z_a , which using the toric data (6.35) reads on the cone

$$\zeta_M = -\partial_{\varphi_2}. \quad (6.50)$$

In the following we assume $R_4 < R_2$. Solving (6.19) for this choice of M-theory circle gives four solutions (recall $\tau = \Lambda\beta$)

$$\tau_1 = -\frac{2\Lambda}{R_5}, \quad \tau_2 = 0, \quad \tau_3 = \frac{2\Lambda}{R_1 + R_2}, \quad \tau_4 = \frac{2\Lambda}{R_1 + R_4}, \quad (6.51)$$

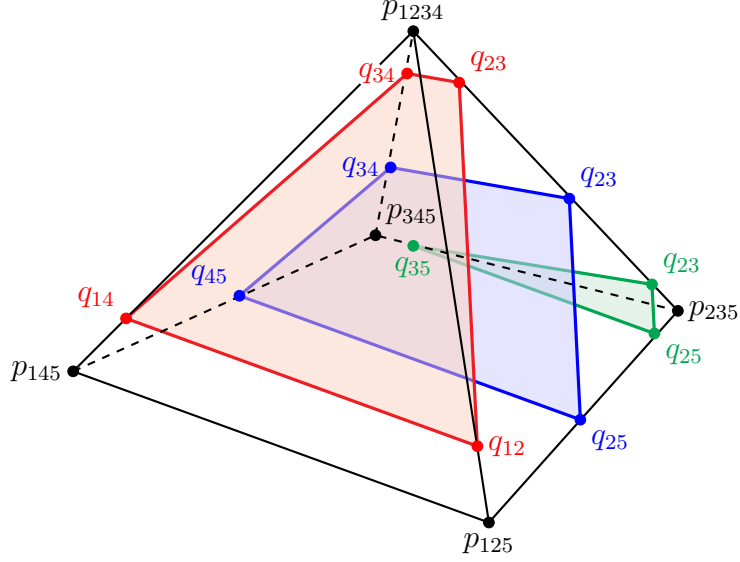


Figure 11: Pyramid describing $\mathbb{C} \times C(T^{1,1})$ and its slicing corresponding to flavoured ABJM. The red slice is \mathcal{Q}_τ for $\tau_1 < \tau < \tau_2$, the blue slice for $\tau_2 < \tau < \tau_3$, and the green slice for $\tau_3 < \tau < \tau_4$. Each vertex p_{abc} denotes the intersection of the facets $\mathcal{P}_a, \mathcal{P}_b, \mathcal{P}_c$, and the Reeb hyperplane. Note that we do not draw the slice at $\tau = \tau_2 = 0$, where $q_{14} = q_{45} = p_{145}$ and $q_{12} = q_{25} = p_{125}$. The perimeter of \mathcal{Q}_τ varies with τ qualitatively as ρ in Figure 18.

and associated non-zero $\alpha_a, \{\alpha_1, \alpha_2, \alpha_3, \alpha_4\}, \{\alpha_1, \alpha_5\}, \{\alpha_3, \alpha_4, \alpha_5\}, \{\alpha_2, \alpha_3, \alpha_5\}$, respectively, as clearly appears in Figure 11. Physically these results correspond to the value of the action of BPS probe M2-branes.

To reproduce ρ we turn to the system (6.26), which in this case admits solutions for any pair of neighbouring v_a , except for q_{15} . The M-theory hyperplane therefore slices the toric polytope parallel to the edge between \mathcal{P}_1 and \mathcal{P}_5 as shown in Figure 11. Then from the inequalities (6.27), we find that \mathcal{Q}_τ has vertices $\{q_{12}, q_{23}, q_{34}, q_{14}\}, \{q_{25}, q_{23}, q_{34}, q_{45}\}, \{q_{25}, q_{23}, q_{35}\}$ in the regions $[\tau_1, \tau_2], [\tau_2, \tau_3], [\tau_3, \tau_4]$ respectively, where we recover the values of τ from (6.51). In the regions where \mathcal{Q}_τ is quadrilateral the area is computed by splitting into two triangles, and summing the two areas computed via the determinant (6.29). After taking the derivative and normalizing properly, see (6.34), we deduce that the density is given by

$$\rho(t) = \frac{1}{\ell_p^3 N^{1/2}} \left\{ \begin{array}{ll} \frac{4\Lambda + 2R_5\tau}{\pi^2(R_2+R_3)(R_3+R_4)(R_1+R_5+R_2)(R_1+R_5+R_4)}, & \tau_1 < \tau < \tau_2 \\ \frac{4\Lambda - (2R_1+R_2R_4-R_3(R_1+R_5))\tau}{\pi^2(R_2+R_3)(R_3+R_4)(R_1+R_5+R_2)(R_1+R_5+R_4)}, & \tau_2 < \tau < \tau_3 \\ \frac{2\Lambda - (R_1+R_4)\tau}{\pi^2(R_2-R_4)(R_4+R_3)(R_1+R_5+R_4)}, & \tau_3 < \tau < \tau_4 \end{array} \right\} \Big|_{\tau = \ell_p^3 N^{1/2} t}. \quad (6.52)$$

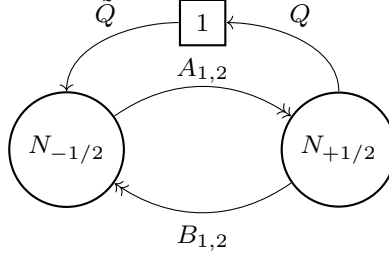


Figure 12: Quiver diagram for the flavoured ABJM theory.

Field theory The field theory dual to $X_4 = \mathbb{C} \times C(T^{1,1})$ equipped with the M-theory circle (6.50) is an instance of the flavoured ABJM theory. That is the Model II with an additional pair of fundamental chiral fields (Q, \tilde{Q}) and with Chern-Simons level $(-1/2, 1/2)$ [27].³⁵ The quiver diagram is shown in Figure 12. The superpotential is the ABJM superpotential, plus a deformation term

$$W = \text{Tr} \left[A_1 B_1 A_2 B_2 - A_1 B_2 A_2 B_1 + Q A_1 \tilde{Q} \right], \quad (6.53)$$

$$T\tilde{T} = A_1 \implies \Delta_T + \Delta_{\tilde{T}} = \Delta_{A_1}. \quad (6.54)$$

The results are derived in Appendix A, assuming $\Delta_{B_1} < \Delta_{B_2}$:

$$\begin{aligned} t_1 &= -\frac{\mu}{\Delta_{\tilde{T}}}, & t_2 &= 0, \\ t_3 &= \frac{\mu}{\Delta_T + \Delta_{B_2}}, & t_4 &= \frac{\mu}{\Delta_T + \Delta_{B_1}}. \end{aligned} \quad (6.55)$$

$$\rho(t) = \begin{cases} \frac{2\mu + 2\Delta_{\tilde{T}}t}{\pi^2(\Delta_{A_1} + \Delta_{B_1})(\Delta_{A_1} + \Delta_{B_2})(\Delta_{A_2} + \Delta_{B_1})(\Delta_{A_2} + \Delta_{B_2})}, & t_1 < t < t_2, \\ \frac{2\mu - (2\Delta_T + \Delta_{B_1}\Delta_{B_2} - \Delta_{A_1}\Delta_{A_2})t}{\pi^2(\Delta_{A_1} + \Delta_{B_1})(\Delta_{A_1} + \Delta_{B_2})(\Delta_{A_2} + \Delta_{B_1})(\Delta_{A_2} + \Delta_{B_2})}, & t_2 < t < t_3, \\ \frac{\mu - (\Delta_T + \Delta_{B_1})t}{\pi^2(\Delta_{A_1} + \Delta_{B_1})(\Delta_{A_2} + \Delta_{B_1})(\Delta_{B_2} - \Delta_{B_1})}, & t_3 < t < t_4. \end{cases} \quad (6.56)$$

$$\mu = \pi \sqrt{\frac{2(\Delta_{A_2} + \Delta_{B_1})(\Delta_{A_2} + \Delta_{B_2})(\Delta_T + \Delta_{B_1})(\Delta_T + \Delta_{B_2})\Delta_{\tilde{T}}}{2 - \Delta_{\tilde{T}}}}. \quad (6.57)$$

³⁵The half-integer level is needed to cancel the parity anomaly due to the additional pair of chiral fields. Note that we exchange k and $-k$ compared to [27], according to the prescription in table 1 of [18].

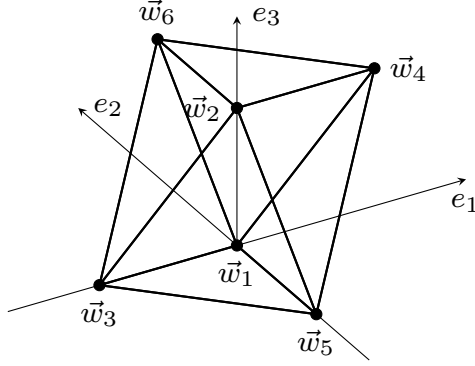


Figure 13: Toric diagram for $Q^{1,1,1}$.

Matching Finally, the parameters on both sides are related by [10]³⁶

$$\begin{aligned} \Delta_{A_1} = R_1 + R_5, \quad \Delta_{A_2} = R_3, \quad \Delta_{B_1} = R_4, \quad \Delta_{B_2} = R_2, \\ \Delta_T = R_1, \quad \Delta_{\bar{T}} = R_5, \end{aligned} \quad (6.58)$$

such that again, $\mu = 2\Lambda/(\ell_p^3 N^{1/2})$, t and τ match and we exactly reproduce ρ in the geometry. Note that the orderings we assumed on each side, namely $R_4 < R_2$ and $\Delta_{B_1} < \Delta_{B_2}$, are equivalent.

6.3 Example: $Y_7 = Q^{1,1,1}/\mathbb{Z}_n$

A second example of a toric cone is $Y_7 = Q^{1,1,1}/\mathbb{Z}_n$. Here we denote the quotient by \mathbb{Z}_n , rather than \mathbb{Z}_k , since in this case the positive integer n is the number of flavours (D6-branes), rather than a Chern-Simons level (RR two-form flux). The toric data are given by the following, with the toric diagram shown in Figure 13:

$$\begin{aligned} v_1 = (1, 0, 0, 0), \quad v_2 = (1, 0, 0, 1), \quad v_3 = (1, -1, 0, 0), \\ v_4 = (1, 1, 0, 1), \quad v_5 = (1, 0, -1, 0), \quad v_6 = (1, 0, 1, 1). \end{aligned} \quad (6.59)$$

We will consider the simplifying ansatz of [9] for the Reeb vector

$$b = (1, 0, b_3, 1/2 + b_3). \quad (6.60)$$

In this case we have

$$\text{Vol}_S(Q^{1,1,1}/\mathbb{Z}_n) = \frac{32\pi^4}{3n} \frac{3 - 4b_3^2}{(1 - 4b_3^2)^2}. \quad (6.61)$$

³⁶Note we used a different toric basis from [10]. In particular, we have $R_1 = \Delta_1^{\text{there}}$, $R_2 = \Delta_3^{\text{there}}$, $R_3 = \Delta_5^{\text{there}}$, $R_4 = \Delta_2^{\text{there}}$, $R_5 = \Delta_4^{\text{there}}$.

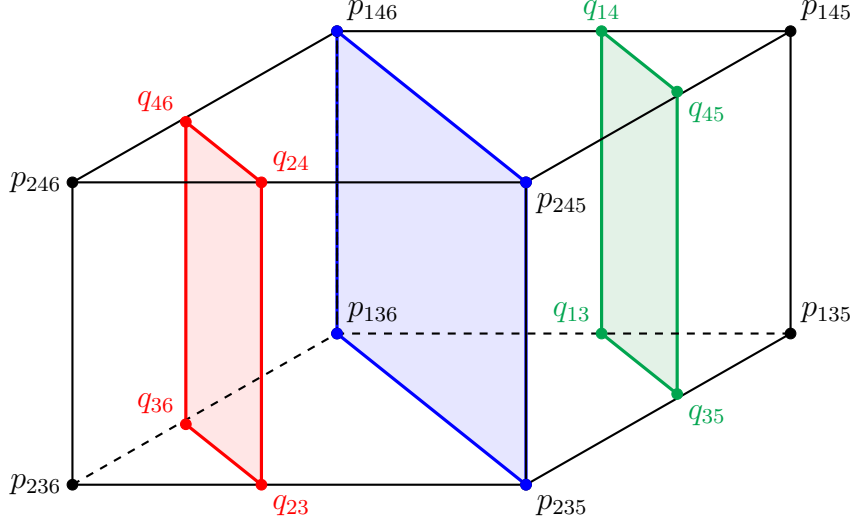


Figure 14: Polytope describing $Q^{1,1,1}$ and its slicing corresponding to flavoured ABJM. The red slice is \mathcal{Q}_τ for $\tau_{\min} < \tau < 0$, the blue slice for $\tau = 0$, and the green slice for $0 < \tau < \tau_{\max}$. Each vertex p_{abc} denotes the intersection of the facets $\mathcal{P}_a, \mathcal{P}_b, \mathcal{P}_c$, and the Reeb hyperplane. Note that \mathcal{Q}_τ is not 0 at $\tau_{\min, \max}$ but an edge of the polytope.

The expressions for the geometrical R-charges in terms of b_3 can be found in [9]. We do not need them here and only notice that their positivity imposes $|b_3| \leq 1/2$. Finally we record that

$$\Lambda = \frac{\ell_p^3 N^{1/2} \pi}{2} \sqrt{n} \frac{1 - 4b_3^2}{\sqrt{3 - 4b_3^2}}. \quad (6.62)$$

6.3.1 Flavoured ABJM

Geometry We pick a $U(1)_M$ action with weights $(-1, 0, 0, 0, 0, 1)$ on the coordinates of the ambient space, which using the toric data (6.59) reads on $Q^{1,1,1}/\mathbb{Z}_n$

$$\zeta_M = \frac{1}{n} (\partial_{\varphi_3} + \partial_{\varphi_4}). \quad (6.63)$$

Then the equation (6.19) admits two³⁷ non-trivial solutions for $\beta = \tau/\Lambda$ (corresponding to BPS M2-brane actions) with non-vanishing $\{\alpha_2, \alpha_6\}$ and $\{\alpha_1, \alpha_5\}$ respectively, which read

$$\tau_{\min} = -\frac{2\Lambda}{n - 2nb_3}, \quad \tau_{\max} = \frac{2\Lambda}{n + 2nb_3}. \quad (6.64)$$

It also admits $\beta = 0$ as a solution with either $\{\alpha_2, \alpha_5\}$ or $\{\alpha_1, \alpha_6\}$ non-zero, as can be observed in Figure 14.

³⁷Actually for general b there are four solutions, which degenerate to these two under the ansatz (6.60).

The system (6.26) has solutions $\{q_{23}, q_{24}, q_{46}, q_{36}\}$ and $\{q_{13}, q_{35}, q_{45}, q_{14}\}$ which, according to the inequalities (6.27) are the vertices of \mathcal{Q}_τ for τ in $[\tau_{\min}, 0]$ and $[0, \tau_{\max}]$ respectively (see Figure 14), reproducing $\tau_{\min, \max}$ given above. The volume of \mathcal{Q}_τ is computed on each region by splitting the quadrilateral into two triangles whose areas are the determinant (6.29). Taking the derivative with respect to Λ and normalizing as in (6.34), we eventually obtain

$$\rho(t) = \frac{1}{\ell_p^3 N^{1/2}} \left\{ \begin{array}{ll} \frac{4\Lambda + (n - 4nb_3)\tau}{\pi^2}, & \tau_{\min} < \tau < 0 \\ \frac{4\Lambda - (n + 4nb_3)\tau}{\pi^2}, & 0 < \tau < \tau_{\max} \end{array} \right\}_{\tau = \ell_p^3 N^{1/2} t}. \quad (6.65)$$

Field Theory The field theory dual is a flavoured ABJM theory with two sets of pairs of fundamental chiral fields $\{Q_j^{(1)}, \tilde{Q}_j^{(1)}\}$, $\{Q_j^{(2)}, \tilde{Q}_j^{(2)}\}$, $j = 1, \dots, n$, and Chern-Simons level 0, see Figure 15. It has the superpotential

$$W = \text{Tr} \left[A_1 B_1 A_2 B_2 - A_1 B_2 A_2 B_1 + \sum_{j=1}^n Q_j^{(1)} A_1 \tilde{Q}_j^{(1)} + \sum_{j=1}^n Q_j^{(2)} A_2 \tilde{Q}_j^{(2)} \right], \quad (6.66)$$

and the monopole operators obey the relations

$$T\tilde{T} = A_1^n A_2^n \implies \Delta_T + \Delta_{\tilde{T}} = n(\Delta_{A_1} + \Delta_{A_2}). \quad (6.67)$$

In terms of these variables the chemical potential for the topological symmetry is

$$\Delta_m = -\frac{1}{2}(\Delta_T - \Delta_{\tilde{T}}). \quad (6.68)$$

The results of interest have been obtained in [19], as explained in Appendix A, and read³⁸

$$t_{\min} = -\frac{\mu}{n + \Delta_m}, \quad t_{\max} = \frac{\mu}{n - \Delta_m}, \quad (6.69)$$

$$\rho(t) = \begin{cases} \frac{2\mu + (n + 2\Delta_m)t}{\pi^2}, & t_{\min} < t < 0, \\ \frac{2\mu - (n - 2\Delta_m)t}{\pi^2}, & 0 < t < t_{\max}, \end{cases} \quad (6.70)$$

with

$$\mu = \frac{\pi}{\sqrt{n}} \frac{|n^2 - \Delta_m^2|}{\sqrt{3n^2 - \Delta_m^2}}. \quad (6.71)$$

Note that $\rho(t_{\min, \max}) \neq 0$, in accordance with the geometric picture.

³⁸Fixing a typo in the sign of Δ_m .

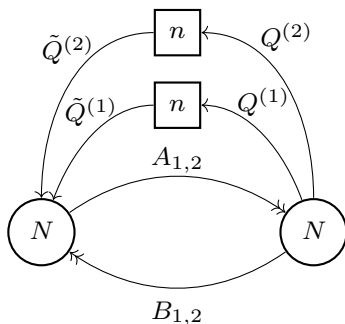


Figure 15: Quiver diagram for the flavoured ABJM theory.

Matching There is one parameter on each side that are related via [9]

$$-\Delta_m = 2nb_3. \quad (6.72)$$

Again under this identification $\mu = 2\Lambda/(\ell_p^3 N^{1/2})$ and $\rho(t)$ is correctly reproduced in the geometry. An interesting observation is that the postivity of the geometrical R-charges, which implies that $|b_3| \leq 1/2$ gives the constraint $|\Delta_m| \leq n$ (such that we could drop the absolute value in μ).

7 Discussion

In this paper we have further studied the relationship between a class of supersymmetric, magnetically charged (and potentially accelerating) black holes in M-theory, and their dual matrix model description. The matching between entropy functions on the two sides (for classes of examples) had already been established in [9, 10]. More recently, a gravitational block formula for the entropy function of accelerating black holes (5.11) was proven in [14, 15] (see also [46]). One observation we have made in this paper is that the gravity formula (5.11) in GK geometry may already be matched to the refined twisted index field theory results in [20], on setting $m_+ = m_- = 1$ so that the spindle horizon becomes simply S^2 . Similarly, the actions of BPS probe M2-branes at the poles of this S^2 then also match with points where the eigenvalue density derivatives ρ'_\pm for the two blocks in the matrix model are discontinuous. These results extend straightforwardly to the accelerating case with a spindle on the gravity side, and it will be fascinating to match the large N limit of the spindle index of [24] to the gravitational results in GK geometry we have presented here.

Perhaps the most interesting open question is to further match quantities in the matrix model to quantities in gravity. For example, it seems likely that there is also

a simple geometric characterization of the fluxes $\mathfrak{s}(t)$. But one also expects a more direct holographic interpretation of these variables, and of the density function $\rho(t)$. The analogous quantity on S^3 was interpreted in [23] in terms of counting operators in the chiral ring of the gauge theory. However, the present paper perhaps suggests a more direct physical interpretation on the gravity side. Specifically, the near-horizon solutions are sourced by N M2-branes, where in AdS/CFT the brane sources disappear and are replaced by N units of dissolved flux over the internal space. On the other hand, in type IIA we have N D2-branes, where $h_M = \tau = \ell_p N^{1/2} t$ is the location of the D2-branes (before the back-reaction and near-horizon limit). This suggests that the eigenvalue density $\rho(t)$ is also playing the role of a density function directly in the gravity dual, describing how the dissolved D2/M2-branes are distributed in the internal space. We leave this speculation, and other questions, for future work.

Acknowledgements

We thank Nikolay Bobev, Pieter Bomans, Matteo Sacchi, and Seyed Morteza Hosseini for helpful discussions. This work was supported in part by STFC grant ST/T000864/1. AL is supported by the Palmer scholarship in Mathematical Physics of Merton college.

A Bethe potential at large N

In this appendix we review the expression for the Bethe potential of topologically twisted Chern-Simons-matter theories at large N , derived in [18]. We focus on flavoured $U(N)$ and ABJM theories, reproducing and completing the discussion of [19] (and fixing some minor typographical errors).

At leading order in N the Bethe potential consists of contributions coming from the various gauge and matter content of the theory³⁹

$$\mathcal{U} = \mathcal{U}^{\text{Gauge}} + \mathcal{U}^{\text{Bifund}} + \mathcal{U}^{\text{Flavour}} . \quad (\text{A.1})$$

For theories with gauge group $\mathcal{G} = \prod_{a=1}^{\mathcal{G}} U(N)_{k_a}$ with $\sum_{a=1}^{\mathcal{G}} k_a = 0$ such that they have an M-theory dual,

$$\mathcal{U}^{\text{Gauge}} = -iN^{3/2} \int dt t \rho(t) \sum_{a=1}^{\mathcal{G}} (k_a v_a(t) + \pi \Delta_m^{(a)}) , \quad (\text{A.2})$$

³⁹There are additional bifundamental contributions to the following equation that are subleading in N . Their role is discussed in [2], but we do not need to consider them in this work.

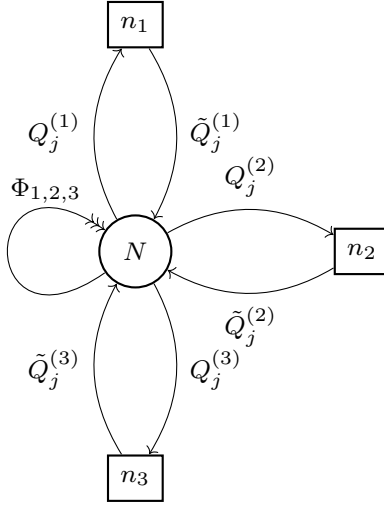


Figure 16: Quiver diagram for the flavoured $U(N)$ theory.

where $\Delta_m^{(a)}$ is the chemical potential of the topological symmetry of $U(N)_{k_a}$. We write $\Delta_m = \sum_a \Delta_m^{(a)}$ in terms of variables $\Delta_T, \Delta_{\tilde{T}}$, identified with the R-charges on S^3 of the diagonal monopole operators, via

$$\Delta_m = -\frac{1}{2}(\Delta_T - \Delta_{\tilde{T}}). \quad (\text{A.3})$$

The general expressions of $\mathcal{U}^{\text{Bifund}}$ and $\mathcal{U}^{\text{Flavour}}$ are given in [18]. Here we want to state their simplification (together with that for $\mathcal{U}^{\text{Gauge}}$) in the special cases of $\mathcal{G} = U(N)$ and $\mathcal{G} = U(N)_k \times U(N)_{-k}$, from which all the examples of the present paper can be recovered.

A.1 Flavoured $U(N)$ theories

A general flavoured $U(N)$ theory contains three sets of pairs of fundamental chiral fields $\{Q_j^{(i)}, \tilde{Q}_j^{(i)}\}_{j=1}^{n_i}$, and three adjoint chiral fields Φ_i , $i = 1, 2, 3$, see Figure 16, and has superpotential

$$W = \text{Tr} \left[\Phi_1 [\Phi_2, \Phi_3] + \sum_{j=1}^{n_1} Q_j^{(1)} \Phi_1 \tilde{Q}_j^{(1)} + \sum_{j=1}^{n_2} Q_j^{(2)} \Phi_2 \tilde{Q}_j^{(2)} + \sum_{j=1}^{n_3} Q_j^{(3)} \Phi_3 \tilde{Q}_j^{(3)} \right]. \quad (\text{A.4})$$

The chemical potentials satisfy constraints coming from the superpotential

$$\sum_{i=1}^3 \Delta_{\Phi_i} = 2, \quad \Delta_{Q_j^{(i)}} + \Delta_{\tilde{Q}_j^{(i)}} + \Delta_{\Phi_i} = 2, \quad (\text{A.5})$$

while the monopole operators obey

$$T\tilde{T} = \Phi_1^{n_1} \Phi_2^{n_2} \Phi_3^{n_3} \implies \Delta_T + \Delta_{\tilde{T}} = \sum_{i=1}^3 n_i \Delta_{\Phi_i}. \quad (\text{A.6})$$

We have

$$\begin{aligned} \mathcal{U}^{\text{Gauge}} &= -iN^{3/2} \int dt t \rho(t) \pi \Delta_m, \\ \mathcal{U}^{\text{Bifund}} &= iN^{3/2} \int dt \rho(t)^2 \sum_{i=1}^3 g_+(\pi \Delta_{\Phi_i}), \\ \mathcal{U}^{\text{Flavour}} &= iN^{3/2} \int dt \frac{1}{2} |t| \rho(t) \sum_{i=1}^3 n_i \pi \Delta_{\Phi_i}, \end{aligned} \quad (\text{A.7})$$

where

$$g_+(v) = \frac{v^3}{6} - \frac{\pi}{2} v^2 + \frac{\pi^2}{3} v. \quad (\text{A.8})$$

Extremizing this potential with respect to ρ , adding a Lagrange multiplier guaranteeing its normalization

$$\frac{\mathcal{U}}{iN^{3/2}} - \pi\mu \left(\int dt \rho(t) - 1 \right), \quad (\text{A.9})$$

gives

$$\begin{aligned} t_{\min} &= -\frac{\mu}{\Delta_{\tilde{T}}}, & t_{\max} &= \frac{\mu}{\Delta_T}, \\ \rho(t) &= \begin{cases} \frac{\mu + \Delta_{\tilde{T}} t}{\pi^2 \Delta_{\Phi_1} \Delta_{\Phi_2} \Delta_{\Phi_3}}, & t_{\min} < t < 0, \\ \frac{\mu - \Delta_T t}{\pi^2 \Delta_{\Phi_1} \Delta_{\Phi_2} \Delta_{\Phi_3}}, & 0 < t < t_{\max}, \end{cases}, \end{aligned} \quad (\text{A.11})$$

with

$$\mu = \pi \sqrt{\frac{2\Delta_{\Phi_1} \Delta_{\Phi_2} \Delta_{\Phi_3} \Delta_T \Delta_{\tilde{T}}}{\Delta_T + \Delta_{\tilde{T}}}}, \quad (\text{A.12})$$

where $t_{\min, \max}$ are obtained as the solutions of $\rho(t) = 0$, and μ imposing $\int_{t_{\min}}^{t_{\max}} dt \rho(t) = 1$. Note that these results only depend on the flavours through the constraint (A.6), while the density takes the exact same form for any flavoured $U(N)$ theory. This is one motivation for introducing the variables $\Delta_{T, \tilde{T}}$.

In this paper we consider the ADHM theory (*i.e.* Model I, which is dual to S^7/\mathbb{Z}_k) corresponding to $n_1 = n_2 = 0$, $n_3 = k$, and the flavoured $U(N)$ dual to $\mathbb{C} \times C(T^{1,1})$ corresponding to $n_1 = n_2 = 1$, $n_3 = 0$.

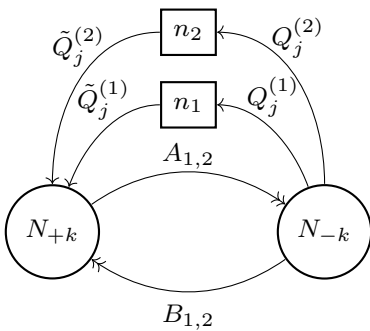


Figure 17: Quiver diagram for the flavoured ABJM theory.

A.2 Flavoured ABJM theories

Flavoured ABJM theories have $U(N)_{+k} \times U(N)_{-k}$ gauge group, contain two sets of pairs of fundamental chiral fields $\{Q_j^{(i)}, \tilde{Q}_j^{(i)}\}_{j=1}^{n_i}$ and bifundamental chiral fields A_i, B_i ($i = 1, 2$), transforming in the $(\mathbf{N}, \bar{\mathbf{N}})$, $(\bar{\mathbf{N}}, \mathbf{N})$ representations respectively, and have superpotential

$$W = \text{Tr} \left[A_1 B_1 A_2 B_2 - A_1 B_2 A_2 B_1 + \sum_{j=1}^{n_1} Q_j^{(1)} A_1 \tilde{Q}_j^{(1)} + \sum_{j=1}^{n_2} Q_j^{(2)} A_2 \tilde{Q}_j^{(2)} \right]. \quad (\text{A.13})$$

We could consider flavouring B_1 and B_2 as well and a similar analysis follows, but we are not interested in spelling out this more general case here. The chemical potentials satisfy the superpotential constraints

$$\Delta_{A_1} + \Delta_{B_1} + \Delta_{A_2} + \Delta_{B_2} = 2, \quad \Delta_{Q_j^{(a)}} + \Delta_{\tilde{Q}_j^{(a)}} + \Delta_{A_a} = 2, \quad (\text{A.14})$$

while the monopole operators obey

$$T\tilde{T} = A_1^{n_1} A_2^{n_2} \implies \Delta_T + \Delta_{\tilde{T}} = n_1 \Delta_{A_1} + n_2 \Delta_{A_2}. \quad (\text{A.15})$$

The two gauge groups have opposite Chern-Simons levels $(k_1, k_2) = (k, -k)$, and we define the following combinations

$$\delta v(t) \equiv v_2(t) - v_1(t), \quad \Delta_m = \Delta_m^{(1)} + \Delta_m^{(2)}, \quad (\text{A.16})$$

such that⁴⁰

$$\begin{aligned}
\mathcal{U}^{\text{Gauge}} &= iN^{3/2} \int dt t \rho(t) (k \delta v(t) - \pi \Delta_m), \\
\mathcal{U}^{\text{Bifund}} &= iN^{3/2} \int dt \rho(t)^2 \sum_{a=1,2} \left[g_+(\delta v(t) + \pi \Delta_{B_a}) - g_-(\delta v(t) - \pi \Delta_{A_a}) \right], \\
\mathcal{U}^{\text{Flavour}} &= iN^{3/2} \int dt \frac{1}{2} |t| \rho(t) \left[n_1 (\pi \Delta_{A_1} - \delta v(t)) + n_2 (\pi \Delta_{A_2} - \delta v(t)) \right],
\end{aligned} \tag{A.17}$$

where

$$g_{\pm}(v) = \frac{v^3}{6} \mp \frac{\pi}{2} v^2 + \frac{\pi^2}{3} v. \tag{A.18}$$

We do not present the solution for extremizing this potential for general flavours. Instead in the next subsection we turn to a specific example, which has not been treated in the literature.

The cases of interest for this paper are the pure ABJM theory (Model II), which has no flavours turned on ($n_1 = n_2 = 0$) and Chern-Simons level k . In this case, the symmetries of the theories allow to set $\Delta_m^{(1)} = \Delta_m^{(2)} = 0$ without loss of generality [2]. Then the instance of the flavoured ABJM dual to $\mathbb{C} \times C(T^{1,1})$ has $n_1 = 1$, $n_2 = 0$, and $k = -1/2$. Finally, the flavoured ABJM dual to $Q^{1,1,1}/\mathbb{Z}_n$ has $n_1 = n_2 = n$, and $k = 0$.

A.2.1 Flavoured ABJM dual to $\mathbb{C} \times C(T^{1,1})$

In the following we present the computations to obtain the eigenvalue density of the flavoured ABJM field theory dual to the $\mathbb{C} \times C(T^{1,1})$ geometry. This computation is interesting to present both because it produces new results, and because it is representative of how the results have been obtained in all of the examples. Indeed, this theory includes both flavours and non-zero Chern-Simons levels. We therefore expect a behaviour that combines the features from Model I and II, *i.e.* both a discontinuity point of $\rho'(t)$ at $t = 0$ coming from the D6-branes, and some $t \neq 0$ and $\rho \neq 0$ discontinuity points.

As explained in section 2.2.3 the analytical expression for $\rho(t)$ is obtained by extremizing the Bethe potential, adding a Lagrange multiplier term

$$\frac{\mathcal{U}}{iN^{3/2}} - \pi\mu \left(\int dt \rho(t) - 1 \right). \tag{A.19}$$

For the model we consider, the Bethe potential is given by (A.17), with $k = -1/2$, $n_1 = 1$, $n_2 = 0$. Extremizing this potential gives solutions for ρ and δv , which are valid

⁴⁰Compared to [19], we add the k term and define Δ_m slightly differently.

for⁴¹

$$0 < \delta v(t) + \pi \Delta_{B_a} < 2\pi, \quad -2\pi < \delta v(t) - \pi \Delta_{A_a} < 0, \quad a = 1, 2. \quad (\text{A.20})$$

As $\sum \Delta = 2$, the 0 bounds are always more restrictive than the 2π bounds, and we only need to consider the former. When δv hits one of these bounds, it stays frozen at that value, creating some “tails” where ρ is obtained again by extremizing \mathcal{U} , but with δv set at its frozen value. For δv extremizing (A.17), the bounds are saturated at

$$\begin{aligned} \delta v(t_1) &= \pi \Delta_{A_2}, & \delta v(t_\star) &= \pi \Delta_{A_1}, \\ \delta v(t_3) &= -\pi \Delta_{B_1}, & \delta v(t_4) &= -\pi \Delta_{B_2}, \end{aligned} \quad (\text{A.21})$$

with

$$\begin{aligned} t_1 &= -\frac{2\mu}{\Delta_{A_1} + 2\Delta_m}, & t_\star &= \frac{2\mu}{\Delta_{A_1} - 2\Delta_m - 2\Delta_{A_2}}, \\ t_3 &= \frac{2\mu}{\Delta_{A_1} - 2\Delta_m + 2\Delta_{B_2}}, & t_4 &= \frac{2\mu}{\Delta_{A_1} - 2\Delta_m + 2\Delta_{B_1}}. \end{aligned} \quad (\text{A.22})$$

By symmetry of the quiver (see Figure 12), we can assume without loss of generality that $\Delta_{B_1} < \Delta_{B_2}$, such that $t_1 < 0 < t_3 < t_4$ (where we have also assumed that $\Delta_{A_1} + 2\Delta_m > 0$). Therefore there is a tail on the right, on which $\delta v(t) = -\pi \Delta_{B_1}$. The extremal values of t are determined by $\rho(t_{\min}) = \rho(t_{\max}) = 0$, which correspond to $t_{\min} = t_1$ and $t_{\max} = t_4$. We discard the t_\star solution, which lies outside of $[t_1, t_4]$ for $\Delta_{A_2} < \Delta_{A_1}$. For $\Delta_{A_2} > \Delta_{A_1}$, we do not have an *a priori* reason to discard t_\star , but we note that if it were a discontinuity point of $\rho'(t)$, it would give a tail on the left, which is not what we expect either from the numerics (see Figure 18) or the gravity dual analysis. We know that there is also a discontinuity point of $\rho'(t)$ at $t_2 = 0$ as D6-branes are present. This is confirmed by the presence of a $|t|$ term in the solution for $\rho(t)$, which in summary is

$$\rho(t) = \begin{cases} \frac{4\mu - (-4\Delta_m + \Delta_{B_1}\Delta_{B_2} - \Delta_{A_1}\Delta_{A_2})t - (\Delta_{A_1} + \Delta_{B_1})(\Delta_{A_1} + \Delta_{B_2})|t|}{2\pi^2(\Delta_{A_1} + \Delta_{B_1})(\Delta_{A_1} + \Delta_{B_2})(\Delta_{A_2} + \Delta_{B_1})(\Delta_{A_2} + \Delta_{B_2})}, & t_1 < t < t_3, \\ \frac{2\mu - (\Delta_{A_1} - 2\Delta_m + 2\Delta_{B_1})t}{2\pi^2(\Delta_{A_1} + \Delta_{B_1})(\Delta_{A_2} + \Delta_{B_1})(\Delta_{B_2} - \Delta_{B_1})}, & t_3 < t < t_4. \end{cases} \quad (\text{A.23})$$

Finally μ is determined by imposing the normalization of ρ and reads

$$\mu = \pi \sqrt{\frac{(\Delta_{A_2} + \Delta_{B_1})(\Delta_{A_2} + \Delta_{B_2})(\Delta_{A_1} + 2\Delta_m)(\Delta_{A_1} - 2\Delta_m + 2\Delta_{B_1})(\Delta_{A_1} - 2\Delta_m + 2\Delta_{B_2})}{8 - 4\Delta_m - 2\Delta_{A_1}}}. \quad (\text{A.24})$$

⁴¹These conditions come from the derivation of $\mathcal{U}^{\text{Bifund}}$, see [18].

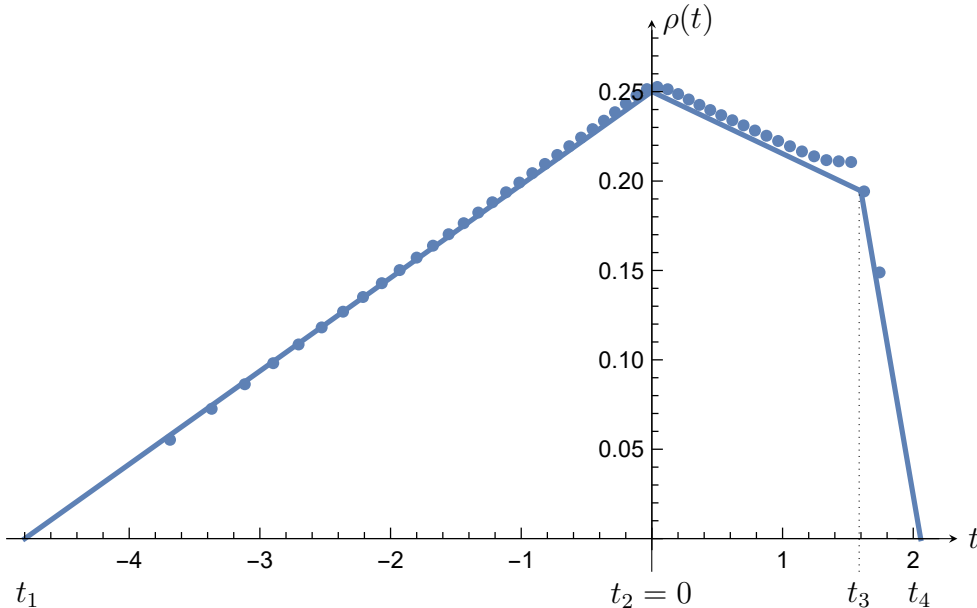


Figure 18: Comparison of the analytical solution in (A.23) (solid line) with the numerics (dots), for $\Delta_{A_1} = 1/2$, $\Delta_{A_2} = 2/3$, $\Delta_{B_1} = 1/3$, $\Delta_{B_2} = 1/2$, $\Delta_m = 0$.

Note that both Δ_1 and Δ_m are related to the monopole variables as $\Delta_1 = \Delta_T + \Delta_{\tilde{T}}$ and $-\Delta_m = \frac{1}{2}(\Delta_T + \Delta_{\tilde{T}})$, such that

$$\Delta_{A_1} - 2\Delta_m = 2\Delta_T, \quad \Delta_{A_1} + 2\Delta_m = 2\Delta_{\tilde{T}}. \quad (\text{A.25})$$

In the main text, we quote the above results in terms of Δ_T and $\Delta_{\tilde{T}}$. This simplifies both the expressions themselves and their comparison with the geometry results.

We also checked our results numerically following the method of [2]. A near-perfect agreement can be observed in Figure 18.

B Example: $Y_7 = S^7/\mathbb{Z}_k$ – Summary of results

The field theories dual to S^7/\mathbb{Z}_k , namely the ADHM and ABJM theories, were used to illustrate the concepts from section 2 to section 4. The aim of this appendix is to gather the results that have appeared scattered in the main text, and present them in the same fashion as in the examples of section 6. Note that $C(S^7) = \mathbb{C}^4$ is also an example of a toric cone, but the geometry in this case is so elementary that the results could be obtained as in section 4, without resorting to the toric machinery introduced in section 6. Here instead we use the general toric framework to present the results.

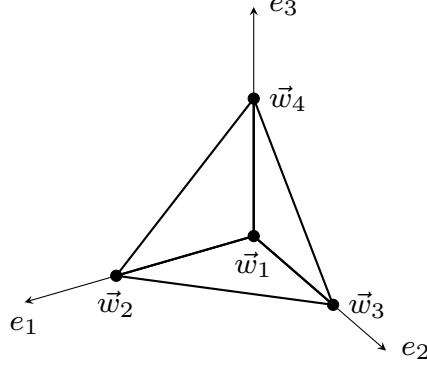


Figure 19: Toric diagram for S^7 .

S^7/\mathbb{Z}_k has the following toric data,

$$v_1 = (1, 0, 0, 0), \quad v_2 = (1, 1, 0, 0), \quad v_3 = (1, 0, 1, 0), \quad v_4 = (1, 0, 0, 1), \quad (\text{B.1})$$

with toric diagram shown in Figure 19. We have

$$\text{Vol}_S(S^7/\mathbb{Z}_k) = \frac{1}{k} \frac{\pi^4}{3b_2 b_3 b_4 (b_1 - b_2 - b_3 - b_4)}, \quad (\text{B.2})$$

$$R_1 = \frac{2}{b_1} (b_1 - b_2 - b_3 - b_4), \quad R_a = \frac{2b_a}{b_1}, \quad a = 2, 3, 4, \quad (\text{B.3})$$

such that

$$\Lambda = \frac{\pi \ell_p^3 N^{1/2}}{2} \sqrt{2k R_1 R_2 R_3 R_4}. \quad (\text{B.4})$$

B.1 ADHM – Model I

Geometry We first consider

$$\zeta_M = \frac{1}{k} (\partial_{\phi_1} - \partial_{\phi_2}) = -\frac{1}{k} \partial_{\varphi_2}, \quad (\text{B.5})$$

leading to

$$\tau_{\min} = -\frac{2\Lambda}{R_2 + R_3}, \quad \tau_{\max} = \frac{2\Lambda}{R_1 + R_4}, \quad (\text{B.6})$$

and

$$\rho(t) = \frac{1}{\ell_p^3 N^{1/2}} \left\{ \begin{array}{l} \frac{2\Lambda + kR_2\tau}{\pi^2 R_3 R_4 (R_1 + R_2)}, \quad \tau_{\min} < \tau < 0 \\ \frac{2\Lambda - kR_1\tau}{\pi^2 R_3 R_4 (R_1 + R_2)}, \quad 0 < \tau < \tau_{\max} \end{array} \right\}_{\tau = \ell_p^3 N^{1/2} t}, \quad (\text{B.7})$$

as shown in Figure 20.

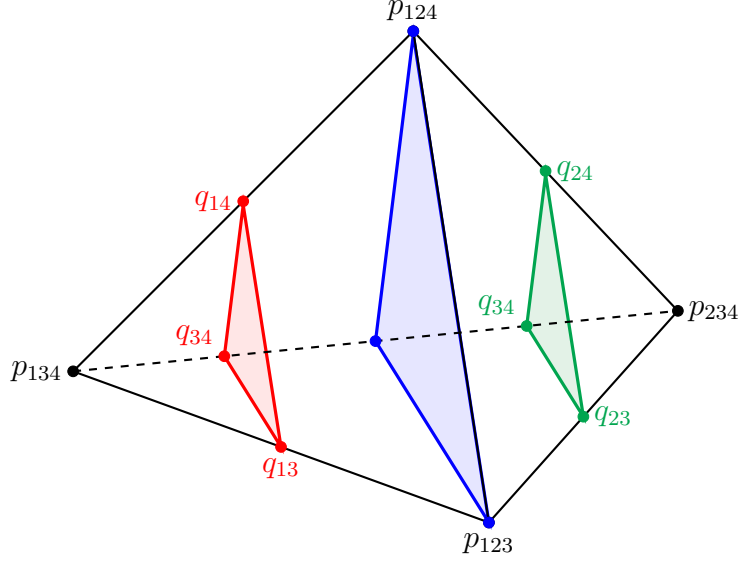


Figure 20: Tetrahedron describing S^7/\mathbb{Z}_k and its slicing corresponding to the ADHM theory. The red slice is \mathcal{Q}_τ for $\tau_{\min} < \tau < 0$, the blue slice for $\tau = 0$, and the green slice for $0 < \tau < \tau_{\max}$. The perimeter of \mathcal{Q}_τ varies with τ qualitatively as ρ in Figure 3.

Field theory The field theory dual to this geometry is the ADHM theory, which corresponds to the instance $n_1 = n_2 = 0$, $n_3 = k$ of the flavoured $U(N)$ theory described in Appendix A.1. The results read

$$t_{\min} = -\frac{\mu}{\Delta_{\tilde{T}}}, \quad t_{\max} = \frac{\mu}{\Delta_T}, \quad (\text{B.8})$$

$$\rho(t) = \begin{cases} \frac{\mu + \Delta_{\tilde{T}}t}{\pi^2 \Delta_{\Phi_1} \Delta_{\Phi_2} \Delta_{\Phi_3}}, & t_{\min} < t < 0, \\ \frac{\mu - \Delta_T t}{\pi^2 \Delta_{\Phi_1} \Delta_{\Phi_2} \Delta_{\Phi_3}}, & 0 < t < t_{\max}, \end{cases}, \quad (\text{B.9})$$

with

$$\mu = \pi \sqrt{\frac{2}{k} \Delta_{\Phi_1} \Delta_{\Phi_2} \Delta_T \Delta_{\tilde{T}}}. \quad (\text{B.10})$$

Matching

$$\Delta_T = kR_1, \quad \Delta_{\tilde{T}} = kR_2, \quad \Delta_{\Phi_1} = R_3, \quad \Delta_{\Phi_2} = R_4, \quad (\text{B.11})$$

such that, $\mu = 2\Lambda/(\ell_p^3 N^{1/2})$, and $\rho(t)$ match.

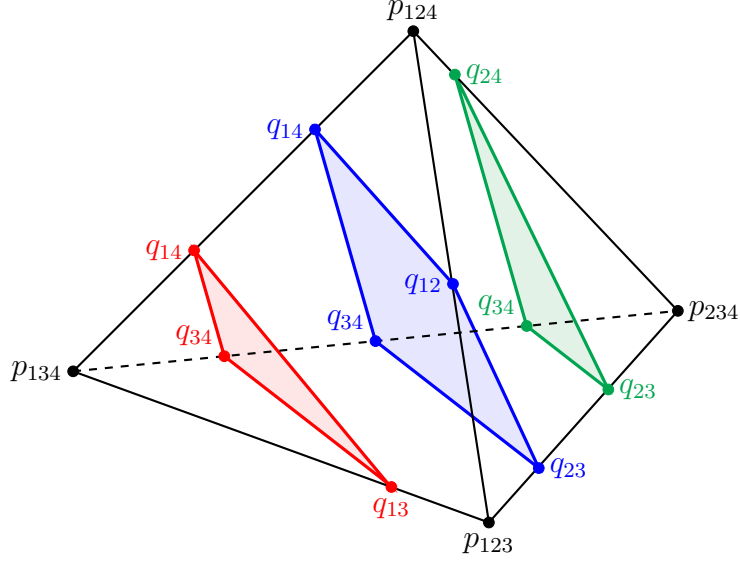


Figure 21: Tetrahedron describing S^7/\mathbb{Z}_k and its slicing corresponding to the ABJM theory. The red slice is \mathcal{Q}_τ for $\tau_1 < \tau < \tau_2$, the blue slice for $\tau_2 < \tau < \tau_3$, and the green slice for $\tau_3 < \tau < \tau_4$. The perimeter of \mathcal{Q}_τ varies with τ qualitatively as ρ in Figure 4.

B.2 ABJM – Model II

Geometry The second choice of M-theory circle is

$$\zeta_M = \frac{1}{k} (\partial_{\phi_1} - \partial_{\phi_2} + \partial_{\phi_3} - \partial_{\phi_4}) = \frac{1}{k} (-\partial_{\varphi_2} + \partial_{\varphi_3} - \partial_{\varphi_4}), \quad (\text{B.12})$$

leading to

$$\tau_1 = -\frac{2\Lambda}{kR_2}, \quad \tau_2 = -\frac{2\Lambda}{kR_4}, \quad \tau_3 = \frac{2\Lambda}{kR_3}, \quad \tau_4 = \frac{2\Lambda}{kR_1}, \quad (\text{B.13})$$

and

$$\rho(t) = \frac{1}{\ell_p^3 N^{1/2}} \left\{ \begin{array}{ll} \frac{2\Lambda + kR_2\tau}{\pi^2(R_1+R_2)(R_2+R_3)(R_4-R_2)}, & \tau_1 < \tau < \tau_2 \\ \frac{4\Lambda + k(R_2R_4 - R_1R_3)\tau}{\pi^2(R_1+R_2)(R_2+R_3)(R_1+R_4)(R_3+R_4)}, & \tau_2 < \tau < \tau_3 \\ \frac{2\Lambda - kR_1\tau}{\pi^2(R_1+R_2)(R_1+R_4)(R_3-R_1)}, & \tau_3 < \tau < \tau_4 \end{array} \right|_{\tau = \ell_p^3 N^{1/2} t} \quad (\text{B.14})$$

as shown in Figure 21.

Field theory The field theory dual to this geometry is the ABJM theory, which corresponds to the unflavoured instance ($n_1 = n_2 = 0$) of the flavoured ABJM theory described in Appendix A.2. The results read

$$t_1 = -\frac{\mu}{k\Delta_{B_1}}, \quad t_2 = -\frac{\mu}{k\Delta_{B_2}}, \quad t_3 = \frac{\mu}{k\Delta_{A_2}}, \quad t_4 = \frac{\mu}{k\Delta_{A_1}}, \quad (\text{B.15})$$

$$\rho(t) = \begin{cases} \frac{\mu + k\Delta_{B_1}t}{\pi^2(\Delta_{A_1} + \Delta_{B_1})(\Delta_{A_2} + \Delta_{B_1})(\Delta_{B_2} - \Delta_{B_1})}, & t_1 < t < t_2, \\ \frac{2\mu + k(\Delta_{B_1}\Delta_{B_2} - \Delta_{A_1}\Delta_{A_2})t}{\pi^2(\Delta_{A_1} + \Delta_{B_1})(\Delta_{A_1} + \Delta_{B_2})(\Delta_{A_2} + \Delta_{B_1})(\Delta_{A_2} + \Delta_{B_2})}, & t_2 < t < t_3, \\ \frac{\mu - k\Delta_{A_1}t}{\pi^2(\Delta_{A_1} + \Delta_{B_1})(\Delta_{A_1} + \Delta_{B_2})(\Delta_{A_2} - \Delta_{A_1})}, & t_3 < t < t_4. \end{cases} \quad (\text{B.16})$$

with

$$\mu = \pi\sqrt{2k\Delta_{A_1}\Delta_{A_2}\Delta_{B_1}\Delta_{B_2}}. \quad (\text{B.17})$$

Matching

$$\Delta_{A_1} = R_1, \quad \Delta_{B_1} = R_2, \quad \Delta_{A_2} = R_3, \quad \Delta_{B_2} = R_4, \quad (\text{B.18})$$

such that, $\mu = 2\Lambda/(\ell_p^3 N^{1/2})$, and $\rho(t)$ match.

C BPS condition for M2-branes

In the following we denote with $M = (0, 1, m)$ the 11d spacetime index and with $A = (0, 1, \mathbf{a})$ the 11d frame indices, and we introduce a local orthonormal frame e^A for the metric (3.9) such that $e^{10} = e^{-B/3}\eta$. If ϵ is the Killing spinor of the background, an M2-brane whose configuration is described by the embedding coordinates X^M does not break supersymmetry if it is such that ϵ satisfies the following Euclidean projection condition [52]

$$\mathbb{P}\epsilon = 0, \quad \text{with} \quad \mathbb{P} \equiv \frac{1}{2} \left(1 - \frac{i}{3!} \varepsilon^{ijk} \partial_i X^M \partial_j X^N \partial_k X^P \Gamma_{MNP} \right). \quad (\text{C.1})$$

Here i, j, k are worldvolume indices, ε^{ijk} is the 3d Levi-Civita tensor, and Γ_{MNP} are antisymmetric products of the 11d gamma matrices in curved space, *i.e.* $\Gamma_M = \Gamma_A e^A_M$. The configuration of branes we are interested in is wrapping EAdS₂ (*i.e.* the (0,1) directions) and S^1_{M2} , which we take to be a generic linear combination of the directions in Y_9 , *i.e.*⁴²

$$\text{vol}_{S^1_{M2}} = \sum_{\mathbf{a}=2}^{10} c_{\mathbf{a}} e^{\mathbf{a}}, \quad c_{\mathbf{a}} \in \mathbb{R}. \quad (\text{C.2})$$

⁴²Of course the fact that S^1_{M2} must be a circle will in principle put restrictions on the coefficients $c_{\mathbf{a}}$, but we will not need them as the projection condition (C.1) is enough to fix all the coefficients.

We choose a parametrization where

$$\begin{aligned}\partial_0 X^0 &= \partial_1 X^1 = 1, & (\partial_3 X^m) e^a_m &= c_a, \\ \partial_0 X^m &= \partial_1 X^m = \partial_3 X^0 = \partial_3 X^1 = 0.\end{aligned}\tag{C.3}$$

Then the only non-zero contributions in the sum in \mathbb{P} are those for which $(M, N, P) = (0, 1, m)$ or permutations, yielding

$$\mathbb{P}\epsilon = 0, \quad \text{with} \quad \mathbb{P} = \frac{1}{2} \left(1 - i \sum_{a=2}^{10} c_a \Gamma_0 \Gamma_1 \Gamma_a \right).\tag{C.4}$$

The next step is to decompose this projection on our $\text{AdS}_2 \times Y_9$ background. Following the conventions of [13, 42] but rotated to Euclidean signature, as those are compatible with our GK backgrounds, we split the 11d gamma matrices as $\Gamma_A = (\beta_0 \otimes \mathbb{I}_9, \beta_1 \otimes \mathbb{I}_9, \beta_* \otimes \gamma_a)$, where $\beta_0 = \sigma_2$ and $\beta_1 = \sigma_1$ are Pauli matrices, $\beta_* = -i\beta_0\beta_1 = -\sigma_3$ is the chiral gamma matrix in 2d, and γ_a generates the 9d Clifford algebra. This gives

$$\mathbb{P} = \frac{1}{2} \left(\mathbb{I}_2 \otimes \mathbb{I}_9 - i\beta_0\beta_1\beta_* \otimes \sum_{a=2}^{10} c_a \gamma_a \right) = \frac{1}{2} \mathbb{I}_2 \otimes \left(\mathbb{I}_9 + \sum_{a=2}^{10} c_a \gamma_a \right),\tag{C.5}$$

where we used the fact that $i\beta_0\beta_1\beta_* = -\mathbb{I}_2$. Notice that in order for \mathbb{P} to be a well-defined projector we have to ensure that $\mathbb{P}^2 = \mathbb{P}$, which implies that $\sum_{a=2}^{10} c_a^2 = 1$. Splitting also the 11d Killing spinor as $\epsilon = \theta \otimes \chi + c.c.$, where θ is a Killing spinor on AdS_2 and χ on Y_9 , the condition $\mathbb{P}\epsilon = 0$ results in the following equation involving the 9d spinor only

$$\sum_{a=2}^{10} c_a \gamma_a \chi = -\chi.\tag{C.6}$$

Finally, taking χ to be normalized as $\bar{\chi}\chi = 1$, it can be shown that for a GK geometry the 1-form η is given by the bilinear [12]

$$\eta = e^{B/3} \bar{\chi} \gamma_a \chi e^a,\tag{C.7}$$

but recall that by definition of the frame $\eta = e^{B/3} e^{10}$, so that χ necessarily satisfies

$$\gamma_{10} \chi = \chi, \quad \bar{\chi} \gamma_a \chi = 0, \quad a \neq 10.\tag{C.8}$$

These equations tell us that χ is an eigenvector of γ_{10} with unit eigenvalue and $\gamma_a \chi$ is orthogonal to $\bar{\chi}$ when $a \neq 10$. Similarly, the Kähler 2-form of the GK background is given by

$$J = -\frac{i}{2} \bar{\chi} \gamma_{ab} \chi e^a \wedge e^b,\tag{C.9}$$

where $\gamma_{\mathbf{ab}} = \gamma_{[\mathbf{a}\mathbf{b}]}$. However, one can always choose a frame such that

$$J = e^2 \wedge e^3 + e^4 \wedge e^5 + e^6 \wedge e^7 + e^8 \wedge e^9, \quad (\text{C.10})$$

so that $i\gamma_{23}\chi = i\gamma_{45}\chi = i\gamma_{67}\chi = i\gamma_{89}\chi = \chi$ and $\bar{\chi}\gamma_{\mathbf{ab}}\chi = 0$ for any other combination of indices \mathbf{a}, \mathbf{b} . As a consequence, one may check that the two sets of spinors

$$\{\chi, \gamma_2\chi, \gamma_4\chi, \gamma_6\chi, \gamma_8\chi\} \quad \text{and} \quad \{\chi, \gamma_3\chi, \gamma_5\chi, \gamma_7\chi, \gamma_9\chi\} \quad (\text{C.11})$$

are both linearly independent. Combining (C.8) with (C.11), we find that (C.6) is solved by setting

$$\begin{cases} c_{\mathbf{a}} = 0, & \mathbf{a} \neq 10 \\ c_{10} = -1 \end{cases} \quad \implies \quad \text{vol}_{S_{\text{M2}}^1} = -e^{10} = -e^{-B/3} \eta. \quad (\text{C.12})$$

We thus conclude that an M2-brane wrapping $\text{EAdS}_2 \times S_{\text{M2}}^1$ is supersymmetric precisely when the circle direction is aligned with the R-symmetry circle.

D Wilson loop duals and flat C -fields

In section 4.4.2 we have matched BPS Wilson loop VEVs in the large N matrix model with the action of M2-branes/fundamental strings in the holographic dual. We have seen that this matching works in a variety of examples throughout the paper, including the toric examples in section 6, and the extension to black holes with spindle horizons/the refined twisted index in section 5.

There is, however, an important subtlety in this matching, which we address in this appendix. The matching of Wilson loops VEVs with the renormalized action of fundamental strings, whose worldvolume ends on the Wilson loop at the conformal boundary, goes back to [22]. However, depending on the topology of the bulk spacetime this Wilson loop VEV in the gravity dual can sometimes be zero, due to integration over a certain bulk zero mode. In particular this can be the case for Euclidean black holes, as first pointed out in a non-supersymmetric context in [44]. One might then be puzzled by why this effect does not lead to the Wilson loops in this paper being zero. They are not zero, and it is instructive to consider the mechanism in [44] more closely to see why.

The type IIA string has a coupling $\exp(i \int B)$, where in the supergravity partition function we should be careful to sum over all bulk configurations with the same boundary conditions on the conformal boundary. In particular, the bulk field B is a two-form

potential for the NS three-form $H = dB$, and one can add a closed/flat B -field to a supergravity background without affecting the gauge-invariant flux H or its equation of motion. In the present set-up, with boundary conditions fixed at conformal infinity, we should then sum over B -fields in the bulk spacetime that are zero at infinity, modulo gauge transformations $B \rightarrow B + d\Lambda$, where the one-form Λ is also zero at conformal infinity. Such physically distinct B -fields are then classified by the compactly supported cohomology group $H_{\text{cpt}}^2(M)$, where M is the spacetime.⁴³

Now for Euclidean black holes the black hole part of the spacetime has topology $\mathbb{R}^2 \times \Sigma$, where Σ is the horizon and \mathbb{R}^2 is parametrized by the Euclidean time circle and the radial direction for the black hole. In fact the topology is the same whether one considers the full black hole, or as in this paper just the near-horizon region of an extremal black hole, where Euclidean AdS_2 also has the topology of \mathbb{R}^2 . The fundamental strings we consider in the paper are precisely wrapping this \mathbb{R}^2 direction. Since $H_{\text{cpt}}^2(\mathbb{R}^2 \times \Sigma, \mathbb{R}) \cong \mathbb{R}$ is generated by a closed two-form that integrates to 1 over the \mathbb{R}^2 direction and has rapid decay towards the boundary of \mathbb{R}^2 (where the conformal boundary is), this naively leads to a moduli space of flat B -fields to integrate over. As we will explain further below, in fact this is not the case, but *if it were the case* the supergravity saddle point approximation for the path integral with the type IIA string inserted would give

$$\langle \text{string} \rangle = \int_{\vartheta=0}^{2\pi} \exp[-I_{\text{string}} + i\vartheta] = 0. \quad (\text{D.1})$$

Here I_{string} is the renormalized string action, for a fundamental string wrapping the \mathbb{R}^2 direction, and $\vartheta = \int_{\mathbb{R}^2} B$ parametrizes the integrals of the inequivalent B -fields. The 2π -periodicity in ϑ arises here precisely due to the large gauge transformations mentioned above.

The above effect was explained in [44], but the conclusion (D.1) is not correct for the set-up we are considering here. In particular, we skipped over two important steps above: (i) the full spacetime M is not simply the black hole part of the geometry, since there is also an internal space geometry, and (ii) we must take into account that the M-theory circle is non-trivially fibred over the type IIA spacetime. In particular the latter introduces a RR field in addition to the B -field, and these couple to each other. In fact it is then simpler to think of the fundamental string as a wrapped M2-brane, wrapping the M-theory circle, and consider instead the M2-brane coupling $\exp(i \int C)$, with compactly support C -field modes in the full 11d spacetime.

⁴³Even more precisely, including large gauge transformations this becomes $H_{\text{cpt}}^2(M, U(1))$.

We denote the 11d Euclidean spacetime by E , and note we are interested in the case where $E = \mathbb{R}^2 \times Y_9$, where the \mathbb{R}^2 factor could be either Euclidean AdS_2 (*i.e.* the Poincaré disk), or the transverse directions to the horizon of a non-extremal deformation of the 4d black hole (*i.e.* the radial and Euclidean time circle). The topology of E is the same in both cases, with the horizon geometry absorbed into Y_9 .

We suppose also that Y_9 is the total space of a circle fibration over a base B_8 . This could be viewed as either the M-theory circle fibration, or a choice of (off-shell) R-symmetry direction for the purposes of the argument that follows. In general B_8 might also have orbifold singularities (for example for a quasi-regular choice of R-symmetry Killing vector), and that also does not affect the following statements in de Rham cohomology. We denote the choice of circle action by $U(1)$, and write $B_8 = Y_9/U(1)$ and $M = E/U(1) = \mathbb{R}^2 \times B_8$.

In general given a total space E which is an S^1 bundle over a non-compact space M , we have the following associated long exact Gysin sequence in cohomology:

$$\cdots \longrightarrow H_{\text{cpt}}^3(M) \xrightarrow{\pi^*} H_{\text{cpt}}^3(E) \xrightarrow{\pi_*} H_{\text{cpt}}^2(M) \xrightarrow{\wedge c_1} H_{\text{cpt}}^4(M) \longrightarrow \cdots \quad (\text{D.2})$$

Here $\pi : E \rightarrow M$ is the projection, π^* the usual pull-back of forms, π_* denotes “integration over the fibre”, which means integrating the form (partially) along the S^1 fibre, and finally $c_1 \in H^2(M)$ denotes the first Chern class of the S^1 bundle, *i.e.* $c_1 = [\mathcal{F}/2\pi]$, where $\mathcal{F} = d\mathcal{A}$ denotes the curvature of a connection \mathcal{A} on this circle bundle.⁴⁴

Viewing $M = \mathbb{R}^2 \times B_8$ as a trivial \mathbb{R}^2 bundle over B_8 , the Thom isomorphism theorem tells us that $H_{\text{cpt}}^{n+2}(M) \cong H^n(B_8)$ for all $n \geq 0$. In particular $H_{\text{cpt}}^2(M) \cong H^0(B_8) \cong \mathbb{R}$, which is generated by a unit integral two-form along \mathbb{R}^2 . Notice this is the same two-form discussed in the argument that led to (D.1), as in [44]. The M2-branes of interest are precisely wrapping this \mathbb{R}^2 direction, together with the S^1 fibre (whether that is the M-theory circle or the R-symmetry direction – for BPS M2-branes they are necessarily aligned for the locus the M2-brane is wrapping).

Examining (D.2) further, the Thom isomorphism above gives us $H_{\text{cpt}}^3(M) \cong H^1(B_8) \cong 0$, which follows since our internal spaces Y_9 (and hence their quotients B_8) all have zero first Betti number, *i.e.* there are no non-trivial closed one-forms. This is a crucial ingredient, as we comment further below. Thus more specifically in this case (D.2)

⁴⁴When the S^1 corresponds to the M-theory circle direction, here \mathcal{F} is naturally represented by the RR two-form field strength. It is precisely when this has a non-trivial cohomology class that the original B -field argument we presented is affected, and from a purely type IIA perspective this is due to the couplings between these fields.

reads

$$\cdots \longrightarrow 0 \longrightarrow H_{\text{cpt}}^3(E) \xrightarrow{\pi_*} \mathbb{R} \xrightarrow{\wedge c_1} H_{\text{cpt}}^4(M) \longrightarrow \cdots \quad (\text{D.3})$$

As long as $c_1 \neq 0$, *i.e.* the circle bundle we have is non-trivial, then wedging the volume form on \mathbb{R}^2 (which generates the \mathbb{R} factor) with c_1 is non-zero in $H_{\text{cpt}}^4(M)$. In fact as already noted the Thom isomorphism tells us $H_{\text{cpt}}^4(M) \cong H^2(B_8)$, with this isomorphism map corresponding to wedging with the above-mentioned volume form. So as long as $c_1 \neq 0 \in H^2(B_8)$, the image in $H_{\text{cpt}}^4(M)$ will also be non-zero, and the kernel of the $\wedge c_1$ map is hence trivial. But then exactness of (D.3) says that the generator of \mathbb{R} is not the image of any class in $H_{\text{cpt}}^3(E)$, when integrated over S^1 under the π_* map.

Coming back to the M2-branes of interest, the cohomology group $H_{\text{cpt}}^3(E)$ precisely captures the flat C -field modes in the bulk that should be integrated over when evaluating the full supergravity partition function. The above argument shows that when the circle bundle we have is non-trivial, the integral of any such C -field mode over the circle direction and \mathbb{R}^2 direction is necessarily zero. There are hence no modes that contribute to an argument similar to that in [44], and the holographic Wilson loop we have is non-zero.

Let us conclude by remarking that this argument is certainly evaded in the case that the circle bundle is trivial: then $Y_9 = S^1 \times B_8$, and there is a flat C -field that is simply the volume form on \mathbb{R}^2 wedged with the volume form along the S^1 . Such M2-branes would lead to zero VEVs, as in (D.1), but in our examples Y_9 always have zero first Betti number, and in particular do not have $S^1 \times B_8$ topology.

References

- [1] A. Strominger and C. Vafa, “Microscopic origin of the Bekenstein-Hawking entropy,” *Phys. Lett. B* **379** (1996) 99–104, [arXiv:hep-th/9601029](#).
- [2] F. Benini, K. Hristov, and A. Zaffaroni, “Black hole microstates in AdS₄ from supersymmetric localization,” *JHEP* **05** (2016) 054, [arXiv:1511.04085](#) [[hep-th](#)].
- [3] F. Benini, K. Hristov, and A. Zaffaroni, “Exact microstate counting for dyonic black holes in AdS₄,” *Phys. Lett.* **B771** (2017) 462–466, [arXiv:1608.07294](#) [[hep-th](#)].

- [4] P. Ferrero, J. P. Gauntlett, J. M. P. Ipiña, D. Martelli, and J. Sparks, “Accelerating black holes and spinning spindles,” *Phys. Rev. D* **104** no. 4, (2021) 046007, [arXiv:2012.08530 \[hep-th\]](#).
- [5] P. Ferrero, J. P. Gauntlett, J. M. Pérez Ipiña, D. Martelli, and J. Sparks, “D3-Branes Wrapped on a Spindle,” *Phys. Rev. Lett.* **126** no. 11, (2021) 111601, [arXiv:2011.10579 \[hep-th\]](#).
- [6] J. P. Gauntlett and O. Varela, “Consistent Kaluza-Klein Reductions for General Supersymmetric AdS Solutions,” *Phys. Rev.* **D76** (2007) 126007, [arXiv:0707.2315 \[hep-th\]](#).
- [7] F. Azzurli, N. Bobev, P. M. Crichigno, V. S. Min, and A. Zaffaroni, “A universal counting of black hole microstates in AdS₄,” *JHEP* **02** (2018) 054, [arXiv:1707.04257 \[hep-th\]](#).
- [8] C. Couzens, J. P. Gauntlett, D. Martelli, and J. Sparks, “A geometric dual of c -extremization,” *JHEP* **01** (2019) 212, [arXiv:1810.11026 \[hep-th\]](#).
- [9] J. P. Gauntlett, D. Martelli, and J. Sparks, “Toric geometry and the dual of \mathcal{I} -extremization,” *JHEP* **06** (2019) 140, [arXiv:1904.04282 \[hep-th\]](#).
- [10] S. M. Hosseini and A. Zaffaroni, “Geometry of \mathcal{I} -extremization and black holes microstates,” *JHEP* **07** (2019) 174, [arXiv:1904.04269 \[hep-th\]](#).
- [11] H. Kim and N. Kim, “Black holes with baryonic charge and \mathcal{I} -extremization,” *JHEP* **11** (2019) 050, [arXiv:1904.05344 \[hep-th\]](#).
- [12] N. Kim and J.-D. Park, “Comments on AdS(2) solutions of D = 11 supergravity,” *JHEP* **09** (2006) 041, [arXiv:hep-th/0607093](#).
- [13] J. P. Gauntlett and N. Kim, “Geometries with Killing Spinors and Supersymmetric AdS Solutions,” *Commun. Math. Phys.* **284** (2008) 897–918, [arXiv:0710.2590 \[hep-th\]](#).
- [14] A. Boido, J. P. Gauntlett, D. Martelli, and J. Sparks, “Entropy Functions For Accelerating Black Holes,” *Phys. Rev. Lett.* **130** no. 9, (2023) 091603, [arXiv:2210.16069 \[hep-th\]](#).

- [15] A. Boido, J. P. Gauntlett, D. Martelli, and J. Sparks, “Gravitational Blocks, Spindles and GK Geometry,” *Commun. Math. Phys.* **403** no. 2, (2023) 917–1003, [arXiv:2211.02662 \[hep-th\]](#).
- [16] D. Martelli, J. Sparks, and S.-T. Yau, “The Geometric dual of a -maximisation for Toric Sasaki-Einstein manifolds,” *Commun. Math. Phys.* **268** (2006) 39–65, [arXiv:hep-th/0503183 \[hep-th\]](#).
- [17] D. Martelli, J. Sparks, and S.-T. Yau, “Sasaki-Einstein manifolds and volume minimisation,” *Commun. Math. Phys.* **280** (2008) 611–673, [arXiv:hep-th/0603021 \[hep-th\]](#).
- [18] S. M. Hosseini and A. Zaffaroni, “Large N matrix models for 3d $\mathcal{N} = 2$ theories: twisted index, free energy and black holes,” *JHEP* **08** (2016) 064, [arXiv:1604.03122 \[hep-th\]](#).
- [19] S. M. Hosseini and N. Mekareeya, “Large N topologically twisted index: necklace quivers, dualities, and Sasaki-Einstein spaces,” *JHEP* **08** (2016) 089, [arXiv:1604.03397 \[hep-th\]](#).
- [20] S. M. Hosseini and A. Zaffaroni, “The large N limit of topologically twisted indices: a direct approach,” *JHEP* **12** (2022) 025, [arXiv:2209.09274 \[hep-th\]](#).
- [21] D. Farquet and J. Sparks, “Wilson loops and the geometry of matrix models in $\text{AdS}_4/\text{CFT}_3$,” *JHEP* **01** (2014) 083, [arXiv:1304.0784 \[hep-th\]](#).
- [22] J. M. Maldacena, “Wilson loops in large N field theories,” *Phys. Rev. Lett.* **80** (1998) 4859–4862, [arXiv:hep-th/9803002](#).
- [23] D. R. Gulotta, C. P. Herzog, and S. S. Pufu, “Operator Counting and Eigenvalue Distributions for 3D Supersymmetric Gauge Theories,” *JHEP* **11** (2011) 149, [arXiv:1106.5484 \[hep-th\]](#).
- [24] M. Inglese, D. Martelli, and A. Pittelli, “The Spindle Index from Localization,” [arXiv:2303.14199 \[hep-th\]](#).
- [25] J. Sparks, “Sasaki-Einstein Manifolds,” *Surveys Diff. Geom.* **16** (2011) 265–324, [arXiv:1004.2461 \[math.DG\]](#).

- [26] I. R. Klebanov and E. Witten, “Superconformal field theory on three-branes at a Calabi-Yau singularity,” *Nucl.Phys.* **B536** (1998) 199–218, [arXiv:hep-th/9807080 \[hep-th\]](#).
- [27] F. Benini, C. Closset, and S. Cremonesi, “Chiral flavors and M2-branes at toric CY4 singularities,” *JHEP* **02** (2010) 036, [arXiv:0911.4127 \[hep-th\]](#).
- [28] D. L. Jafferis, “Quantum corrections to $\mathcal{N} = 2$ Chern-Simons theories with flavor and their AdS₄ duals,” *JHEP* **08** (2013) 046, [arXiv:0911.4324 \[hep-th\]](#).
- [29] M. Aganagic, “A Stringy Origin of M2 Brane Chern-Simons Theories,” *Nucl. Phys. B* **835** (2010) 1–28, [arXiv:0905.3415 \[hep-th\]](#).
- [30] D. Gaiotto and A. Tomasiello, “The gauge dual of Romans mass,” *JHEP* **01** (2010) 015, [arXiv:0901.0969 \[hep-th\]](#).
- [31] O. Aharony, O. Bergman, D. L. Jafferis, and J. Maldacena, “N=6 superconformal Chern-Simons-matter theories, M2-branes and their gravity duals,” *JHEP* **10** (2008) 091, [arXiv:0806.1218 \[hep-th\]](#).
- [32] D. Martelli and J. Sparks, “Moduli spaces of Chern-Simons quiver gauge theories and AdS(4)/CFT(3),” *Phys. Rev. D* **78** (2008) 126005, [arXiv:0808.0912 \[hep-th\]](#).
- [33] F. Benini and A. Zaffaroni, “A topologically twisted index for three-dimensional supersymmetric theories,” *JHEP* **07** (2015) 127, [arXiv:1504.03698 \[hep-th\]](#).
- [34] F. Benini and A. Zaffaroni, “Supersymmetric partition functions on Riemann surfaces,” *Proc. Symp. Pure Math.* **96** (2017) 13–46, [arXiv:1605.06120 \[hep-th\]](#).
- [35] D. L. Jafferis, I. R. Klebanov, S. S. Pufu, and B. R. Safdi, “Towards the F-Theorem: N=2 Field Theories on the Three-Sphere,” *JHEP* **06** (2011) 102, [arXiv:1103.1181 \[hep-th\]](#).
- [36] V. Pestun, “Localization of gauge theory on a four-sphere and supersymmetric Wilson loops,” *Commun. Math. Phys.* **313** (2012) 71–129, [arXiv:0712.2824 \[hep-th\]](#).
- [37] J. P. Gauntlett, D. Martelli, and J. Sparks, “Toric geometry and the dual of c -extremization,” *JHEP* **01** (2019) 204, [arXiv:1812.05597 \[hep-th\]](#).

- [38] D. Berenstein, C. P. Herzog, and I. R. Klebanov, “Baryon spectra and AdS /CFT correspondence,” *JHEP* **06** (2002) 047, [arXiv:hep-th/0202150 \[hep-th\]](#).
- [39] F. Kirwan, “Momentum maps and reduction in algebraic geometry,” *Differential Geometry and its Applications* **9** no. 1, (1998) 135–171.
- [40] S.-y. Wu, “An Integration formula for the square of moment maps of circle actions,” *Lett. Math. Phys.* **29** (1993) 311–328, [arXiv:hep-th/9212071](#).
- [41] E. Bergshoeff, E. Sezgin, and P. K. Townsend, “Supermembranes and Eleven-Dimensional Supergravity,” *Phys. Lett. B* **189** (1987) 75–78.
- [42] J. P. Gauntlett, “Branes, calibrations and supergravity,” [arXiv:hep-th/0305074 \[hep-th\]](#).
- [43] L.-Y. Hung, R. C. Myers, M. Smolkin, and A. Yale, “Holographic Calculations of Renyi Entropy,” *JHEP* **12** (2011) 047, [arXiv:1110.1084 \[hep-th\]](#).
- [44] E. Witten, “Anti-de Sitter space, thermal phase transition, and confinement in gauge theories,” *Adv. Theor. Math. Phys.* **2** (1998) 505–532, [arXiv:hep-th/9803131](#).
- [45] P. Ferrero, J. P. Gauntlett, and J. Sparks, “Supersymmetric spindles,” *JHEP* **01** (2022) 102, [arXiv:2112.01543 \[hep-th\]](#).
- [46] D. Martelli and A. Zaffaroni, “Equivariant localization and holography,” *Lett. Math. Phys.* **114** no. 1, (2024) 15, [arXiv:2306.03891 \[hep-th\]](#).
- [47] K. Hristov, S. Katmadas, and C. Toldo, “Rotating attractors and BPS black holes in AdS_4 ,” *JHEP* **01** (2019) 199, [arXiv:1811.00292 \[hep-th\]](#).
- [48] S. M. Hosseini, K. Hristov, and A. Zaffaroni, “Gluing gravitational blocks for AdS black holes,” *JHEP* **12** (2019) 168, [arXiv:1909.10550 \[hep-th\]](#).
- [49] D. Cassani, J. P. Gauntlett, D. Martelli, and J. Sparks, “Thermodynamics of accelerating and supersymmetric AdS4 black holes,” *Phys. Rev. D* **104** no. 8, (2021) 086005, [arXiv:2106.05571 \[hep-th\]](#).
- [50] C. Beem, T. Dimofte, and S. Pasquetti, “Holomorphic Blocks in Three Dimensions,” *JHEP* **12** (2014) 177, [arXiv:1211.1986 \[hep-th\]](#).

- [51] J. P. Gauntlett, D. Martelli, and J. Sparks, “Fibred GK geometry and supersymmetric AdS solutions,” *JHEP* **11** (2019) 176, [arXiv:1910.08078](#) [[hep-th](#)].
- [52] K. Becker, M. Becker, and A. Strominger, “Five-branes, membranes and nonperturbative string theory,” *Nucl. Phys. B* **456** (1995) 130–152, [arXiv:hep-th/9507158](#).